FORGE

Fate Of Repository Gases

European Commission FP7

WP 4.2.1/WP 5.2.2: Gas transport processes at Mont Terri Test Site (EDZ and host rock)- Field results and conceptual understanding of selfsealing processes

FORGE Report D4.16 – Final

	Name	Organisation	Signature	Date
Compiled	P. Marschall	Nagra		29.5.2013
Verified	L. Johnson	Nagra		29.5.2013
Approved	P. Zuidema	Nagra		10.6.2013

Keywords.

Opalinus Clay; Gas flow; transport; field experiments

Bibliographical reference

P. MARSCHALL, B. LANYON, I. GAUS, J. RÜEDI. 2013. Gas transport processes at Mont Terri Test Site (EDZ and host rock)- Field results and conceptual understanding of self-sealing processes

FORGE Reports D4.16. 61pp.

Euratom 7th Framework Programme Project: FORGE

EURATOM

Fate of repository gases (FORGE)

The multiple barrier concept is the cornerstone of all proposed schemes for underground disposal of radioactive wastes. The concept invokes a series of barriers, both engineered and natural, between the waste and the surface. Achieving this concept is the primary objective of all disposal programmes, from site exploration and characterisation to repository design and construction. However, the performance of the repository as a whole (waste, buffer, engineering disturbed zone, host rock), and in particular its gas transport properties, are still an area of ongoing research and development. Issues still to be further examined that relate to improved understanding of basic processes include: dilational versus visco-capillary flow mechanisms; long-term performance of seals, in particular gas flow along contacts; role of the EDZ as a conduit for preferential flow; laboratory to field up-scaling. Understanding gas generation and migration is thus an important aspect in the quantitative assessment of repositories and is the focus of the research in this integrated, multi-disciplinary project. The FORGE project is a pan-European project with links to international radioactive waste management organisations, regulators and academia, specifically designed to tackle key research issues associated with the generation and movement of repository gasses. Of particular importance are the long-term performance of bentonite buffers, plastic clays, indurated mudrocks and crystalline formations. Further experimental data are useful to reduce uncertainty relating to the quantitative treatment of gas in performance assessment. FORGE will address these issues through a series of laboratory and field-scale experiments, including the development of new methods for up-scaling allowing the optimisation of concepts through detailed analysis. The FORGE partners are committed to training and CPD through a broad portfolio of training opportunities and initiatives which form a significant part of the project.

Further details on the FORGE project and its outcomes can be accessed at www.FORGEproject.org.

Contact details:

Paul Marschall
Nagra
Tel: +41 (0)56 4371 330 Fax +41 (0)56 4371 207
email: marschall@nagra.ch
web address: www.nagra.ch
Address: Hardstrasse 73, CH 5430 Wettingen

Bill Lanyon
Fracture Systems Ltd
Tel: +44 (0) 1736 795142 Fax +44 (0) 1736 793210
email: bill@fracture-systems.co.uk
web address: www.fracture-systems.co.uk
Address: Tregurrian, Ayr, St Ives, Cornwall, TR26 1EQ, UK

Irina Gaus
Nagra
Tel: +41 (0)56 4371 334 Fax +41 (0)56 4371 207
email: gaus@nagra.ch
web address: www.nagra.ch
Address: Hardstrasse 73, CH 5430 Wettingen

Jörg Rüedi
Nagra
Tel: +41 (0)56 4371 312 Fax +41 (0)56 4371 207
email: joerg.rueedi@nagra.ch
web address: www.nagra.ch
Address: Hardstrasse 73, CH 5430 Wettingen

Foreword

This report is a joint product of WP 4.2.1 ("Gas transport in EDZ at Mont Terri Test Site") and WP 5.2.2 ("The HG-C gas injection experiment in intact Opalinus Clay at the Mont Terri URL"), compiling experimental evidence on phenomena and processes associated with gas transport along the excavation damage zone of a sealed tunnel section (WP 4.2.1) and through the intact host rock (WP 5.2.2). The data bases presented in this report were disseminated to the FORGE project partners, forming the basic input for a series of benchmark exercises on modelling of gas transport processes in Opalinus Clay (see Deliverable D4.18). The data deliveries were distributed in electronic form together with a short note containing the data description (Deliverables D4.2, D4.3, D4.10, D5.2, D5.6).

Acknowledgements

A large number of individuals have contributed to the project. We would particularly like to thank the individuals who have contributed to the collection of the laboratory and field data in the context of the Mont Terri project. The continuous support of the delegates of the Mont Terri HG-A project team (R. De La Vaissiere/Andra, H. Leung/NWMO, D. Jäggi/Swisstopo, H. Shao/BGR, B. Lanyon/FSL, T. Trick/Solexperts) and, respectively, the HG-D project team (R. De La Vaissiere/Andra, D. Jäggi/Swisstopo, T. Trick/Solexperts) is greatly acknowledged. Chr. Nussbaum and T. Theurillat (Swisstopo) provided important on-site support at the Mont Terri URL. R. Senger/Intera, E. Romero/UPC Barcelona and A. Ferrari/LMS-EPFL Lausanne contributed with their comprehensive knowledge in the field of laboratory testing of unsaturated Opalinus Clay and the corresponding data interpretation of the laboratory data.

Contents

Foreword ii

Acknowledgements ii

Contents iii

1 Introduction 1
- 1.1 Scope 1
- 1.2 Objectives 1
- 1.3 Report outline 2

2 Laboratory testing 3
- 2.1 Overview 3
- 2.2 Geotechnical characterisation of core samples 3
- 2.3 Complementary information From the Mont Terri URL 22

3 HG-A experimental results and interpretation 27
- 3.1 Description of the HG-A experiment 27
- 3.2 Experimental results 28
- 3.3 Conceptual model 31
- 3.4 Interpretation 39
- 3.5 Outlook 41

4 HG-C/D experimental results and interpretation 43
- 4.1 Description of the sequence of experiments at site 43
- 4.2 Experimental results and Interpretation 46
- 4.3 Summary and conclusions 54

5 Summary and conclusions 56

References 59

Appendix – Data Packages 1 - 11 62

FIGURES

Figure 2.1: Field data from the HG-D1 borehole ate the Mont Terri Site:(a) Geophysical logging comprising induction, total magnetic field and natural gamma log; (b) optical image of the dry borehole and (c) photo documentation of the core samples retrieved. **5**

Figure 2.2: Core samples as received by UPC: the resin coating for core preservation during shipment is removed and the inner part of the sample is sub-cored for preparing the raw samples. **6**

Figure 2.3: Grain size distribution by sedimentation analysis of the core BHG-D1/4 (left graph). The sample can be classified as a sandy clay (CM). **7**

Figure 2.4: Pore size distribution and cumulative intrusion void ratio of the core BHG-D1/4. ..... **8**

Figure 2.5: Water retention behaviour of the core BHG-D1/4: water content (a), void ratio (b) and degree of saturation (c) as a function of total suction. **9**

Figure 2.6: The high pressure oedometric cell at the LMS-EPFL. **10**

Figure 2.7: (a) Oedometric curve for the core BHG-D1, volumetric strain computed from total settlement and the end-of-primary consolidation settlement; (b) consolidation coefficient, oedometric modulus, secondary compression coefficient and permeability over void ratio as back-calculated from the settlement versus time curves. **10**

Figure 2.8: Water retention behaviour of the core BHA-8/1: the water retention curves determined with the desiccator method and comparison with back-calculated MIP curves. The data were fitted with a van Genuchten model. **12**

Figure 2.9: Triaxial cell for water/gas permeability measurements: photograph and schematical sketch. **12**

Figure 2.10: Empirical relationship between (a) total stress and water permeability and (b) void ratio and water permeability for samples parallel and normal to bedding. **13**

Figure 2.11: Measured pressure transients at the injection and outflow sides together with outflow volume and axial displacements. The tests were conducted parallel (thick lines) and perpendicular to bedding (thin lines). **14**

Figure 2.12: Graph of the axial strain versus the axial effective stress for the different stages of the experiment: AB – gas injection phase; BC-shut in phase (p – confining/isostatic stress; Pup – gas injection pressure). **15**

Figure 2.13: Mercury instrusion porosimetry: Pore size distribution of two samples from core BHG-D1/15. ..... **16**

Figure 2.14: Water retention behaviour of Opalinus Clay: Fittings to the van Genuchten expression as a function of the confinement conditions for total and matric suction (the dotted lines correspond to drying paths) **17**

Figure 2.15: Water retention behaviour of Opalinus Clay: Compilation of results from previous studies in other boreholes at the Mont Terri URL (BVE-99-102: Villar et al. 2009) **17**

Figure 2.15: Evolution of injection and confining pressure and outflow in test OPA3 ..... **19**

Figure 2.16: Desaturation and resaturation experiments in a hermetically sealed drying cabinet at the Grimsel Test Site. **20**

Figure 2.17: Large caliper Opalinus Clay subjected to a long-term desaturation experiment in a hermetically sealed drying cabinet at the Grimsel Test Site: (a) photo of the sample and (b) upper side of the sample with TDR probe. The resin filled pre-drillings were aimed at stabilizing the core during core recovery. **20**

Figure 2.18: Desaturation and resaturation experiments in a hermetically sealed drying cabinet at the Grimsel Test Site **22**

Figure 2.19: Gas transport experiments on core samples by Krooss&Alles (2007): Sample configuration and experimental results **25**

Figure 3.1: Location and layout of HG-A a) location at the Mont Terri Laboratory; b) Schematic drawing of the Microtunnel and the site instrumentation. Colour coding refers to the steel liner (red), the seal section (green) and the backfilled test section (orange). **27**

Figure 3.2: Microtunnel stress, pore pressure, water content and flowrate measurements from start of saturation. **29**

Figure 3.3: Geosphere pressure measurements from start of saturation: a) Near-field piezometers in HG-A02 and HG-A03; b) piezometers HG-A08 to HG-A13, HG-A24 &HG-A25. ..... **30**

Figure 3.4: a) Linear and b) log-log plots of delta pressure from GI1-3. ..... **30**

Figure 3.5: Microtunnel stress, pore pressure, water content and flowrate measurements during gas injection. **31**

Figure 3.6: Schematic representation of the damage zone around the HG-A microtunnel (after Marschall et al. 2008), showing key processes and features that affect stability: slab-like breakouts on the upper left side are due to extensile failure along tectonic fractures. Wedge-like breakouts occur on the right side. Direction of view is towards the rear of the microtunnel. **32**

Figure 3.7: Sealing section of the Microtunnel with the surface breakouts at 11 and 4 H radial positions as of April 2006. View

is looking towards test section. The wooden dummies are for the emplacement of the total pressure cells **33**

Figure 3.8: Relationship between gas entry pressure and intrinsic permeability for low permeability rock formations (claystones, shales, sandstones). Data from Benken and Mont Terri added to the compilation of Davies (1991). **35**

Figure 3.9: Compilation of pressure observations in boreholes of the Mont Terri rock laboratory on 30.06.2000 (unless indicated otherwise in the figure legend), illustrated with respect to the distance along bedding to the nearest gallery. **35**

Figure 3.11: Reduction in interval transmissivity with resaturation time from (Blümling et al 2007). **38**

Figure 3.12: Sealing Index during water injection. Periods of reduced Megapacker pressure (low effective stress) are marked. . **39**

Figure 3-13: Test and seal section pressure and stress during a) high b) low effective stress testing. **40**

Figure 3.14: EDZ schematic (from Marschall et al. 2008) with stages of gas injection: a) EDZ structure, b) storage & dissolution, c) storage & leakage, d) breakdown and gas flow into the EDZ. **41**

Figure 4.2 Pressure responses in the injection borehole (BGS2-2) and observation borehole (BGS1-1, BGS1-2, BGS1-3) during the HG-C multi-step water injection (a), measured flow rates (b) and axial displacements (c). **46**

Figure 4.3: Simulated response of the entire test sequence based on the best-fit parameters from the HI5 optimization for injection flow rates. **47**

Figure 4.4: Computed 95% confidence regions of parameter estimates based on the optimization of the log-log flow rates for HI1 through HI6. ..... **48**

Figure 4.5: Pressure responses in the injection borehole (BGS2-2) and observation borehole (BGS1-1, BGS1-2, BGS1-3) during the HG-C multi-step gas injection (a), measured flow rates (b) and axial displacements (c). **49**

Figure 4.6: Simulated pressure responses in BGS2-1 (injection) and BGS1-2 (observation) during the HG-C Experimental Phases 2, based on individual fits of Sequences GHI1–3, GHI4 and GHI5. ..... **51**

Figure 4.7: Simulated pressure responses in BGS2-1 (injection) and BGS1-2 (observation) during the HG-C Experimental Phases 2 based on individual fits of Sequences GHI1–3, GHI4 and GHI5, whereby GHI5 includes the simulated results assuming pressure-dependent permeability. **52**

Figure 4.8: HG-D testing: a) flow and pressure response; b) FIM response **53**

Figure 4.9: HG-D testing gas injection flow and pressure response. **54**

TABLES

Table 2.1: Overview of core samples from the shaly facies of the Mont Terri URL, subjected to geotechnical characterisation.....4

Table 2.2: Results of the geotechnical characterization of the core BHG-D1/4.....7

Table 2.3: Results of the geotechnical characterization of the core BHA-8/1 and BDR-1_OC14.....11

Table 2.4: Results of the geotechnical characterization of the core BHA-8/15 16

Table 2.5: Activity logbook of the long-term core desaturation experiment 21

Table 2.6: Geotechnical reference parameters of the Opalinus Clay at the Mont Terri underground laboratory after (Bock 2000). 23

Table 2.8: Range of hydraulic properties for different facies of the Opalinus Clay at Mont Terri (from Marschall et al. 2004). 23

Table 2.9: Stress tensor for Mont Terri Rock Laboratory (from Martin&Lanyon 2003a, Bossart&Wermeille 2003 and Corcum&Martin 2007).....24

Table 2.10: Reports on laboratory testing of the Opalinus Clay. 26

Table 3.1: HG-A experiment instrumentation.....28

Table 3.2: HG-A experiment chronology.....29

Table 3.3: Summary of Sealing Mechanisms as Identified by Bock et al. (2010) 38

Table 4.1: Overview of the HG-C site instrumentation.....44

Table 4.2: Overview of GS/GP-A, HG-C and HG-D experimental phases 45

Table 4.3: Summary of parameter estimates from nSights optimization of HI1 through HI6.....48

Table 4.4: Summary of parameter estimates from ITOUGH optimization of GHI13-GHI5. 50

1 Introduction

1.1 SCOPE

The understanding and prediction of the evolution of repository systems over geological timeframes requires a sufficiently detailed knowledge of a series of highly-complex coupled phenomenological processes. There remains uncertainty regarding the mechanisms and processes governing gas generation and migration in natural and engineered barrier systems. It is thus important to understand a system to an adequate level of detail to allow confidence in the assessment of site performance, recognising that a robust treatment of uncertainty is desirable. Of particular importance to the European radioactive waste management programmes are the long-term engineering performance of bentonite buffers, plastic clays, indurated mudrocks and crystalline formations. The EU 7th FP project FORGE was launched to tackle key research issues associated with the generation and movement of repository gases using a series of laboratory and fieldscale experiments, including the development of new methods for up-scaling allowing the optimisation of concepts through detailed analysis.

While progress has been made in recent years in our understanding of the EDZ through EU-projects like SELFRAC and NF-PRO, there remains a paucity of representative data for both the definition of hydro-mechanical responses to complex stress paths induced during repository construction, and to the role of gas migration on issues including fracture self-sealing, tunnel convergence, radionuclide displacement and repository over-pressuring. These complex issues are the subject of recent state-of-the-art laboratory and field-based test programmes. It has been the aim of WP 4 to provide process-based knowledge and the production of a unique representative dataset for the development and validation of theoretical frameworks and predictive numerical tools for different lithological units in support of repository performance assessment. Nagra's particular focus has been on the phenomena and processes, associated with gas transport in Opalinus Clay. The experimental data bases have been acquired in the context of the Mont Terri research programme.

In order to better evaluate the conditions under which gas can migrate from the loci of gas generation in the backfilled underground structures of a closed repository through the host rock formation and/or along the engineered access structures to the biosphere, it is essential to understand the phenomena, processes and mechanisms governing gas migration in the intact host rock at a certain level which allows at least to bound the consequences. WP 5 addressed these issues through a detailed programme of laboratory and field-scale experiments. These provided important new data for the validation of numerical models for use in the evaluation of repository evolution. Nagra's interests in this context concentrated on the hydro-mechanical processes, associated with gas transport in the (initially) intact Opalinus Clay, assuming that the rock is fully saturated prior to the application of the elevated gas pressures. As for WP4, the experimental data bases have been acquired in the context of the Mont Terri research programme.

1.2 OBJECTIVES

A comprehensive gas-related data base has been elaborated in the context of the Mont Terri project, comprising both laboratory investigations on core samples and in-situ experiments in the Mont Terri URL. These data bases are of high importance for the identification of gas-related phenomena and for the development of conceptual models of coupled THM processes associated with gas transport in intact and fractured Opalinus Clay. This report is aimed at

compiling relevant data from the Mont Terri URL as input for the benchmark exercises to be tackled by the THM-modelling groups of WP4 (WP 4.3.1: Modelling of gas migration through disturbed argillaceous media) and WP5 (WP 5.3.1 Modelling of gas transport in indurated clay). The data bases are related to the following issues of gas related research:

- Laboratory experiments, suitable for the derivation of basic two-phase flow parameters of Opalinus Clay (intrinsic properties, capillary pressure and relative permeability relationships);
- Laboratory experiments, which reveal gas-related phenomena and HM processes in intact Opalinus Clay;
- Field data, which allow for the validation of coupled models of multiphase flow in deformable media. Model validation includes not only the drainage process (gas invasion into saturated rock) but also the resaturation process after gas invasion (imbibition of pore water and self-sealing of the rock);
- Derivation of new methodologies for up-scaling from laboratory to field to repository scales.

1.3 REPORT OUTLINE

Chapter 1 presents background information on the EU-FORGE project and on the scope of this report. The objectives are defined and the endusers' expectations are reviewed.

Chapter 2 is dedicated to the gas-related laboratory experiments in the context of the Mont Terri project. Key laboratory experiments are described and references are given.

Chapter 3 reviews the experimental set-up of the HG-A experiment in the Mont Terri Underground Laboratory (URL). The chronology of the experiment is described and the monitoring data are discussed. Furthermore, a brief description of the site descriptive model is given.

Chapter 4 reviews the experimental set-up of the HG-C / HG-D experiment at Mont Terri URL. The chronology of the experiment is described and the monitoring data are discussed. Furthermore, a brief description of the site descriptive model is given.

Chapter 5 summarises the main achievements and provides conclusions regarding the gas related data base from within the Mont Terri Project.

2 Laboratory testing

2.1 OVERVIEW

Data packages were distributed to the THM-modelling groups participating in the benchmark exercises of WP 4.3.1 and WP 5.3.1. The packages comprised experimental data from laboratory tests in the HG-D site, relevant laboratory data from other locations in the Mont Terri URL and further references of scientific papers on gas transport in Opalinus Clay. In chapter 2, the following data sets will be discussed in greater detail:

- Chapter 2.2: Geotechnical characterisation and permeability testing of core samples, which had been retrieved from the HG-D-1 borehole in the HG-D site;
- Chapter 2.3: Complementary geotechnical information from the Mont Terri URL, which is of potential interest for the modelling groups

As part of WP4 and WP5 the following deliverables have been distributed to date:

- D4.2: Contribution to the report "Description of proposed in situ experimental set-ups (within URLs)"
- D4.3: Compilation of existing data (Mont Terri)
- D4.10: Progress report on HG-A experimental activities
- D5.2: Design, installation and compilation of existing data for the HG-C experiment at Mont Terri
- D5.6: Progress report on HG-C experiment at Mont Terri

Electronic data bases on long-term monitoring data from the HG-A and HG-C/HG-D experiments have been handed over to the modellers on request.

2.2 GEOTECHNICAL CHARACTERISATION OF CORE SAMPLES

2.2.1 General information on core samples

The borehole HG-D1 was drilled in June 2009 as to complement the borehole array in the HG-D site for a new campaign of gas injection tests (see chapter 4). The borehole was directed from the floor of Gallery 98 of the Mont Terri URL parallel to bedding at a dip of around 50° downwards (borehole mouth: X-2579384.15; Y-1247613.61; Z-513.38; azimuth: 323°; diameter 101 mm; length: 13.3 m). A dry drilling, single barrel technique was applied to retrieve high quality core samples. All cores recovered were subjected to geological mapping with focus on sedimentary and tectonic structures. Several cores were shipped to geoscientific laboratories (EPFL, UPC, CIEMAT and BGS) for further geotechnical characterisation. After completion of the drilling a geophysical logging campaign was conducted, comprising an induction log with SS (51 cm) and LS (81 cm) spacing, total magnetic field measurements and natural gamma logging. Figure 2.1 displays the results of geological logging in HG-D1 and core recovery. The rock fabric along the borehole looks rather uniform with only a few sandy nodules and thin carbonate layers, respectively. A total of 9 discrete structures (joints / fractures) were found, mostly oriented sub-parallel to bedding at a depth between 10 and 12 m ah.

Another core sample (BHA8/1) was recovered in June 2008 from the short borehole BHA8 in the MI niche nearby the HG-D site (Girardin et al. 2008). The borehole was drilled perpendicular to bedding into the shaly facies (borehole mouth: X-2579427.014; Y-1247556.48; Z-511.396;

azimuth: 330°; diameter 150 mm; length: 1.82 m) and a special overcoring technique was used for core recovery in order to minimize sample damage (Steiger & Bossart, 2003). The core BHA8/1 was used by UPC / Barcelona for comprehensive water and gas permeability testing (chapter 2.2.3). Figure 2-2 shows the core samples as received by UPC and illustrated core preservation and the adopted sub-coring procedure.

As part of the Mont Terri / DR experiment a large diameter drilling campaign was conducted in 2010, aimed at retrieving an overcore of the diffusion test section in DR-1 (drilling orientation perpendicular to bedding). Subsequently, the borehole was extended and core material was recovered for geotechnical characterisation. Core sample DR-1_OC14 was shipped to the geotechnical laboratories of UPC. It turned out that the core sample was very fissile and did not allow any testing beyond determination of basic index properties. Table 2.1 gives an overview of the core samples which were submitted to several geotechnical laboratories for the determination of index properties and permeability testing.

Table 2.1: Overview of core samples from the shaly facies of the Mont Terri URL, subjected to geotechnical characterisation

Core ID	Depth (m ah)	Lab	Tests performed
BHG-D1 / 4	3.0 – 3.9	EPFL	- Index properties - Atterberg Limits - Mercury intrusion - Water retention - High pressure oedometric testing
BHG-DR_OC14	10.2 – 11.0	UPC	- Index properties
BHA-1	1.1 – 1.8	UPC	- Index properties - Mercury intrusion - Water retention - High pressure oedometric testing
BHG-D1 / 15	11.8 – 12.5	Ciemat	- Index properties - Mercury intrusion - Water retention - High pressure oedometric testing

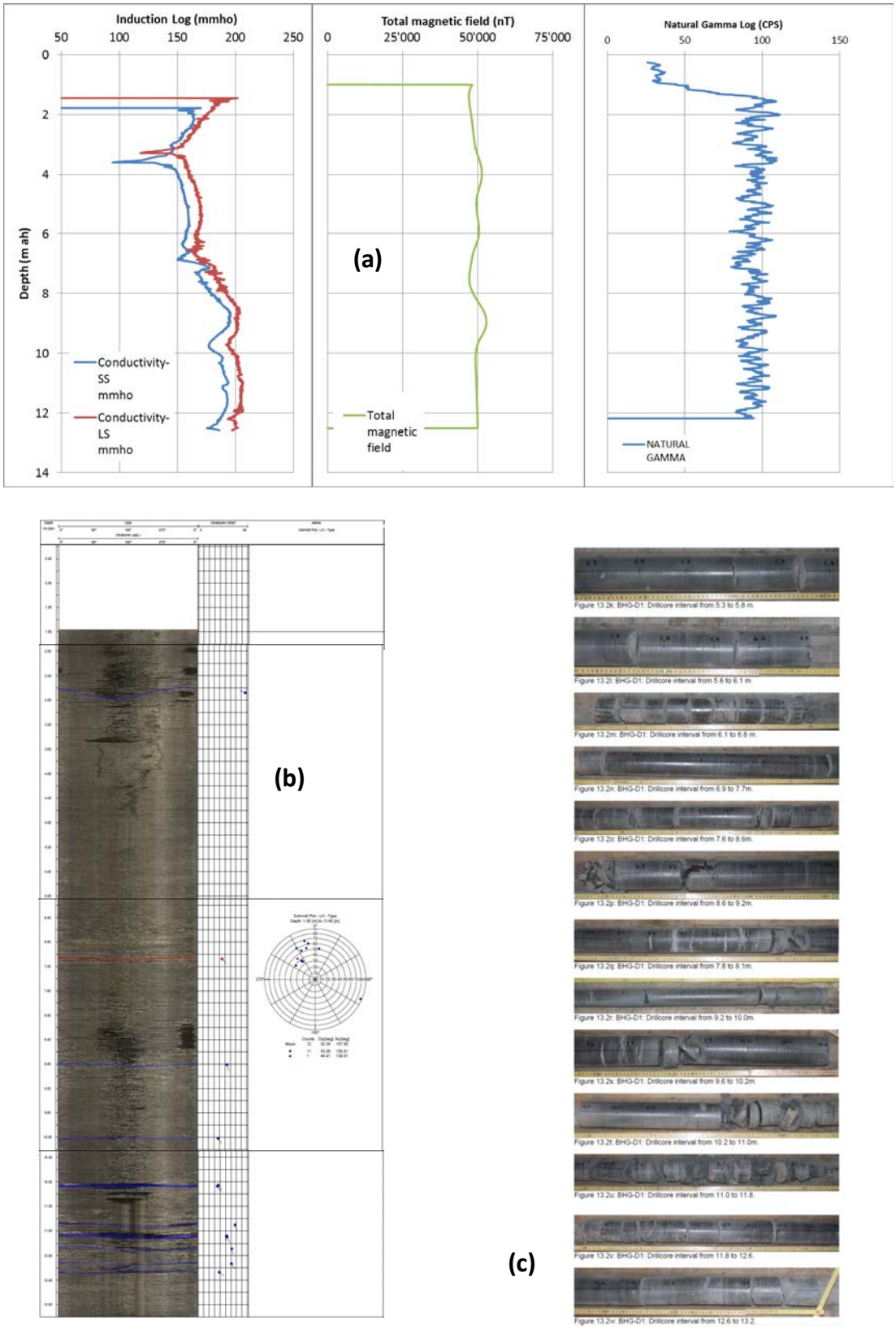

Figure 2.1: Field data from the HG-D1 borehole at the Mont Terri Site: (a) Geophysical logging comprising induction, total magnetic field and natural gamma log; (b) optical image of the dry borehole and (c) photo documentation of the core samples retrieved.

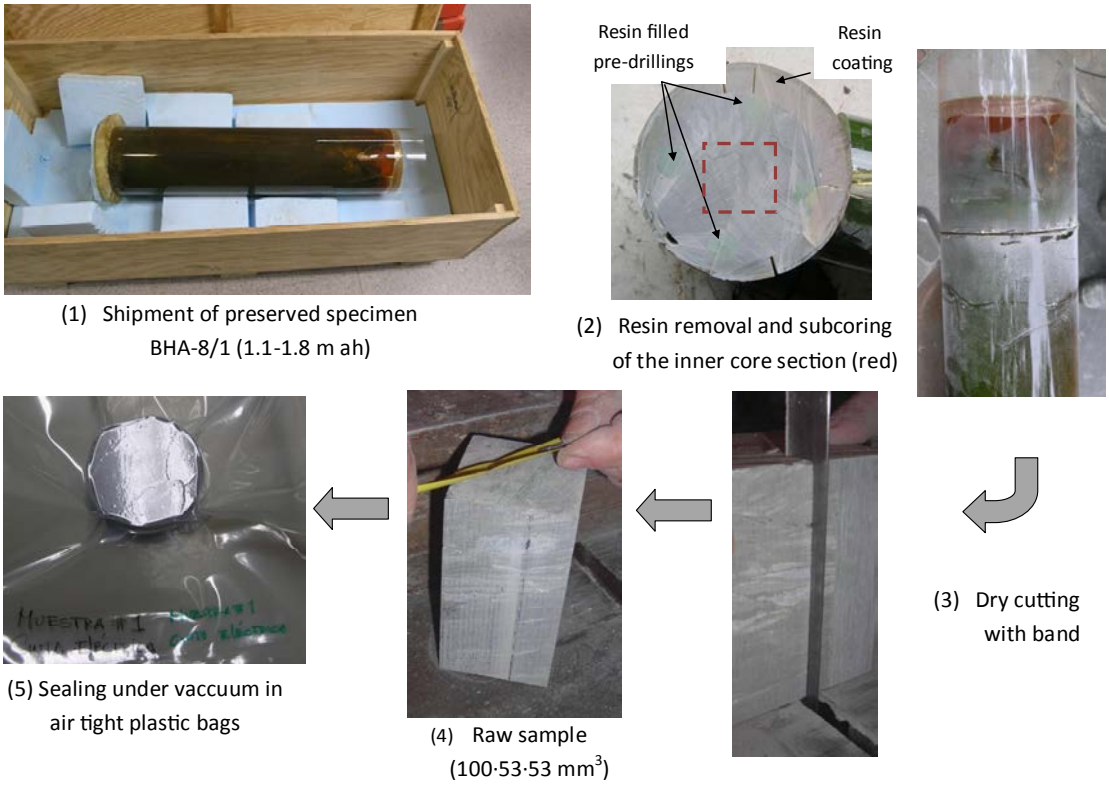

Figure 2.2: Core samples as received by UPC: the resin coating for core preservation during shipment is removed and the inner part of the sample is sub-cored for preparing the raw samples.

2.2.2 Geotechnical characterisation of core BHG-D1/4 by LMS/EPFL

The core material BHG-D1/4 was subjected to comprehensive geotechnical characterisation by the Laboratory of Soil Mechanics (LMS) of the Swiss Federal Institute of Technology in Lausanne (EPFL). The focus was on its geotechnical material properties and the geomechanical behaviour, including particle density, bulk density, water content, void ratio, degree of saturation, Atterberg limits, grain and pore size distributions. Furthermore, initial total suction was measured, as well as the water-retention and the stress-strain behaviour. The study has been reported in Ferrari et al. (2012).

Geotechnical characterization

The result of the geotechnical identification of the cores is reported in Table 2-2 which presents:

- the grain density (ρ_s, ratio of the mass to the volume of the solid phase),
- the bulk density (ρ, ratio of the mass to the total volume of the material),
- the gravimetric water content (w, ratio of the weight of the water to the weight of the solid phase),
- the void ratio (e, the ratio of the volume of pores to the volume of the solid phase),
- the degree of saturation ($S_{r,i}$, the ratio of the volume of water to the volume of pores at initial state),

- the Atterberg limits (liquid limit w_L; plastic limit w_P, plasticity index PI),
- the grain size distribution, and
- the classification of the materials.

Table 2.2: Results of the geotechnical characterization of the core BHG-D1/4

ρ_s (Mg/m3)	ρ (Mg/m3)	*w* (%)	*e* (-)			$S_{r,i}$(%)
2.74	2.46	6.9	0.21			92
			Grain size fraction (%)			Classification
w_L(%)	w_P(%)	*PI*(%)	sand	silt	clay	
38	23	15	5	60	35	CM

The grain size distribution of core BGD-D1/4 was obtained by sedimentation analysis according to the SN 670 816. In order to carry out the sedimentation analysis, the material is crushed initially by means of a grinder and the fraction passing the ASTM No. 35 sieve is selected. The crushed material is placed in distilled water along with a dispersing agent and shaken overnight. The obtained grain size distributions are shown in 2-3 (left graph). The core was classified as CM (sandy clay; Figure 2-3, right graph) and can be discriminated clearly from the CL-ML category (silty clay with sand), which may be more characteristic for the sandy facies of the Opalinus Clay at Mont Terri.

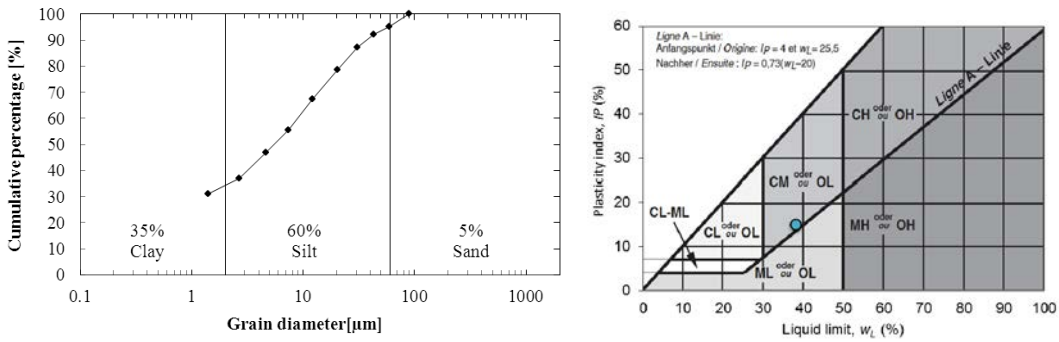

Figure 2.3: Grain size distribution by sedimentation analysis of the core BHG-D1/4 (left graph). The sample can be classified as a sandy clay (CM).

Mercury Intrusion Porosimetry (MIP) was used to determine the Pore Size Distribution (PSD) for core BHG-D4/1. The MIP technique consists in forcing the penetration of mercury inside a sample and measuring the intruded volume of mercury as a function of the applied pressure. The required pressure is inversely proportional to the size of the pores that are filled progressively. Washburn equation relates the applied pressure to the equivalent pore throat diameter (assuming a circular shape for the pores) of the intruded porosity. Details of the test procedure are described in Ferrari et al. (2012).

The results from the MIP tests are depicted in Figure 2-4 in terms of cumulative intruded void ratio (ratio of the cumulative intruded mercury volume to the weight of the solid phase) and pore size density function versus the equivalent pore diameter (*D*). The cumulative void ratio graphs show that not the entire porosity is intruded with the MIP method (see Table 2.1; e=0.21); this indicates that there is a significant residual porosity with small pore sizes and occluded pores, respectively, which are not intruded by the mercury. The PSD function is found to be unimodal, showing a pore mode at approximately 20 nm.

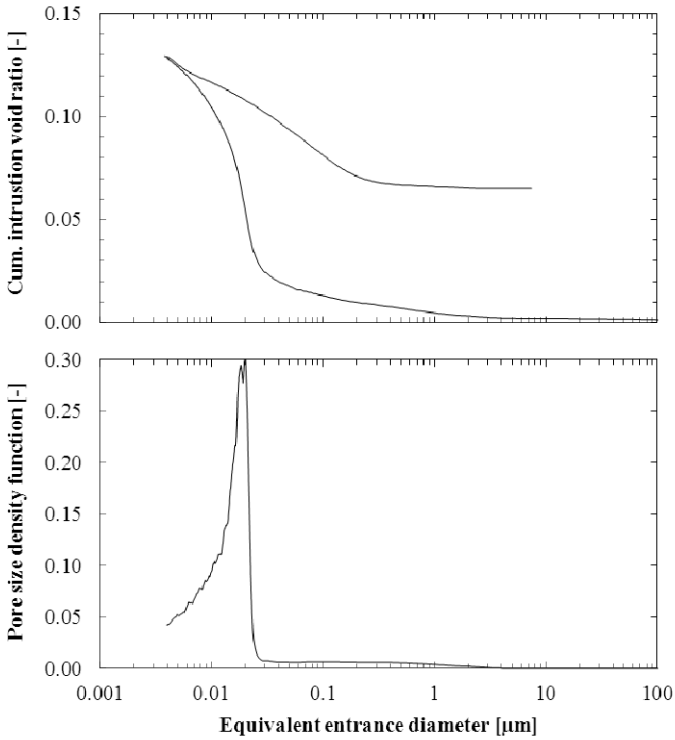

Figure 2.4: Pore size distribution and cumulative intrusion void ratio of the core BHG-D1/4.

Water retention behaviour

To determine the water-retention behaviour, the water content of the shale specimen was imposed, before the suction and the volume of the specimen was measured. A detailed description of the experimental procedure is given in Ferrari et al. (2012).

The water retention behaviour of the core sample is displayed in Figure 2-5. Results are depicted in terms of water content, void ratio and degree of saturation versus total suction. Each point represents an average of the measurement done on three specimens which followed an identical drying/wetting path. The initial state of the sample is also depicted. The material has an initial degree of saturation close to one, indicating that the core samples had been well preserved during shipment (no damage, no significant desaturation). The initial state for both materials was found on the main drying paths, as a consequence of the coring process and the exposition to atmosphere before preservation.

Main drying and wetting paths are well distinguished and hysteresis zones are observed. The void ratio evolution with total suction (Figure 2-5a and 2-5b) shows that porosity changes are more significant for suction variations in the lowest ranges. Void ratios at lowest measured suctions were in very good agreement with the results of free swelling tests carried out with the same synthetic waters used for determining the water retention curves.

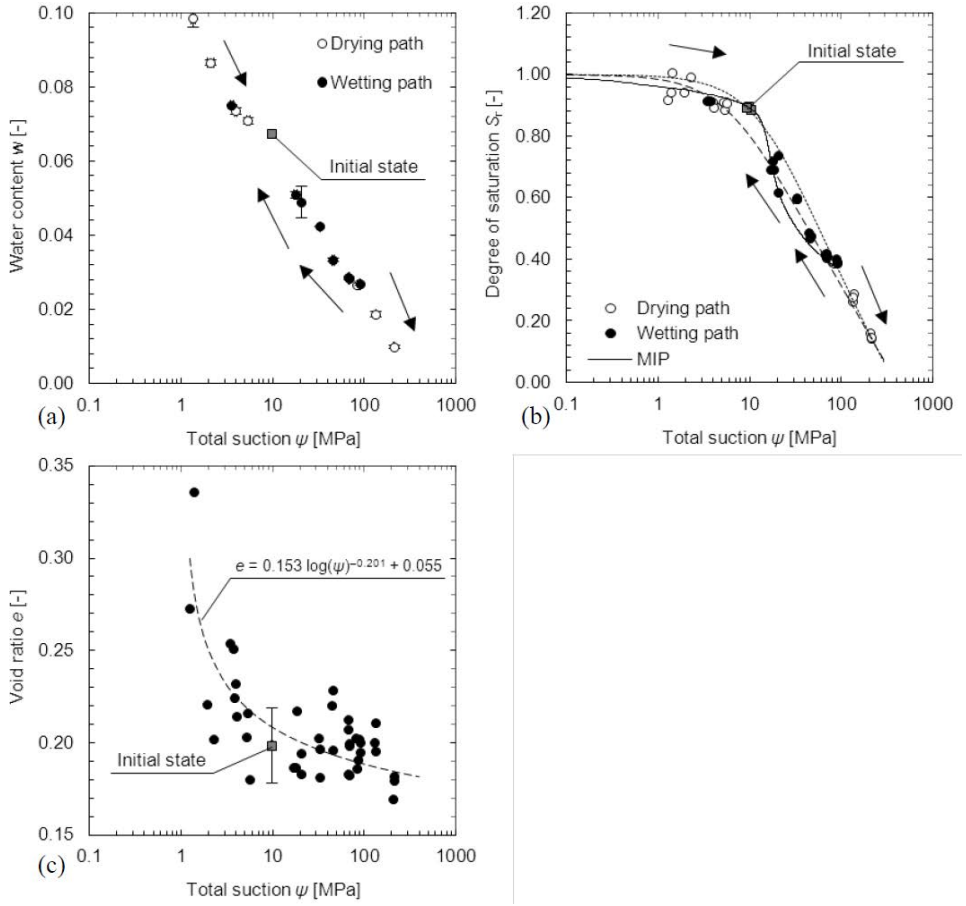

Figure 2.5: Water retention behaviour of the core BHG-D1/4: water content (a), void ratio (b) and degree of saturation (c) as a function of total suction.

Volumetric response on mechanical loading

High-pressure oedometer tests are carried out on the core BHG-D1. The apparatus used for these tests is a specially designed high-pressure oedometer cell (Ferrari et al. 2012) allowing a maximum attainable vertical stress of 100 MPa. The high level of applicable vertical stress is required in order to observe the transition from the over- to the normally-consolidated behaviour of the material. The layout and a picture of the apparatus are depicted in Figure 2-6. The vertical pressure is applied by means of a hydraulic jack, in which the pressure is maintained by a pressure/volume controller. The vertical displacement is measured via three LVDTs (Linear Variable Differential Transformer) fixed on the loading piston and in contact with the base of the cell (accuracy of 1 μm). The tests are done in drained conditions, allowing water exchange between the specimen and the cell circuit.

The oedometric curve along with the determination of the yield stress and the swelling and compression coefficients are reported in Figure 2.7 (a) in terms of axial (or vertical) strain versus applied vertical effective stress. The figure depicts the volumetric strain relative to the end of the primary consolidation. The yield stress is approximately 2 MPa, whereas the compression index C_c = 0.038, the swelling index upon first unloading C_{s1} = 0.007 and the swelling index upon second unloading C_{s2} = 0.016. A systematic increase of the swelling coefficient with the yield stress is observed.

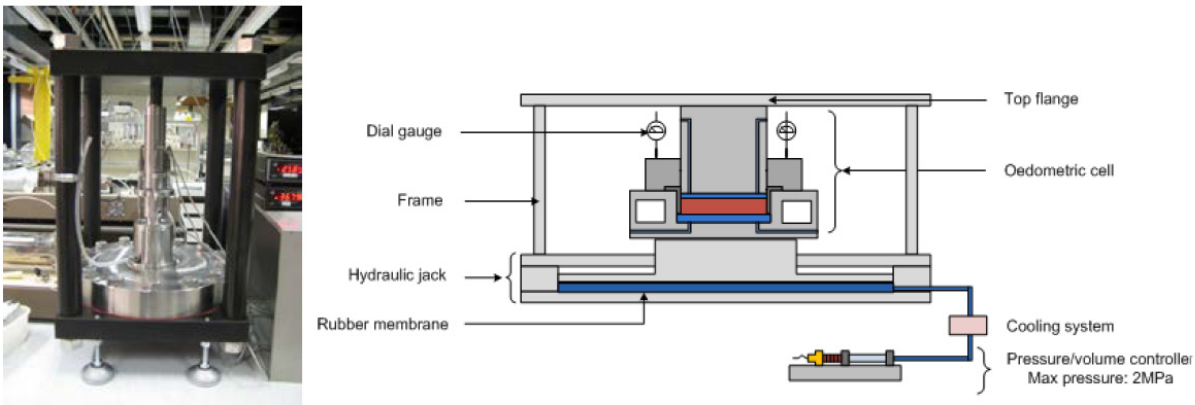

Figure 2.6: The high pressure oedometric cell at the LMS-EPFL.

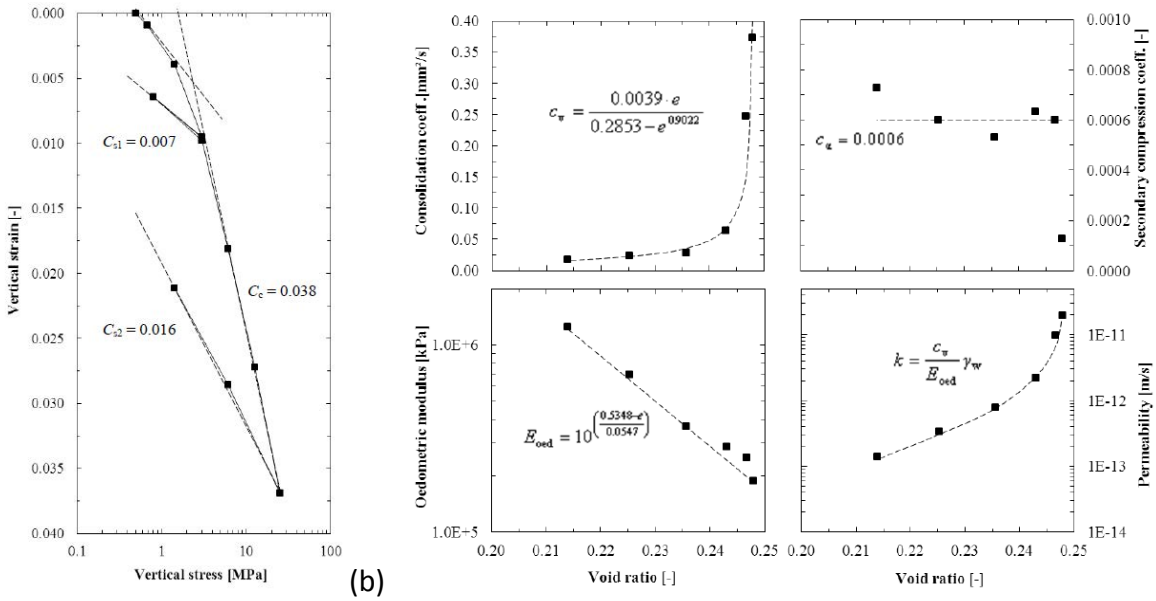

Figure 2.7: (a) Oedometric curve for the core BHG-D1, volumetric strain computed for total settlement and the end-of-primary consolidation settlement; (b) consolidation coefficient, oedometric modulus, secondary compression coefficient and permeability over void ratio, back-calculated from settlement versus time curves.

End-of-primary strains are used not only to compute the compression and the swelling indices and to assess the vertical effective yield stresses, but also for estimating the permeability of the sample perpendicular to the loading axis. The oedometric modulus (E_{oed}) and the coefficient of consolidation (c_v) as a function of the applied vertical effective stress are depicted in Figure 2.7b. Eventually, the permeability (k) can be back-calculated for each load increment using the definition of the coefficient of consolidation:

$$k = \frac{c_v \cdot \gamma_w}{E_{oed}}$$

2.2.3 Gas/water permeability tests by UPC/Barcelona

Core samples from boreholes BHG-D1/13, BHA-8/1 and BDR-1_OC14 were sent to UPC for geotechnical characterisation and for water/gas permeability testing. Core BDR-1_OCR14 turned out to be delicate to handle and thus, the test program was quite limited.

Geotechnical characterization

The result of the geotechnical identification of the cores is reported in Table 2-2 which presents:

- the grain density (ρ_s, ratio of the mass to the volume of the solid phase),
- the bulk density (ρ, ratio of the mass to the total volume of the material),
- the water content (w, ratio of the weight of the water to the weight of the solid phase),
- the void ratio (e, the ratio of the volume of pores to the volume of the solid phase),
- the degree of saturation ($S_{r,i}$, the ratio of the volume of water to the volume of pores at initial state),
- the Atterberg limits (liquid limit w_L; plastic limit w_P, plasticity index PI).
- Swelling strain
- Young's modulus
- Mercury porosimetry

The results from basic geotechnical characterisation of the cores are given in Table 2.3.

Table 2.3: Results of the geotechnical characterization of the core BHA-8/1 and BDR-1_OC14

Sample ID	ρ_s (Mg/m³)	ρ (Mg/m³)	*w* (%)	*e* (-)	S_r(%)
BHA8/1	2.70	2.34 - 2.38	6.6 - 6.9	0.21 - 0.23	77 - 88
BDR-1_OC14	-	2.31	6.9 – 7.1	0.25	79
	w_L(%)	w_P(%)	Swelling strain (%)	Young's Modulus (GPa)	
BHA8/1	38 ± 5	23 ± 2	1 - 8	1 - 7	

Mercury porosimetry of sample BHA-8/1 indicated a dominant pore mode of 23 nm. The initial (total) suction of the sample was 15 MPa.

Water retention behavior and water permeability

The water-retention behaviour of sample BHA-8/1 was determined using a conventional desiccator method (weight measurements of samples, which are exposed to well defined suction). Measurements were performed on the wetting and drying path. Figure 2-8 compares the suction measurements with the back-calculated suction curves from MIP.

An instrumented high-pressure triaxial cell was used for water and gas permeability testing, which was specifically designed to apply isotropic/anisotropic stress states up to a maximum of 40 MPa, while injecting air at controlled volume rate (Romero et al. 2012). Figure 2-9 shows a schematic of the triaxial cell jointly with the test set-up. The axial deformation of low-height specimens –confined by several neoprene membranes and aluminium foils– is registered with an external LVDT. Each cap of the triaxial cell has inlet and outlet lines, prepared for gas and liquid connections. The equipment uses four automatic pressure / volume controllers (P/V in the figure), two for gas (injection and extraction at downstream point), and two for water, which can be used in combination (for example, air injection and water pressure at downstream, which is the setup used in the present investigation). The gas injection pressure / volume controller has a maximum range of 20 MPa (maximum volume 500 mL), and is able to

control volume rates between 10^{-4} mL/min and 100 mL/min (volume resolution < 5 mm^3). The 2 MPa P/V controllers for air and water at downstream present a volumetric resolution of 1 mm^3 (pressure resolution 1 kPa).

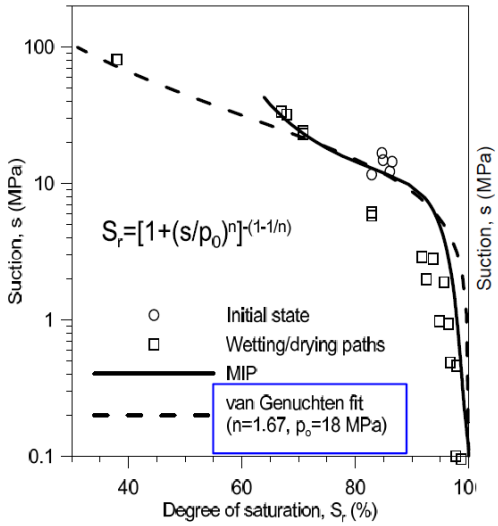

Figure 2.8: Water retention behaviour of the core BHA-8/1: the water retention curves determined with the desiccator method and comparison with back-calculated MIP curves. The data were fitted with a van Genuchten model.

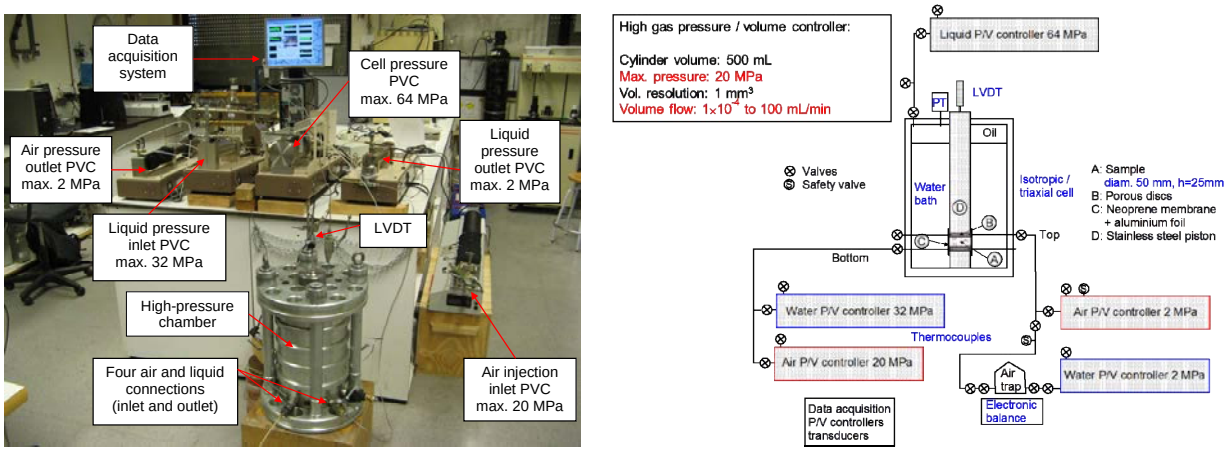

Figure 2.9: Triaxial cell for water/gas permeability measurements: photograph and schematical sketch.

Figure 2-10a presents the relationship between water permeability and confining stress for the direction normal and parallel to bedding, displaying clear anisotropic features. Figure 2-10b exhibits an exponential relationship between water permeability and void ratio. Clear evidence is shown for the important dependency of water permeability on void ratio. Furthermore, for constant void ratio, the anisotropy ratio $K_{II}/K_{\perp}$ (ratio of intrinsic permeability parallel to bedding to intrinsic permeability orthogonal to bedding) is in the range 3 to 5. The experiments fit well with previous laboratory investigations by Munoz (2007) on core samples from the shaly facies of the Opalinus Clay in the HE site of the Mont Terri URL.

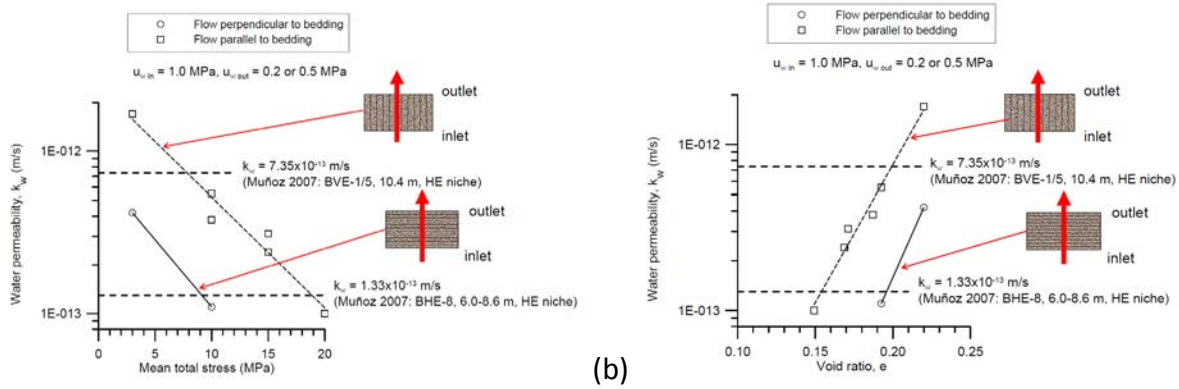

(a) (b)

Figure 2.10: Empirical relationship between (a) total stress and water permeability and (b) void ratio and water permeability for samples parallel and normal to bedding (from Romero et al., 2012).

Gas permeability tests

Gas permeability testing was initiated after completion of the water permeability tests. This procedure ensured that the samples were fully saturated and in hydro-mechanical and hydro-chemical equilibrium at the onset of the gas injection phase. Details of the experimental procedure are given in Romero et al. (2012).

Figure 2.11 shows the time evolution of air injection pressure during a fast controlled volume-rate tests (100 mL/min) at 15 MPa isotropic confining stress under different orientations (flow parallel and orthogonal to bedding). Gas injection was stopped when the injection pressure had reached a level between 12 and 13 MPa (depending on the test). A shut-in and recovery period followed at constant volume. For the flow parallel to bedding (thick lines), the outflow response was immediately observed after shut-in corresponding to a sudden drop in the injection pressure, followed by a subsequent gradual decline. For the flow orthogonal to bedding, the injection pressure remained initially flat and the outflow response was significantly delayed indicating also anisotropy during air permeability tests. After the apparent air breakthrough process corresponding to an increase in the outflow pressure, the injection pressure showed a steep decline.

Another important observation is the axial displacement of the test samples in response to the increase in gas pressure (Fig. 2.11), suggesting a marked dependency of volumetric strain on the constitutive stress changes during air injection/dissipation tests. Figure 2.12 presents a graph of the axial strain versus the axial effective stress (effective stress = confining stress – injection pressure) for the different stages of the experiment. During injection (stage AB) the injection pressure rises and effective stress decreases, resulting in an expansion of the sample. The corresponding mechanism is most probably the swelling due to effective stress reduction. In the early shut-in period (stage B to peak strain) the strain increases slightly in response to the gas pressure change, which could be interpreted as a dilation mechanism. Alternatively, it can be explained as a swelling response on the increase of the pore pressure at the outlet. Eventually, in the late shut-in phase (stage BC), a linear negative trend is observed in the effective stress – strain relationship, which is broadly consistent with the slope of the swelling/reconsolidation line of the rock (see Figure 2.11). Notably, the mechanical response is observed for both flow directions (parallel and orthogonal) in a similar magnitude. In the early stage of the test orthogonal to bedding, the axial strains were not monitored due to a technical problem.

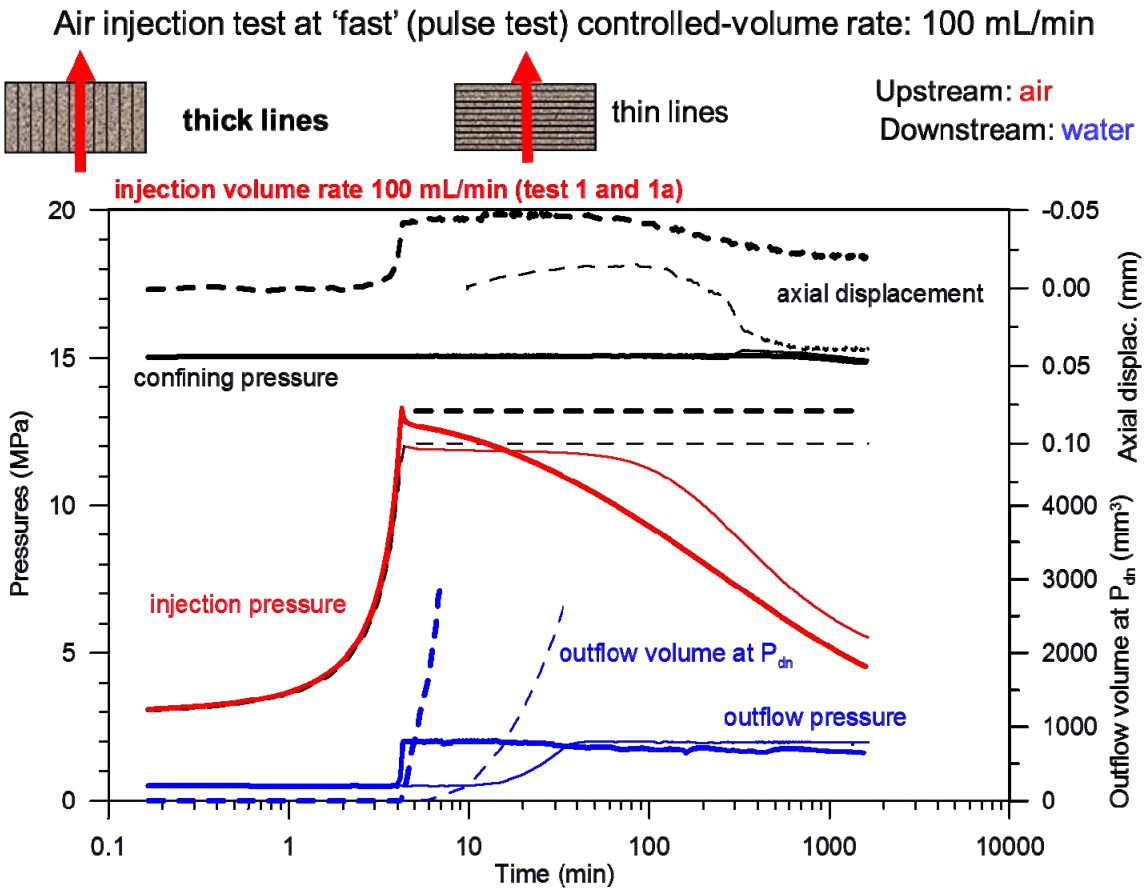

Figure 2.11: Measured pressure transients at the injection and outflow sides together with outflow volume and axial displacements. The tests were conducted parallel (thick lines) and perpendicular to bedding (thin lines). Graphs from Romero et al. (2012).

The examination of the measured axial deformation revealed different deformation regimes. For the test parallel to bedding (Fig. 2.11), the initial pressure increase shows axial deformation to negative values indicating expansion. During the early period after shut-in, the pressure slightly decreased but the axial strain continued to expand. Afterwards, as the pressure continued to decrease, the axial deformation reversed indicating compression as the effective stress increased.

For the gas test with flow normal to bedding (Fig. 2.11), the axial deformation indicates a similar pattern, whereby no measurements were available during the early injection period. During the early period after shut-in very little change in pressure occurred, whereas the axial deformation went negative indicating expansion. At late time, the axial deformation reversed as the pressure decline steepened indicating compression. The axial deformation, reflecting the changes in void ratio, indicate that during the injection period expansion and a corresponding increase in void ratio occurred associated with gas migration into the pore space of the core sample and effective stress decrease due to pore pressure increase. This expansion continued beyond the shut-in as the gas pressure front propagated into the sample causing the fluid pressure to further increase and the effective stress to decrease. At late time after the pressure in the outflow chamber started to increase, the injection pressure declined and the effective stress increased, indicating compression.

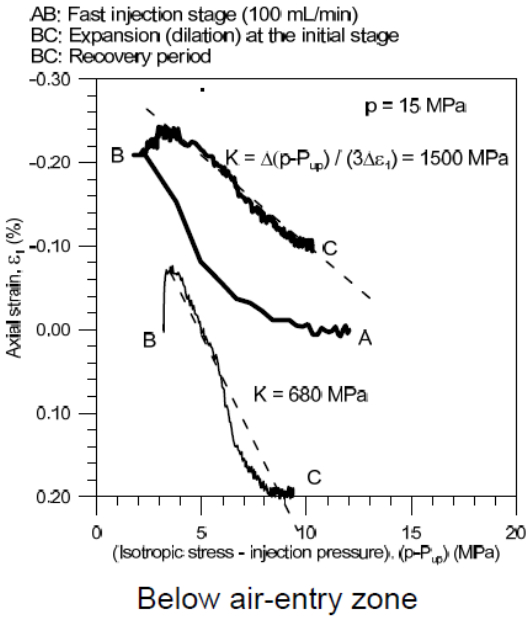

Figure 2.12: Graph of the axial strain versus the axial effective stress for the different stages of the experiment (Romero et al.; project report in preparation): AB – gas injection phase; BC-shut in phase (p – confining/isostatic stress; Pup – gas injection pressure).

In summary, the water and air permeability experiments revealed some important hydromechanical characteristics of the claystone samples. Specifically, the intrinsic permeability (as measured in water flow tests) exhibits an anisotropy ratio $K_{\parallel}/K_{\perp}$ (ratio of intrinsic permeability parallel to bedding to intrinsic permeability orthogonal to bedding) in the range 3 to 5 at constant void ratio. Furthermore, clear evidence is shown for the important dependency of water permeability with void ratio and thus constitutive stress (coupling between pore compressibility and effective stress). The samples display quasi-reversible features with expansion at the early fast air injection stage in response to mean effective stress decrease, and progressive compression towards approximately the initial volume on air pressure dissipation (mean effective stress increase). Further studies are currently being undertaken to analyse these features and their implications on changes in the air transport properties.

2.2.4 Geotechnical characterisation by CIEMAT

CIEMAT accomplished as part of FORGE WP5.1 “Gas transport laboratory experiments” a comprehensive laboratory programme on Opalinus Clay samples (Forge Deliverable D5.11; Villar & Romero 2012). Focus was on the determination of two-phase flow parameters, gas permeability and gas breakthrough pressure determinations. For the determination of the gas permeability and gas breakthrough pressure a setup was designed and fine-tuned. It allowed the application of gas injection pressures of up to 18 MPa to cylindrical samples while keeping higher confining pressures and measuring the gas outflow.

Geotechnical characterization and water retention behaviour

The core sample BHG-D1/15 was shipped in March 2010 to CIEMAT. A basic geotechnical identification of the cores was performed; the results thereof are reported in Table 2-2.

Table 2.4: Results of the geotechnical characterization of the core BHA-8/15

Borehole	Water content (-)	Dry density (Mg/m^3)	Grain density (Mg/m^3)	Initial total suction (MPa)	Dominant pore mode / MIP (nm)
BHG-D1/15	6.4%	2.33	2.71	31.3±0.1	11 nm

The total suction of a core was measured at laboratory temperature (21°C) with two capacitive sensors inserted in a suitable perforated hole. The equilibrium suction value was found to be 31.3±0.1 MPa for a dry density of 2.33 g/cm^3 and water content of 6.4% (determined in samples drilled from the core). The measured grain density for this sample was 2.71 g/cm^3.

A sample from the BHG-D1 core of dry density 2.4 g/cm3 and water content 3.4% (slightly air-dried) was lyophilised and analysed by mercury intrusion porosimetry (MIP). The mercury intrusion method allows access only to the macroporosity (pores smaller than 600 µm) and to part of the mesopores (pores of diameter larger than 0.006 µm). An estimation of the percentage of pores actually intruded can be made by comparing the actual void ratio of the samples (computed from their dry density and density of solid particles) and the apparent void ratio calculated from mercury intrusion. Thus, the pore size distribution curves obtained by MIP were corrected to take into account the percentage of pores not intruded and are shown in Figure 2-13 for two subsamples. Most of the pore sizes were comprised in the range 2-50 nm, i.*e*. in the mesopore range, with a dominant pore mode of 11 nm. The air entry value corresponding to this dominant pore mode calculated from the Laplace's equation is 27.8 MPa.

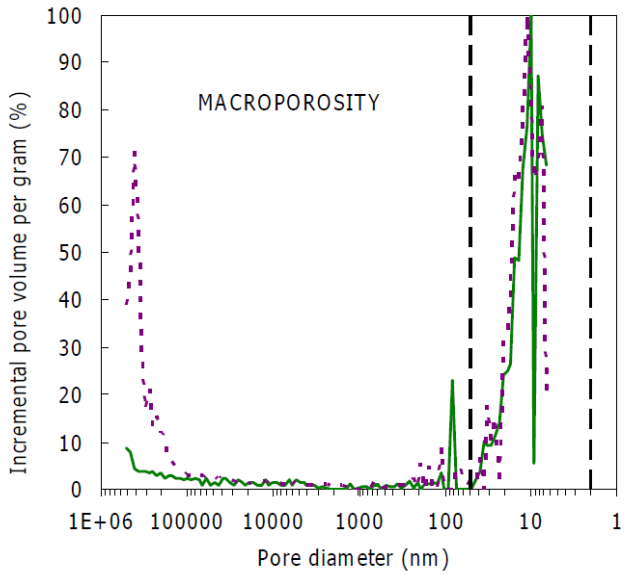

Figure 2.13: Mercury instrusion porosimetry: Pore size distribution of two samples from core BHG-D1/15.

In order to analyse the effect of stress on the water retention capacity and the air entry value, the retention curve of the Opalinus Clay was determined in similar samples without and with external stress (0 MPa and 8 MPA, respectively), both in desiccators applying total suction and in membrane cells applying matric suction. A detailed description of the test protocols is given in Villar et al. (2012) / FORGE D-5.11.

Figure 2.14 shows a comparison of the curves fitted for tests performed under free volume conditions and under vertical stress of 8 MPa. In the range of suctions tested, and when matric suction was applied, the degrees of saturation obtained for a given suction were higher for samples tested under confinement, but this trend was not so clear when total suction was

applied. In the latter case and in wetting paths, the curves obtained under free or confined volume conditions were practically identical.

Drying paths recorded higher degrees of saturation than wetting paths when total suction was applied, which is the expected behaviour, but this was not the case when matric suction was applied. This is due to the difficulty in fitting right curves to results showing a large dispersion.

A comparison of the results with previous studies (Villar et al. 2009) is shown in Figure 2-15, confirming a well-established and consistent data base for the water retention behavior of the Opalinus Clay at Mont Terri.

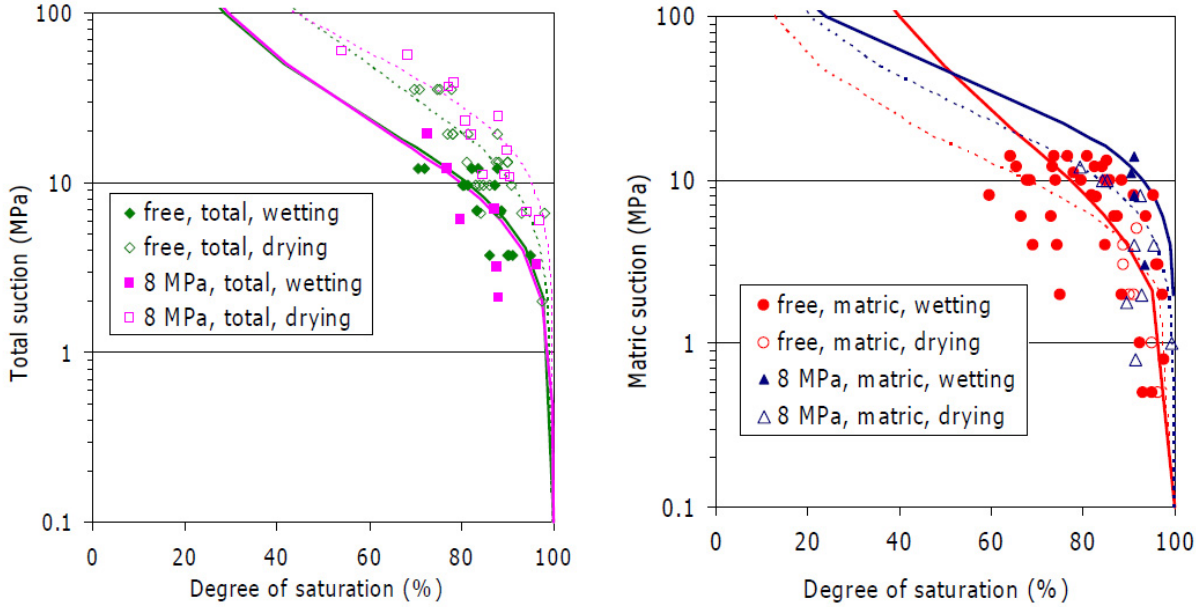

Figure 2.14: Water retention behaviour of Opalinus Clay: Fittings to the van Genuchten expression as a function of the confinement conditions for total and matric suction (the dotted lines correspond to drying paths)

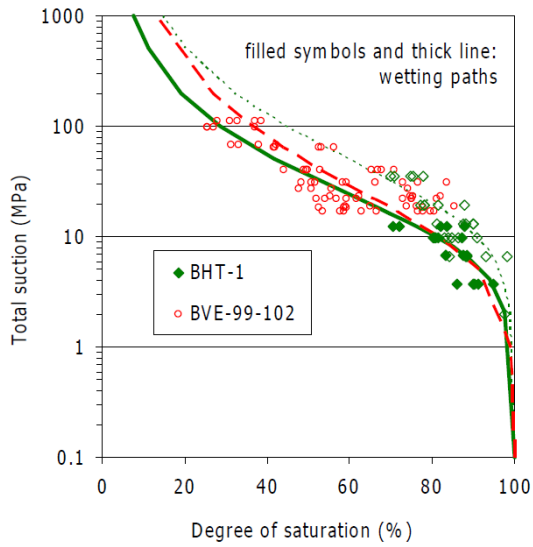

Figure 2.15: Water retention behaviour of Opalinus Clay: Compilation of results from previous studies in other boreholes at the Mont Terri URL (BVE-99-102: Villar et al. 2009)

Water and gas permeability testing

An experimental set-up was designed and tested for the determination of the gas permeability and gas breakthrough pressure. It was specified to cope with gas injection pressures of up to 18 MPa, applied to cylindrical samples while keeping higher confining pressures and measuring the gas outflow.

The hydraulic conductivity (k_w) measured in one of the samples in the direction perpendicular to bedding was $2.2 \cdot 10^{-11}$ m/s, corresponding to an intrinsic permeability (k_{iw}) of $2.3 \cdot 10^{-18}$ m^2. Laloui et al. (2012) and Romero et al. (2012) found for similar void ratios (0.20-0.24) water permeabilities measured in the laboratory an order of magnitude lower (see chapters 2.2.2 and 2.2.3).

The set-up for gas permeability measurements was yet in an early design phase and the results of testing may be considered as preliminary. In this context, the main challenge was associated with the low gas flow rates, which were significantly below the detection limit of the applied flow controllers.

As an example, the gas test on sample 3 / BHG-D1/15 is discussed in the following section. The sample was mounted in a triaxial cell. The pressure path followed during the test and the flow measured are shown in Figure 2-15. Initially the cell was pressurised to 8 MPa and a gas injection pressure of 0.5 MPa was applied to the top of the sample and increased (approximately) every 24 h. When the injection pressure reached 7 MPa, the confining pressure was increased to 15 MPa. The injection pressure was subsequently increased up to 14 MPa, resulting in a progressive increase in flow that would be linked to the reduction in effective stress. Afterwards, the confining pressure was stepwise increased to 19 MPa and the injection pressure to 18 MPa. This last pressure situation was kept for 27 days.

The flows measured during the test (time-integrated value of intermittent flow) were always very low, in most of the cases below the turndown value (accurate detection limit) of the flowmeters, which is the reason why they can only be used as a qualitative indicator of the actual gas flow. Nevertheless, the flow slightly reflected the changes in the stress conditions, tending to decrease with the increase in confining pressure and to increase with the reduction in effective pressure caused by the injection pressure rise. In spite of some spikes in the gas flow measurements, an significant decrease in effective stress (to values of around 1 MPa) was needed to observe a “steady” gas flow.

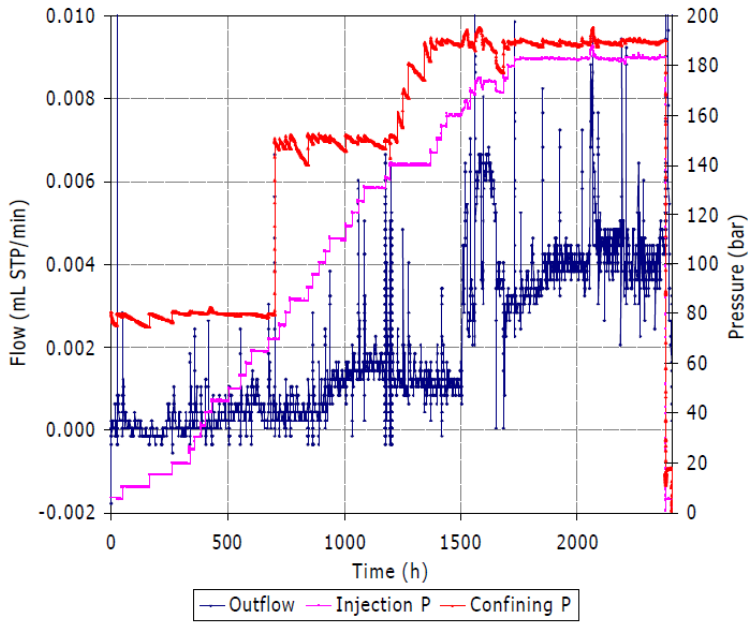

Figure 2.15: Evolution of injection and confining pressure and outflow in test OPA3

2.2.5 Long-term desaturation of a large diameter core sample

Unlike the in-situ tests performed at Mont Terri URL, small and medium scale columns are set up to investigate specific features and processes under well controlled boundary conditions. The experiment described in this section was initially aimed at calibrating dual-rod TDR probes, which had been emplaced in the tunnel near-field of the Mont Terri VE experiment. As a by-product of the calibration procedure, the acquired long-term monitoring data can be used for quantifying the desaturation and resaturation behaviour of the Opalinus Clay. For this, a large diameter Opalinus Clay core sample from the Mont Terri URL was recovered and subjected to long-term ventilation in a hermetically sealed laboratory set-up, a so-called drying chamber. The experiment was started in 2007 and is still ongoing at Nagra's Grimsel Test Site. The GTS is ideally suited for long-term monitoring experiments, because of naturally occurring constant temperature conditions that are necessary to prevent unwanted perturbations of the actual experiments. Moreover, the large amount of data produced can be easily accessed remotely.

The investigated core sample originated from the short borehole BHG-A28 (borehole length 1.12 m), which was oriented perpendicular to bedding in the shaly facies nearby the EZ-B niche. The core sample eventually used for the long-term desaturation experiment was retrieved from the lower borehole section between 0.6 m and 1.1 m along hole (ah). A special overcoring technique was used to minimise core damage during sample recovery; for this, the core was stabilised by resin filled pre-drillings before it was broken off and recovered from the borehole (see also Figure 2.17b). Eventually, the core was coated with resin to prevent any mechanical damage or desaturation during shipment. Details of core recovery and core preservation are documented in Meier et al. (2006).

Experimental set-up

The experimental set-up consists of a drying chamber, which is operated at very stable humidity and temperature conditions, a balance for continuous measurements of the weight of the core sample, a time domain reflectometer for monitoring the distribution of water content in the sample and a data logger, which can be operated remotely. Figure 2.16 shows a picture and a schematic sketch of the device.

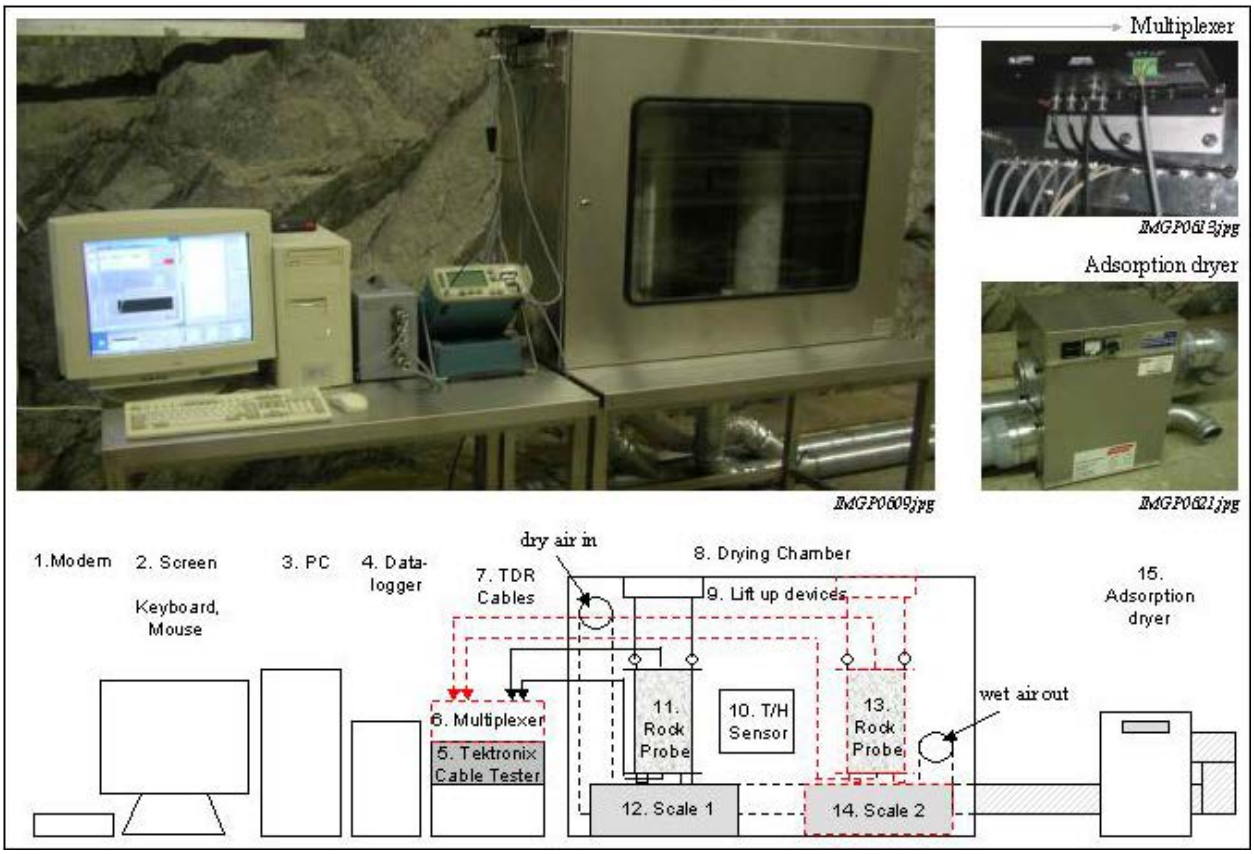

Figure 2.16: Desaturation and resaturation experiments in a hermetically sealed drying cabinet at the Grimsel Test Site.

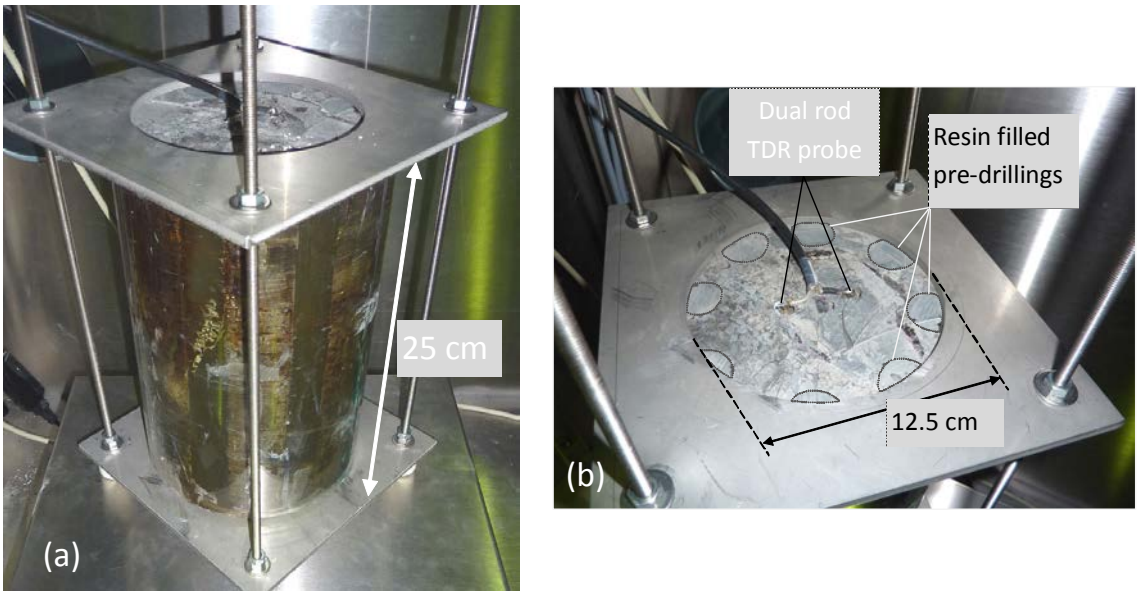

Figure 2.17: Large diameter Opalinus Clay subjected to a long-term desaturation experiment in a hermetically sealed drying cabinet at the Grimsel Test Site: (a) photo of the sample and (b) upper side of the sample with TDR probe. The resin filled pre-drillings were aimed at stabilizing the core during core recovery.

The drill core from Mont Terri URL (Fig. 2.17) was cut to a length of 250 mm without removing the resin coating of the core annulus. Upper and lower end of the sample were flattened to

ensure a well-defined surface for humidity exchange of the core sample with the atmosphere of the dryer cabinet. Eventually, a 2-rod TDR probe was emplaced along the axis of the cylindrical sample to allow for measurements of saturation profiles in the sample. In June 2012, the instrumentation was complemented by a strain-meter for measuring axial displacement of the sample in response to desaturation / resaturation events.

Experimental procedure and results

The long-term dryer experiment was started on 13th April 2007 by setting the humidity in the cabinet to a value of 70%. In August 2007, the desaturation was enforced to 40% RH until February 2008. A short period at a humidity of 10% followed, before the 40% level was re-established for more than two years. In June 2012, complementary instrumentation was mounted (distometer for axial strain measurements) and the humidity was increased to 70%; this stage is still ongoing. During the entire monitoring phase the experimental data, comprising weight, temperature and humidity measurements have been monitored remotely by a data acquisition system. The balance was recalibrated periodically. Table 2.5 presents an overview of the test activities since 2007.

Table 2.5: Activity logbook of the long-term core desaturation experiment

Date	**Work**
01.02.2007-09.02.2007	Shipment of Opalinus Clay sample and instrumentation of TDR
07.03.2007	Emplacement of core sample in dryer chamber at FLG; initial weight of the core: 12602 g ; several pretests
13.04.2007	Rh set back to 70% in the dryer chamber
20.08.2007	Rh in the drying chamber set to 40% at 12:30
06.12.2007	Re-calibration of balance; weight of the core: 12501.4g (before) / 12500.9 g (after recalibration)
05.09.2007	Rh set to 40% in the dryer chamber
03.02.2009-04.02.2009	Removal of dryer cabinet to the VE cavern / GTS; Re-Installation of sensors and data acquisition; recalibration of balance (b:12372g / a:12374.7g); re-setting of humidity to 10%.
13.03.2009	Re-setting of humidity to 40%.
20.06.2012	Installation of distometer for axial strain measurements
11.07.2012	Re-setting of humidity to 40%.

The measured weight of the core at the beginning of the experiment was 12602 g. It can be assumed due to the air-tight preservation during shipment that the core was close to full saturation when it was emplaced in the dryer cabinet. In the cabinet the sample was placed on a balance, such that desaturation of the sample took place via the upper and the lower face, whereas the resin coated circumferential surface remained tight. The temperature in the cabinet remained remarkably constant during the entire monitoring phase with slight seasonal variations between 14 and 16°C. A clear change of the sample weight in response to humidity changes could be observed. The total loss of weight during the drying phase of more than 5

years was around 250g, corresponding to a weight loss of less than 2%. The long-term monitoring data are displayed in Figure 2-18.

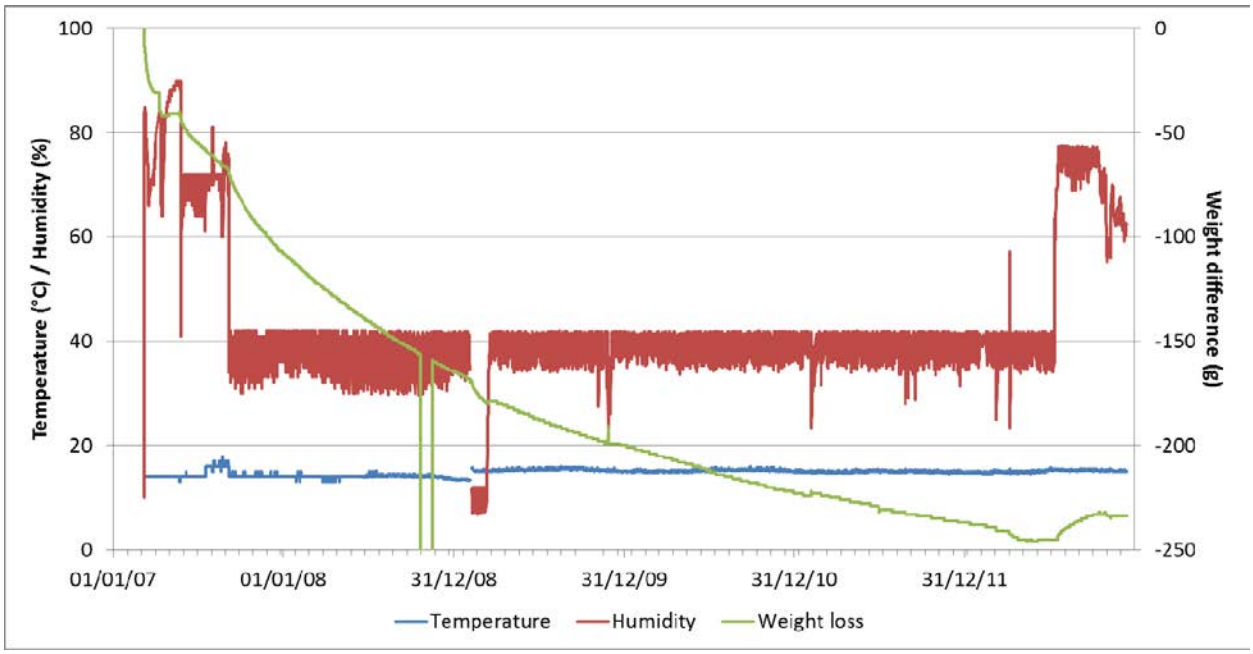

Figure 2.18: Desaturation and resaturation experiments in a hermetically sealed drying cabinet at the Grimsel Test Site

2.3 COMPLEMENTARY INFORMATION FROM THE MONT TERRI URL

The modelling teams of WP4 and WP5 have been provided with both, reference geotechnical rock properties and laboratory test data to help them develop suitable constitutive models for the Opalinus Clay at Mont Terri. This section lists the reference parameter for the clay rock properties and the environmental conditions and provides a brief description of some complementary laboratory testing. Full descriptions of the laboratory testing were provided in reports distributed to the modellers.

2.3.1 Reference mechanical properties

Reference values have been derived for selected mechanical properties of the intact Opalinus Clay at Mont Terri in previous projects for various purposes – these reference parameters are indicative for the geomechanical behaviour of the Opalinus Clay at Mont Terri, but may not be applicable to all modelling applications considered within the FORGE project. Hence, it is the responsibility of the modelling teams to decide upon the appropriateness of the reference data sets in the context of their modelling tasks. The reference values are summarised in Table 2.6.

2.3.2 Reference hydraulic properties

Marschall et al. (2004) describe a conceptual model of groundwater flow in the Opalinus Clay at Mont Terri and note that at the core scale "layering can be interpreted as an indication for pronounced anisotropy of the hydraulic conductivity at the centimetre and decimetre scale." They provide information on permeameter tests on core from Mont Terri and packer tests performed at Mont Terri. Packer test derived hydraulic conductivities ranged from 2×10^{-14} to 2×10^{-12}m/s. Results from tests in different facies showed some variation, which was thought to be largely due to variations in testing and which could not be used to identify systematic variations in conductivity between the different facies. Summary hydraulic conductivity values

are given in Table 2.7. A limited number of permeameter tests were performed and the database is insufficient to estimate the hydraulic anisotropy.

Table 2.6: Geotechnical reference parameters of the Opalinus Clay at the Mont Terri underground laboratory after (Bock 2000).

Parameter	Value	Remarks
Bulk density [Mg/m^3]	2.45	
Grain density [Mg/m^3]	2.71	
Porosity [%]	13.7	Range: 10 - 16 %
Water content [% wt]	6.1	Range: 6 - 7 %
Young's modulus [GPa]	10 4	parallel to bedding normal to bedding
Shear modulus	1.2	
Poisson's ratio [-]	0.27	
Uniaxial compressive strength [MPa]	10 16	parallel to bedding normal to bedding
Tensile strength [MPa]	2 1	parallel to bedding normal to bedding
P-wave velocity [m/s]	3410 2620	parallel to bedding normal to bedding
S-wave velocity [m/s]	1960 1510	parallel to bedding normal to bedding
Fracture toughness [MN/m$^{1.5}$]	0.53 0.12	K_{IC} parallel to bedding K_{IC} normal to bedding

Table 2.7: Range of hydraulic properties for different facies of the Opalinus Clay at Mont Terri (from Marschall et al. 2004).

Scale	Facies	Hydraulic conductivity (m/s)	Specific storage (1/m)
0.1m-10m	Carbonate rich sandy facies	4×10^{-13}-9×10^{-13}	2×10^{-7}-6×10^{-7}
	Sandy facies	2×10^{-14}-2×10^{-13}	-
	Shaly facies	2×10^{-14}-2×10^{-12}	3×10^{-7}-3×10^{-5}

Nagra (2002) presents results from permeability and diffusion tests on Opalinus Clay core from the Benken boreholes (Zürcher Weinland). Nagra (2002) suggested "anisotropy factor" $K_{II}/K_{\perp}$ ranging between 1 and 10. The anisotropy in the diffusion constant was found to be about a factor of 5. Microscopic observation of the fabric of the Opalinus Clay at Mont Terri suggests that there may be a significant core-scale hydraulic anisotropy. However the database of

permeameter tests on core from Mont Terri is insufficient to provide robust estimates of hydraulic anisotropy of the Opalinus Clay. The value of the anisotropy factor $K_{II}/K_{\perp}$ is thought to lie between 1 and 10, with a suggested value of 5.

2.3.3 Stress state

Martin & Lanyon (2003) and Bossart & Wermeille (2003) report results from several stress measurement campaigns at the Mont Terri Rock Laboratory including the results of a previous data compilation. Martin & Lanyon (2003) suggest that the stress tensor given in Table 2.8 is representative of the stress state at the laboratory although the greatest uncertainty is in the estimate of σ_3. In particular the low range value of 0.6 (derived from analysis of an undercore experiment) is below the best estimate of pore pressure at the laboratory (Marschall et al. 2004).

More recent studies by Corkum & Martin (2007) led to a revised estimate of σ_3 magnitude as shown in Table 2.8 (lower table). Note that there are minor orientation differences (note: Table 1 and Figure 6 of Corkum & Martin [2007] are in error. The values given in Table 2.8 are correct). The recommended full tensor for the Mont Terri rock laboratory is that from Corkum & Martin (2007).

Table 2.8: Stress tensor for Mont Terri Rock Laboratory (from Martin&Lanyon 2003, Bossart&Wermeille 2003 and Corkum&Martin 2007).

	Martin & Lanyon (2003), Martin et al (2002)				
	Orientation	Trend (°)	Plunge (°)	Magnitude Estimate	Range (MPa)
σ_1	Vertical	210	70	6.5	6-7
σ_2	NW-SE	320	10	4.0	4-5
σ_3	NE-SW	50	15	0.6	0.6-2

	Bossart&Wermeille (2003)			
	Trend (°)	Plunge (°)	Magnitude Estimate	Range (MPa)
σ_1	210	70	6.5	6-7
σ_2	320	10	4.4	4-5
σ_3	50	20	2.2	2-3

	Corkum & Martin (2007)				
	Orientation	Trend (°)	Plunge (°)	Magnitude Estimate	Range (MPa)
σ_1	Vertical	210	70	6.5	6-7
σ_2	NW-SE	320	7	4.0	4-5
σ_3	NE-SW	52	18	2.2	2-3

More recent studies have involved stress measurements in the surrounding lithologies at Mont Terri to avoid problems of measurement in the anisotropic moisture-sensitive Opalinus Clay (see Martin et al. 2002 for a discussion of the difficulties of measurements in the Opalinus Clay). Results from these studies are not currently available.

2.3.4 Gas related laboratory tests

A total of 6 gas injection and breakthrough tests using either helium or argon gas on small cylindrical samples (Ø 2.4 cm, height ≈ 2 cm) of Opalinus Clay from the Mont Terri underground laboratory have been performed by Krooss & Alles (2007). An isostatic cell was used to confine the sample axially and radially with a confining pressure of 6 MPa, which corresponds to the natural stress conditions in the field (Mont Terri, max. principal stress). The experimental procedure starts with a water permeability test performed on each sample followed by the gas injection test. After creating a gas filled volume at each end of the sample, gas is injected into the upstream compartment (tubing and porous disc) and closed hermetically. The pressure evolution in the two (upstream and downstream) compartments is continuously monitored over time: a steady decrease is observed in the upstream compartment, a steady increase at the downstream compartment. The differences between upstream and downstream gas pressure were kept low (probably below gas entry pressure).

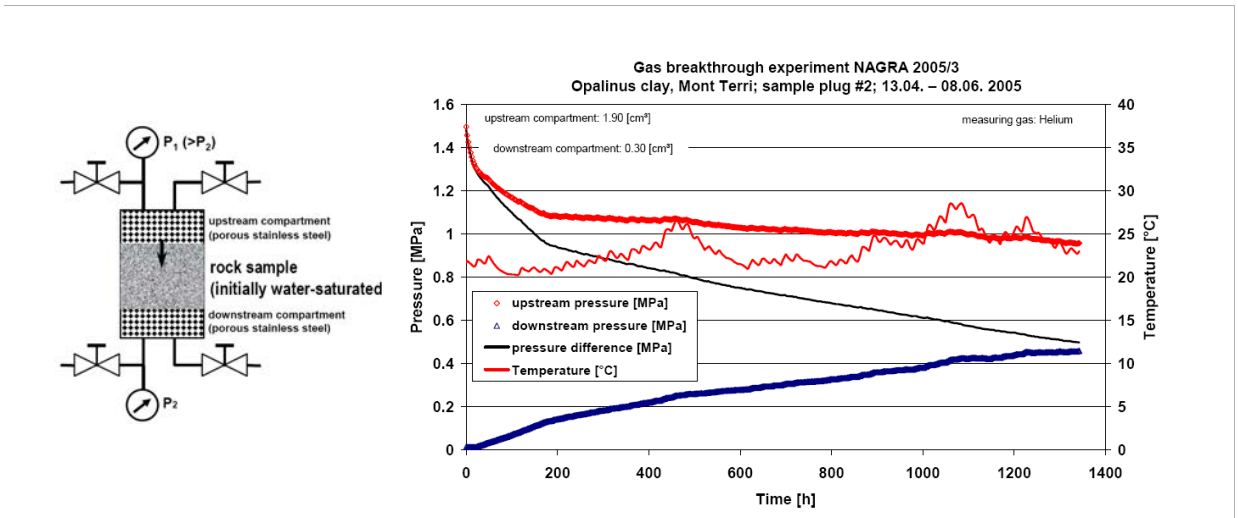

Figure 2.19: Gas transport experiments on core samples by Krooss&Alles (2007): Sample configuration and experimental results

A comprehensive description of the experimental configuration and of the test procedures is given in Krooss & Alles (2007). The test interpretation is documented in Croisé&Mayer (2006) and Brommundt & Croisé (2010).

2.3.5 Summary of laboratory testing data provided to modellers

In addition to the aforementioned experiments, mainly focused on gas transport and water retention behaviour of Opalinus Clay, the Mont Terri project has generated a comprehensive number of technical notes and technical reports, related to mechanical and hydraulic properties of the Opalinus Clay. Among the multitude of documents a small selection of reports of potential relevance was distributed to the modellers of WP4 and WP5. The corresponding reports are listed in Table 2.9.

Table 2.9: Reports on laboratory testing of the Opalinus Clay.

Reference	Testing	Data	Core source
Birchall DJ , Harrington JF, , Noy DJ, Cuss RJ. 2007. Laboratory study examining permeability evolution along an isotropic unloading stress path. BGS Open report OPEN REPORT OR/07/016.	Permeability during unloading under isotropic stress field.	Yes	Mont Terri BHA-5
Horseman ST, Harrington JF, Birchall DJ, Noy DJ, Cuss RJ. 2003. Hydrogeologic analyses and synthesis (HA experiment): Consolidation and rebound properties of Opalinus Clay: a long-term, fully drained test. Mont Terri Project, Technical note 2003-03	Drained consolidation, creep and rebound behaviour.	Yes	
Horseman, S.T., Harrington, J.F. (2002). Laboratory Experiments On Gas Migration In Opalinus Clay Samples From The Benken Borehole, Switzerland. Nagra Internal Report NIB 02-31	Flow of gas and water (pre/post gas test).	Yes	Benken
Laloui L, Ferrari A. 2008. Analysis of Opalinus Clay self sealing: experimental investigation (swelling tests). HA-project, Technical Note 2008-45.	Swelling tests	Yes	Mont Terri Sandy: BWS-H2 Shale: BRC1
Krooss, B., M., Alles, S. 2007. Investigation of Gas Transport Processes in the Opalinus Clay. Mont Terri Technical Note TN 2007-53	Permeability to gas and water (pre/post breakthrough). Porosimetry Deformation Tests	Yes	Mont Terri BH 4/1
Peron, H., Salager, S., Eichenberger, J, Rizzi, M., Laloui, L. 2008. HG-A Experiment: EXPERIMENTAL AND NUMERICAL ANALYSIS OF EXCAVATION DAMAGED ZONE (EDZ) ALONG TUNNELS. Mont Terri Technical Note TN 2008-54	Oedometer test WRC (drying)	No	Shale and sandy facies specimens
Laloui, L, Francois B. 2008. Benchmark on Constitutive Modelling of the Mechanical Behaviour of Opalinus Clay Focus on the Material Anisotropy. EPFL Report	Compilation of uniaxial, triaxial, oedometric and direct shear tests	No	Shale and sandy facies specimens

3 HG-A experimental results and interpretation

3.1 DESCRIPTION OF THE HG-A EXPERIMENT

The experiment ("Gas path through host rock and along seal sections / HG-A") was designed as a long-term gas experiment in a backfilled microtunnel, to investigate both leak-off rates and gas release paths from a sealed tunnel section in an ultra-low permeability host rock (Opalinus Clay). The aims of the HG-A experiment are to:

- Provide evidence for barrier function of the Opalinus Clay on the tunnel scale (scale effects in rock permeability);
- Investigate self-sealing of the EDZ after tunnel closure (mechanical self-sealing in response to packer inflation and pore pressure changes);
- Provide evidence for gas transport capacity of Opalinus Clay (intact host rock and EDZ).

The HG-A experiment is located in the southern part of the Mont Terri Rock Laboratory off Gallery 04 (see Fig. 3.1). The 1m diameter, 13m long microtunnel was excavated during February 2005 using a steel auger from a niche in Gallery 04. The microtunnel was excavated parallel to bedding strike and bedding parallel features run along the tunnel replicating the expected relationship between bedding and emplacement tunnel orientation in a deep repository (Nagra, 2002) where bedding is expected to be flat-lying and emplacement tunnels to be sub-horizontal. Excavation was monitored by a borehole array containing piezometers and deformation gauges (clino-chain and chain deflectometers). The borehole array was subsequently augmented with additional piezometer boreholes and borehole stressmeters (Fig. 3.1b).

The first 6m of the microtunnel was lined with a steel casing immediately after excavation to stabilize the opening. The gap behind the liner was then cement-grouted, but not sealed. The purpose-built hydraulic Megapacker (diameter 940mm and sealing section length 3000mm) was installed in 2006. The sealing section was located at 6-9m with a 1m grouted zone containing the non-sealing part of the packer and retaining wall from 9-10m. The final 3m of the microtunnel from 10-13 m forms the test section which was instrumented and backfilled prior to packer emplacement.

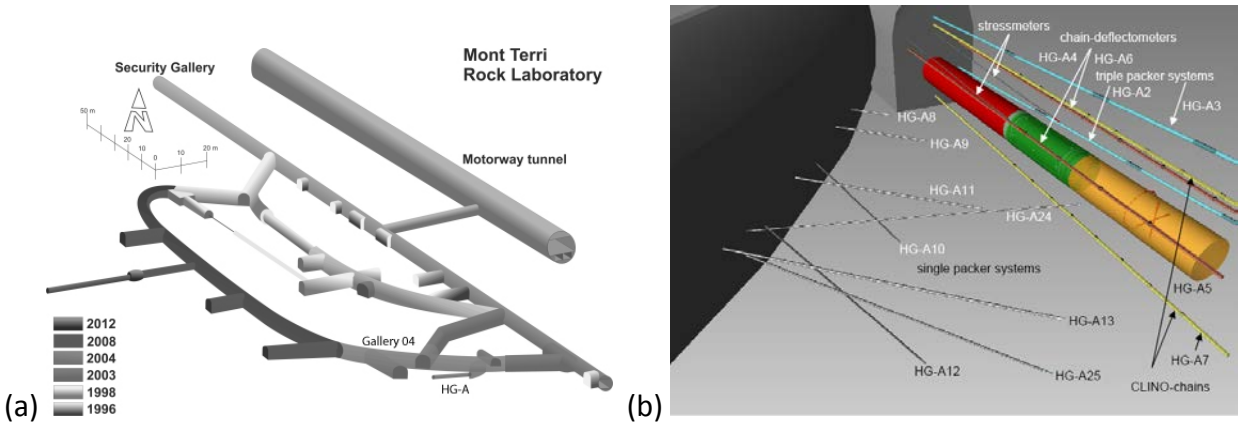

Figure 3.1: Location and layout of HG-A a) location at the Mont Terri Laboratory; b) Schematic drawing of the Microtunnel and the site instrumentation. Colour coding refers to the steel liner (red), the seal section (green) and the backfilled test section (orange).

The test section was instrumented with piezometers, extensometers, strain-gauges and Time Domain Reflectometers (TDRs) to measure pressure, deformation and water content. After instrumentation the test section was backfilled with sand behind a retaining wall.

The seal section was instrumented with piezometers, total pressure cells and TDRs prior to the installation of the megapacker. Following the installation of the megapacker the volume between the retaining wall and the megapacker was filled with a cement grout. Table 3.1 lists the instruments in the geosphere, test and sealing sections.

Table 3.1: HG-A experiment instrumentation

Section	Instrument	Count	Measurement
Test Section	Piezometers	2	Pore pressure
	Extensometers	2	Horizontal/vertical deformation
	Strain gauges	22	Circumferential deformation
	TDRs	8	Volumetric water content
	Geophones	8	Acoustic emission
Seal Section	Piezometers	12	Pore pressure
	Total pressure cells	6	Load on tunnel wall + temperature
	TDRs	2	Volumetric water content
Geosphere	Piezometers	14	Pore pressure
	Deflectometers	2	Deformation (8-point)
	Clino-chains	2	Deformation (8-point)
	Stressmeters	3	Deformation and stress + temperature

3.2 EXPERIMENTAL RESULTS

An overall chronology of the HG-A experiment from excavation to the current day (November 2012) is given in Table 3.2. Saturation of the test section and surrounding rock was started in November 2006 following emplacement of the megapacker (June 2006) and subsequent grouting of the section between the Megapacker and Test Section. A variety of saturation tests were performed using a synthetic pore water (Pearson et al., 2002) until January 2008 when a long-term multirate hydraulic test was initiated. This test continued until February 2010 and involved a series of constant rate injection steps. During the test the injection rate declined from ~10 ml/min to 0.1 ml/min (144 ml/day). Figure 3.2 displays an overview of the available long-term monitoring data in terms of microtunnel stress, pore pressure, water content and flowrate measurements from start of saturation. The geosphere pore pressure measurements from start of saturation are shown in Figure 3.3, comprising near-field piezometers in HG-A02 and HG-A03 and the piezometers in Gallery 04 (HG-A08 to HG-A13, HG-A24 &HG-A25).

The gas injection phase included three separate Nitrogen gas injections (GI1-3). After each gas injection, following a shut-in period, water was extracted from the test section and depressurized to remove trapped gas (gas-water exchange). The degassed water was then re-injected into the test section. This procedure provided a well-defined initial gas saturation in the test section pore water for the subsequent gas injection. During gas injection a low constant rate (~0.02 ml/min) water injection was maintained into the test section.

Table 3.2: HG-A experiment chronology

Start	End	Activity
17/02/2005	25/02/2005	Excavation of Micro-tunnel and installation of liner 0-6m
25/02/2005	29/06/2006	Tunnel open instrumentation and backfill of test section
29/06/2006	29/06/2006	Megapacker emplacement
29/06/2006	21/11/2006	Tunnel closed grouting between Megapacker & backfill
21/11/2006	23/01/2008	Saturation Tests
23/01/2008	15/02/2010	Long Term Multirate Hydraulic test
15/02/2010	21/04/2010	GI1 -initial flow 20 mln/min, switch to constant pressure 1200kPa
21/04/2010	01/06/2010	GI1 Recovery and gas/water exchange
01/06/2010	28/10/2010	GI2 - 10 mln/min constant rate
28/10/2010	29/03/2011	GI2 Recovery and gas/water exchange
29/03/2011	16/09/2011	GI3 - 20 mln/min constant rate
16/09/2011	30/09/2011	GI3 Recovery and gas/water exchange
30/09/2011	Ongoing	Post-Gas Hydraulic test: constant rate injection

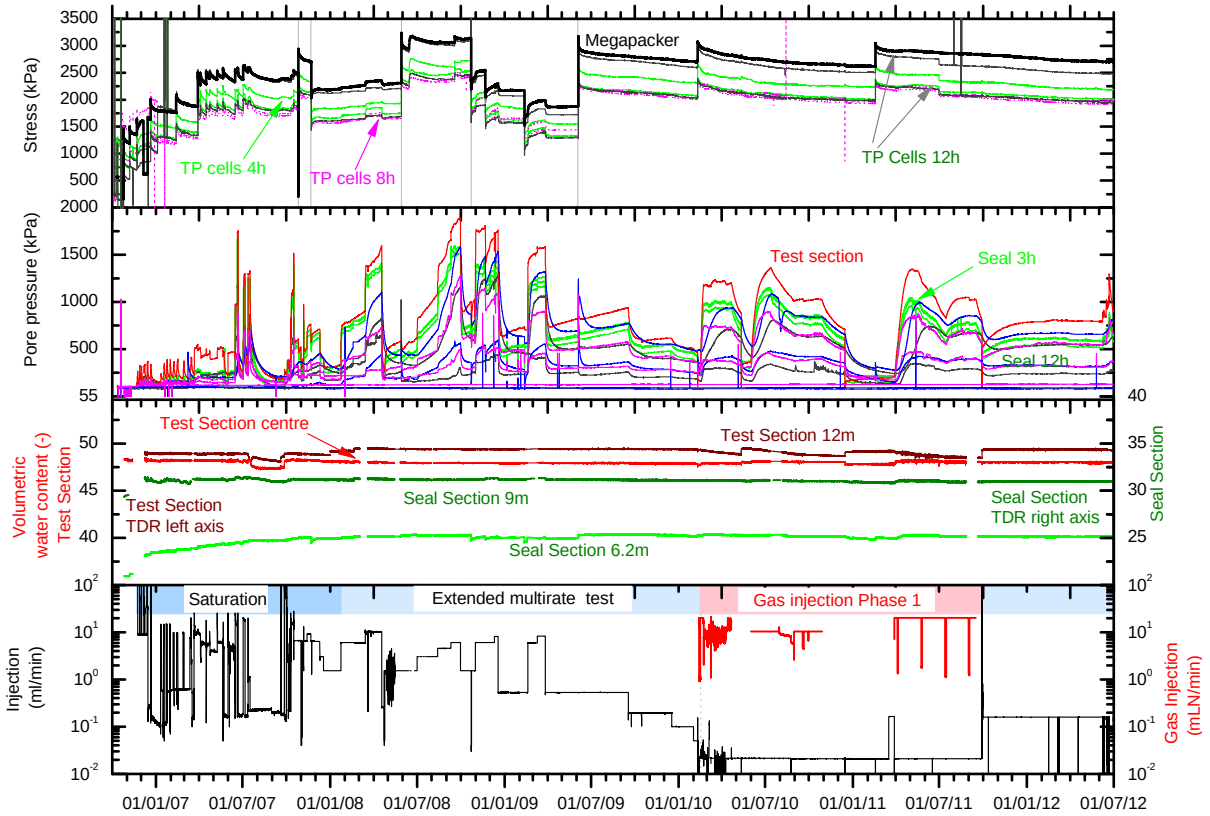

Figure 3.2: Microtunnel stress, pore pressure, water content and flowrate measurements from start of saturation.

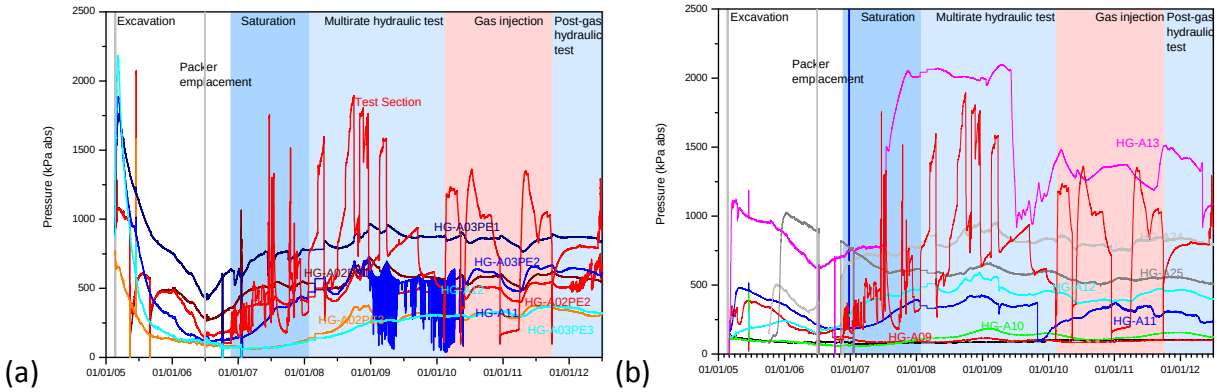

Figure 3.3: Geosphere pressure measurements from start of saturation: a) Near-field piezometers in HG-A02 and HG-A03; b) piezometers HG-A08 to HG-A13, HG-A24 &HG-A25.

Typically measured pressures are below 1000 kPa with the lowest pressures measured in those piezometers closest to Gallery 04 and to the lined section of the Microtunnel (HG-A08 to 10). Pressures in HG-A11 and 12 are relatively stable at about 500-600 kPa but show the influence of testing in the Microtunnel. The pressure measured in HG-A13 show an unusual response that is believed to be a real reflection of the local pressure but potentially affected by hydromechanical or other effects (e.g. borehole closure).

Fig. 3.4 shows a comparison between the test section pressures in GI1 GI2 and GI3. Inspection of the log-log plots (Fig. 3.4b) shows a roughly linear behaviour for the first 20 days prior to the subsequent breakdown in GI2 and GI3. In GI1 pressure is held constant and no breakdown was observed.

Gas pressure during GI1 was limited to 1200 kPa, significantly below the minimum stress, to avoid coupled mechanical effects. After an initial 20 mlN/min injection when pressure rose quickly, the injection rate was reduced to about 10 mlN/min to maintain roughly constant test section pressure.

During GI2 the test section pressure rose more slowly than in GI1 and then peaked at 1363kPa on 12/07/10. After the pressure breakdown, the test section pressure drops over about a month by about 350 kPa to 975 kPa and then stabilises at about 1040kPa.

During GI3, test section pressure again peaks at 1347 kPa but with a broader peak than in GI2 and then drops to about 840 kPa due to an interruption in injection before recovering (after resumption of gas injection) and stabilizing at about 1040 kPa.

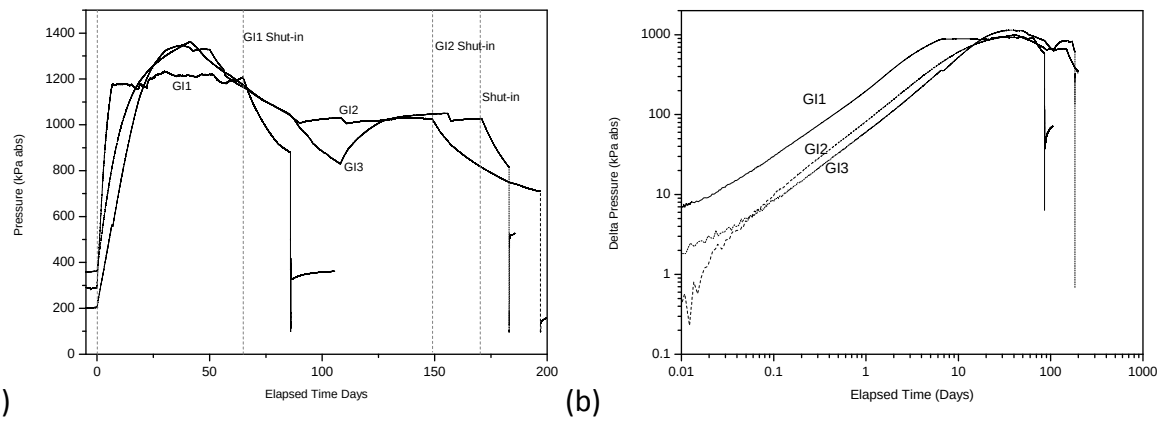

Figure 3.4: a) Linear and b) log-log plots of delta pressure from GI1-3.

Pressures in the sealing section during gas injection were lower and lagged those in the test section as would be expected (Figure 3.5). Pressure response is highly heterogeneous. Pressure along the 3 o'clock sensors reacts most strongly and quickly to the test section suggesting a high hydraulic diffusivity connection. However, the pressure at Section 1 in PES-S1-3h (sensor close to the rear of the sealing element) is high (in fact higher than PES-S2-3h a sensor in the centre of the seal section) and comparable to PES-S3-3h closest to the test section. This suggests that this piezometer is not well connected to the open tunnel. All other piezometers in Section 1 show no response to gas injection and remain at close to atmospheric pressure.

After shut-in and depressurisation remnant high pressures were observed at some piezometers in the sealing section indicating possible closure after gas injection or some other loss of connectivity, perhaps, due to water invasion and blocking.

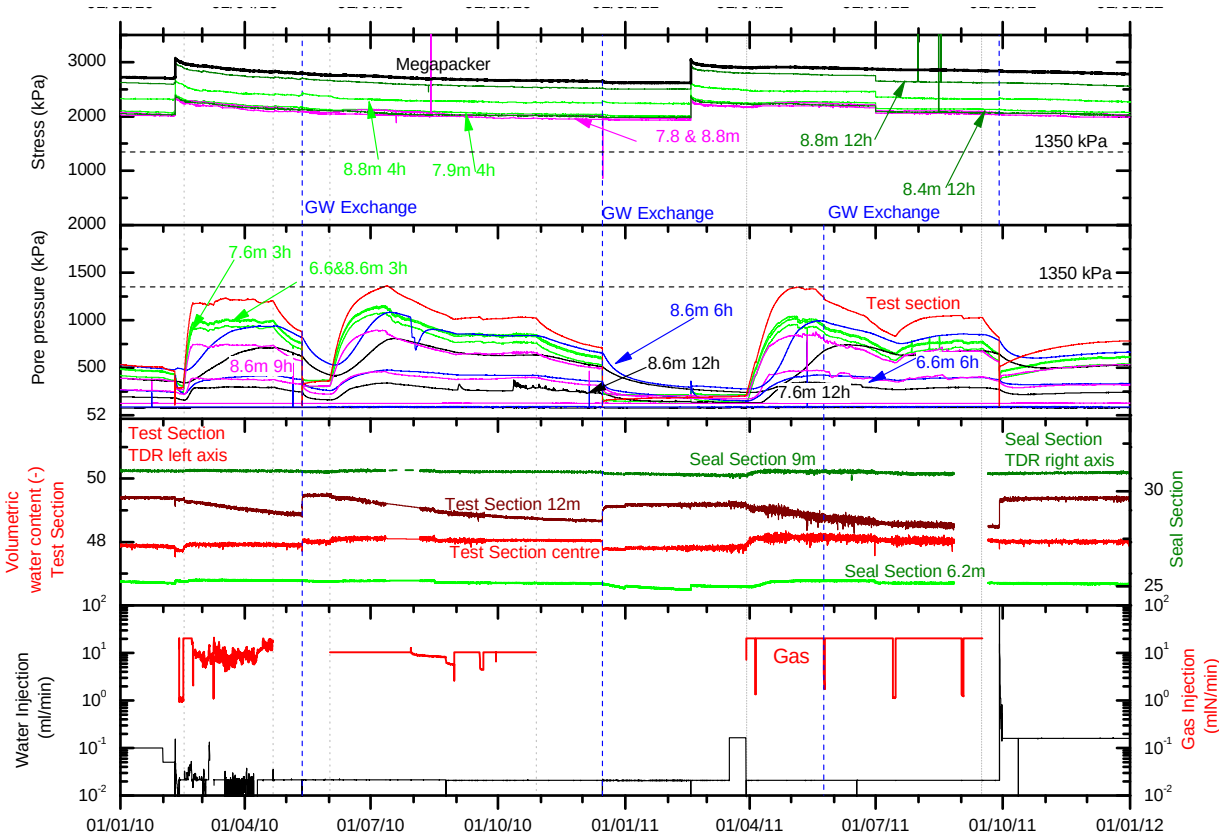

Figure 3.5: Microtunnel stress, pore pressure, water content and flowrate measurements during gas injection.

3.3 CONCEPTUAL MODEL

This section sets out a conceptual framework for gas and water flow in the HG-A experiment. It builds on previous work and interpretations from Marschall et al. (2008), Lanyon et al. (2009), Lanyon (2012) and Lanyon et al. (2012). The structural understanding of the EDZ (believed to be the main water/gas conducting feature) relies on mapping studies by Nussbaum & Bossart (2006).

3.3.1 Water and Gas Conducting Features

Excavation Damaged Zone

The geometry and development of the EDZ around the HG-A Microtunnel have been described by Marschall et al. (2008). The evolution of the EDZ during the period when the Microtunnel was open can be observed from the two geological mapping campaigns performed in March

2005 and February 2006. The first 6m of the Microtunnel were not mapped due to the installation of the steel liner immediately after excavation. Bedding dips of about 48° towards SSE, and bedding planes are tangential to the tunnel wall a) between 10.0 and 11.00 o'clock (310-320°) and b)between 4.00 and 5.00 o'clock (130-140°). Two sets of tectonic fractures are present, one sub parallel to bedding and a second sub-horizontal S-SW dipping system. The bedding parallel fractures are observed in the Microtunnel from TM 8.5-3. The S-SW dipping fractures are present from TM 9-13 but are not believed to have been involved in the development of the EDZ.

Three main types of artificial discontinuities have been observed on the HG-A Microtunnel walls: 1) Extensional brittle fractures, 2) Shear brittle fractures related to the (re)activation of bedding plane and fault plane slip, and 3) Anisotropy- and stress-induced borehole breakouts. Figure 3.6 shows a schematic of the damage zone structure illustrating the relationships between the different feature types.

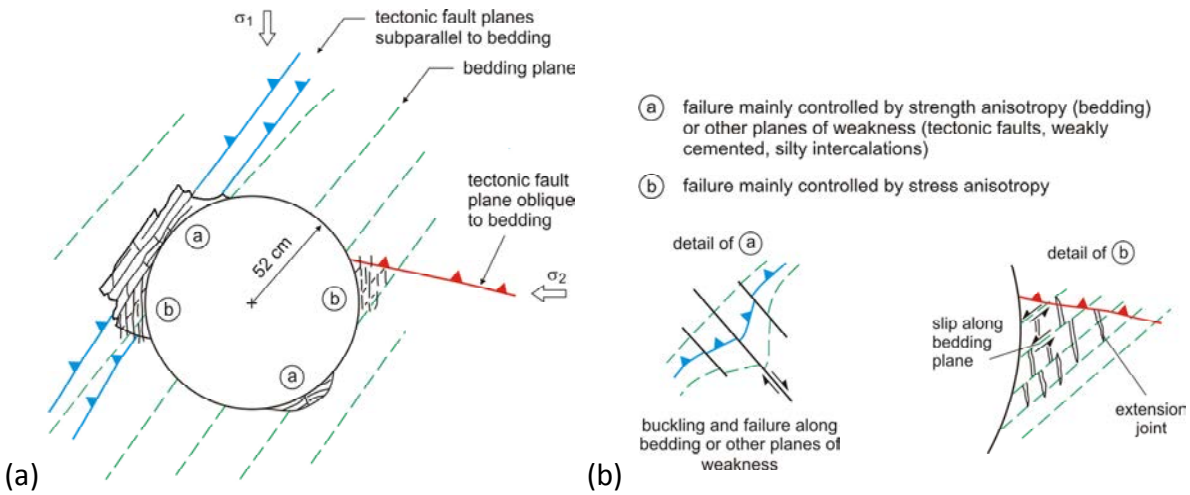

Figure 3.6: Schematic representation of the damage zone around the HG-A microtunnel (after Marschall et al. 2008), showing key processes and features that affect stability: slab-like breakouts on the upper left side are due to extensile failure along tectonic fractures. Wedge-like breakouts occur on the right side. Direction of view is towards the rear of the microtunnel.

Additional desaturation fractures have been identified in the tunnel mapping but are thought to be isolated and not to form part of a connected fracture network.

Extensional brittle features are normally sub-parallel to the tunnel and therefore mainly mapped in the breakout zones where the notch allows access to features in the tunnel wall. The occurrence of extensional fractures is suspected behind the tunnel walls at 3 and 9 o'clock as these locations show well developed breakouts. In one area, near the seal section, the rock forms pencil-like structures where extensional EDZ fractures and bedding planes intersect. Early interpretations emphasised the role of bedding-parallel tectonic fractures but were revised due to greater exposure allowing the identification of sheared bedding planes (Nussbaum & Bossart, 2006).

It is likely that the EDZ developed further after the February 2006 mapping prior to backfilling the tunnel and the emplacement of the Megapacker in May-July 2006. However the overall structure shown in Figure 3.6 and observed in the 2006 mapping is expected to have remained the same.

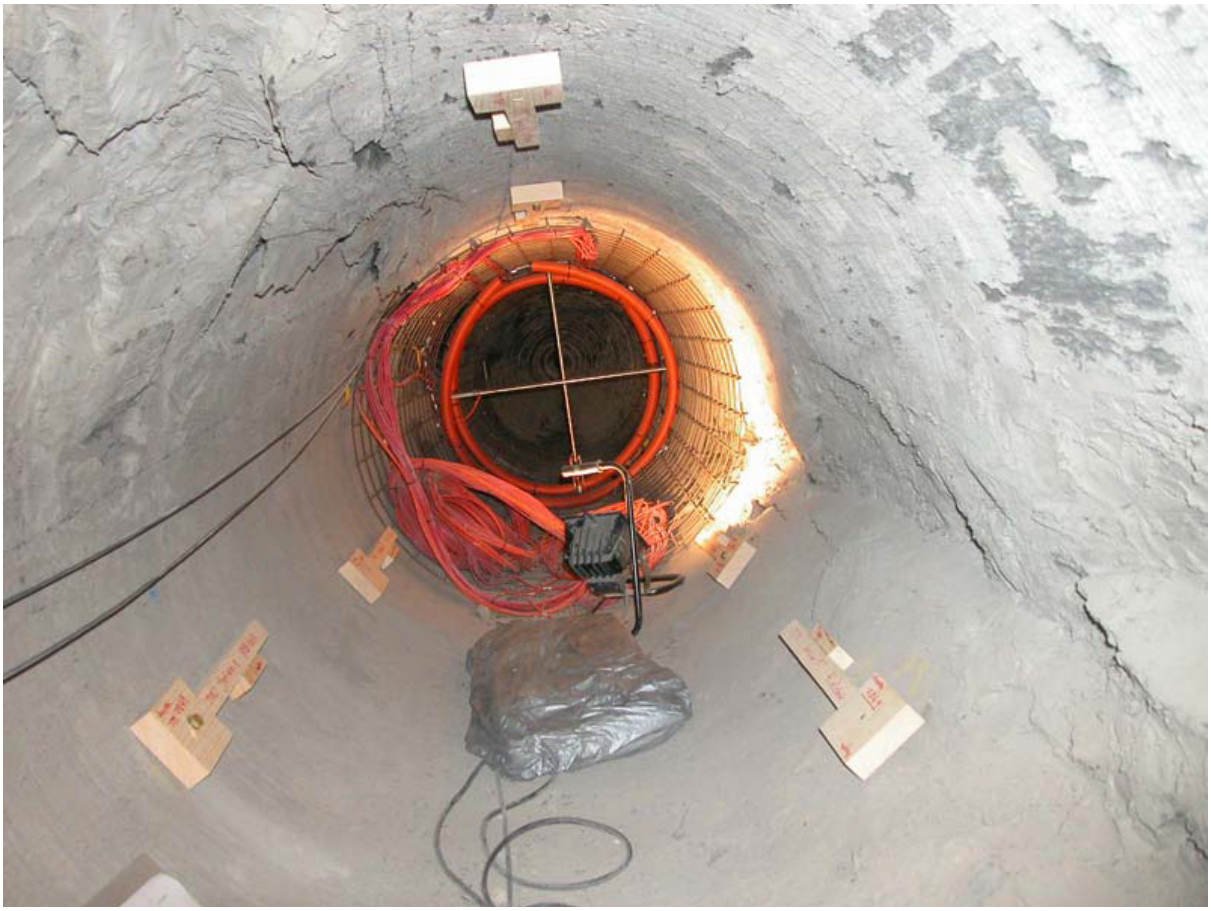

Figure 3.7: Sealing section of the Microtunnel with the surface breakouts at 11 and 4 H radial positions as of April 2006. View is looking towards test section. The wooden dummies are for the emplacement of the total pressure cells

After emplacement of the Megapacker the EDZ was no longer accessible for mapping but during saturation and the long term multirate hydraulic tests it probably provided a water flow path from the pressurised test section. Over time the rate of water injected into the test section was reduced as the resistance to flow increased.

A time-dependent self-sealing of the EDZ has been suggested by Lanyon et al. (2009) on the basis of the observed pressure/flow behaviour during the long-term multirate test that followed the saturation phase.

The effective stress around the seal zone was varied by changing the Megapacker pressure. Hydraulic data from periods of low effective stress suggest that features in the EDZ may become more permeable (dilate) at low effective stress. Porous medium models (Lanyon et al. 2009) were able to replicate the overall pattern of test section water flow and pressure behaviour during the saturation and multirate testing by incorporating time dependent permeability reduction (self-sealing) and pressure dependent permeability (dilation at low effective stress).

The fractures within the EDZ around the seal are likely to have formed a preferential flow path immediately after Megapacker emplacement but ongoing resaturation and recompaction have caused self-sealing via a range of possible mechanisms (see Bock et al., 2010). At the beginning of the gas injection test the partially sealed fracture network may still have provided a preferential flow path compared to the undisturbed rock.

The rock within the EDZ may also have been microfractured resulting in some possible permeability increase (Davy et al., 2007). It is possible that recompaction and resaturation

resulted in a reduction of permeability, but the properties of the in situ material is difficult to characterise and whether there is any significant permeability increase over that of the undisturbed rock is uncertain.

Within the seal section, prior to emplacement of the Megapacker the tunnel profile was restored by filling the notches with Sika Monotop 615 cement. It is possible that some flow paths may be associated with the cement/rock or cement/packer interfaces.

Excavation Disturbed Zone

Outside the Excavation Damage Zone there is a second region, the Excavation Disturbed Zone, where the rock may have been disturbed by the presence of the tunnel. This disturbance is typically related to changes in state (stress, saturation, pore pressure, temperature) that is likely to be reversible and to have recovered after resaturation and recompaction.

Pre-existing fractures and faults

Borehole cores and mapping of the HG-A tunnel show pre-existing fault planes. These planes are sealed and their main influence is to provide some local control of the EDZ (see Marschall et al. 2008 and Lanyon et al., 2009). Unless they have been reactivated by the excavation process they are not believed to be significantly more permeable than the undisturbed matrix.

Matrix

Marschall et al. (2004) describe a conceptual model of groundwater flow in the Opalinus Clay at Mont Terri and note that at the core scale "layering can be interpreted as an indication for pronounced anisotropy of the hydraulic conductivity at the centimetre and decimetre scale." They provide information on permeameter tests on core from Mont Terri and packer tests performed at Mont Terri. Packer test hydraulic conductivity ranged from 2×10^{-14} - 2×10^{-12} m/s. Results from tests in different facies showed some variation, which was thought to be largely due to variations in testing and which could not be used to identify systematic variations in conductivity between the different facies. Summary hydraulic conductivity values are given in Table 2.8. A limited number of permeameter tests were performed and the database is insufficient to estimate the hydraulic anisotropy.

Nagra (2002) presents results from permeability and diffusion tests on Opalinus Clay core from the Benken boreholes (Zürcher Weinland) and suggests a range of "anisotropy factor" $K_{II}/K_{\perp}$ of between 1 and 10. The anisotropy in the diffusion constant was found to be about a factor of 5. Microscopic observation of the fabric of the Opalinus Clay at Mont Terri suggests that there may be a significant core-scale hydraulic anisotropy. However, the database of permeameter tests on core from Mont Terri is insufficient to provide robust estimates of hydraulic anisotropy. The value of the anisotropy factor $K_{II}/K_{\perp}$ is thought to lie between 1 and 10, with a suggested value of 5. Gas entry pressure for the undisturbed matrix is high at about 1MPa (see Fig. 3.8).

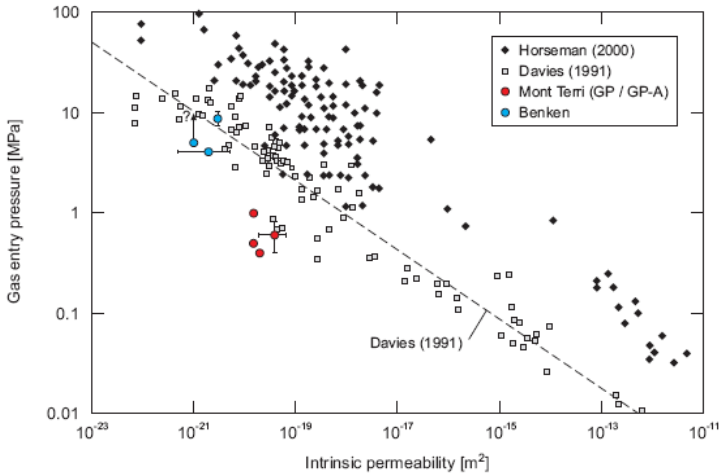

Figure 3.8: Relationship between gas entry pressure and intrinsic permeability for low permeability rock formations (claystones, shales, sandstones). Data from Benken and Mont Terri added to the compilation of Davies (1991).

3.3.2 Boundary conditions

Hydraulic head/pressure

A range of piezometers have been installed around the HG-A site to monitor formation pressure. Piezometers close to the Microtunnel have also shown the effects of tunnel excavation and water/gas injections testing. The appropriate boundary conditions for models are likely to be complex due to the experiment geometry and the ongoing recovery from excavation of both the Microtunnel and the galleries. The galleries are normally shotcreted, but measured pressures close to the tunnel wall are typically low suggesting that they do not act as no-flow boundaries. There are no pressure measurements to the SE of the Microtunnel where we might expect pressures to be higher.

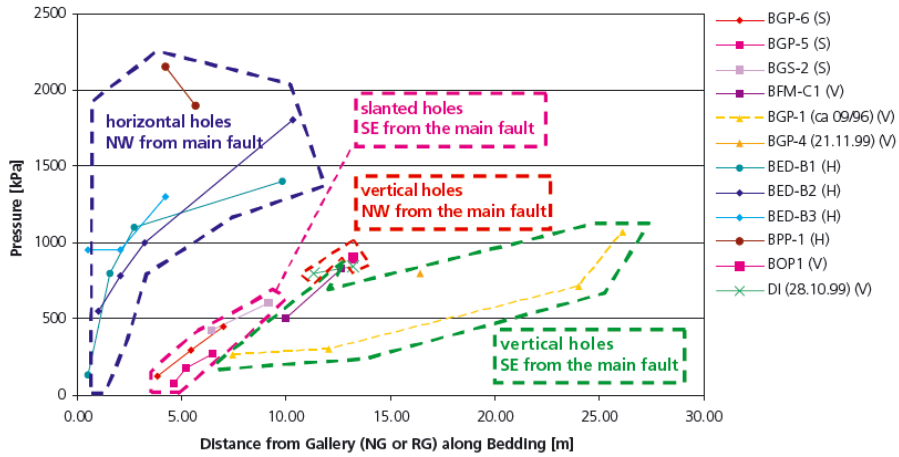

Figure 3.9: Compilation of pressure observations in boreholes of the Mont Terri rock laboratory on 30.06.2000 (unless indicated otherwise in the figure legend), illustrated with respect to the distance along bedding to the nearest gallery (from Marschall et al 2004).

The undisturbed pressures at the Mont Terri URL have been described in Marschall et al. (2004) using data gathered prior to excavation of the Gallery 04 and show a complex pattern probably due to a range of influences (see Figure 3.9). The highest pressures are seen in horizontal boreholes NW of the main fault while pressures to the SE of the fault are typically lower between 0.3 and 0.8 MPa. Vertical boreholes show typically lower pressures than

horizontal boreholes. The pressure in the lined section of the Microtunnel are likely to be low – close to atmospheric as there was no sealing behind the liner and the tunnel surface is open between the liner and the Megapacker. This is supported by the low pressures measured in HGA-08 to 10.

3.3.3 Processes

Porewater flow (from Marschall et al. 2004)

The Opalinus Clay is a very low permeability (aquitard) clay stone. There is no evidence from Mont Terri that pre-existing tectonic fractures have any significant effect on groundwater flow. At elevated hydraulic gradients (~1000) porewater flow is governed by Darcy's Law as demonstrated on the laboratory scale by permeameter experiments. There was no evidence from single hole hydraulic tests of any significant deviations from Darcy's Law at gradients ~50. Anomalous flow responses have been observed in cross-hole tests at gradients of <1. The overall validity of Darcy's law is supported by observations of a drawdown cone around the excavations. In undisturbed conditions at low hydraulic gradients, diffusion is the dominant transport process.

Hydromechanical processes have been observed at low effective stress. In the context of packer testing, evidence was seen for permeability enhancement at elevated injection pressures. Within HG-A Lanyon et al. (2009) found it necessary to include a pressure dependent permeability to represent possible fracture opening in the EDZ when effective stress approached zero.

Gas dissolution

It is expected that the dissolution of nitrogen gas will be governed by Henry's Law relating the mass of gas dissolved in the solute (water) to the absolute pressure using the Henry's law constant H (-).

Transient dissolution models incorporating the surface area for gas dissolution and diffusion of the dissolved gas within the liquid are available. The test section was filled with gravel on 5/05/06. About 3 m^3 of quartz gravel was emplaced. Assuming a porosity of 30% for the gravel, this suggests a pore volume of 0.8 m^3 for the gravel filled test section from 10-13m. Assuming a solubility of 1.70E-5 kg N_2/kg water at 15°C and 101.3 kPa the pore volume could dissolve ~112 lN (i.e. volume normalised to atmospheric conditions) of Nitrogen gas at an interval pressure of ~1000kPa abs.

Gas flow

Gas transport through low-permeability rock formations is controlled not only by the hydraulic and mechanical properties of the rock mass (intrinsic permeability, porosity, rock strength), but also by the gas pressure at the place of gas entry and the hydromechanical state of the rock (i.e. water saturation, porewater pressure, stress state). Phenomenological considerations suggest the following subdivision of the basic transport mechanisms:

- advective-diffusive transport of gas dissolved in the porewater
- visco-capillary two-phase flow
- dilatancy-controlled gas flow
- gas transport along macroscopic tensile fractures (hydro- and gas-fracturing)

At close to full saturation an indication for the required overpressure to generate dilatancy controlled flow can be drawn from the Mont Terri HG-C / HG-D experiment and from laboratory tests presented in chapter 2.2. Gas entry and gas breakthrough under isostatic (total) stress conditions caused moderate volume expansion in the order of a few millistrains, which could be explained as a swelling mechanisms or as the onset of dilatancy, respectively. When gas injection stopped, the gas pressure in the clay drops rapidly and then continues to decrease slowly with time. The associated recovery of deformation supports the assumption of an elastic response of the rock (i.e. swelling rather than dilatancy). In contrast, the HG-C/HG-D in-situ experiment indicated opening of discrete pathways in response to gas injection, as soon as gas pressure approached a certain threshold value. In this case, clear evidence of pathway dilation was found.

For HG-A these considerations lead to the following conclusion about gas flow into the formationin an environment with EDZ:

- There is likely to be a high dependence on the local entry pressure and heterogeneity associated with the EDZ (even after self-sealing) creating a favourable path for gas.
- Pathway dilation processes are only likely if the test section pressure approaches the local minimum stress.
- The observation of possible fracture opening in the EDZ during the multirate test suggests that this may be a dominant process rather than the pathway dilation process.
- Entry pressure for the undisturbed Opalinus Clay is high 500-1000 kPa (see Fig. 3.8) and more generally in the range 1-10 MPa (Marschall et al., 2004) which might not be reached before pore pressure in the test section breaks through along the EDZ.

Self-sealing

An important aspect of the transient behaviour of the EDZ around the HG-A Microtunnel is the self-sealing of EDZ fractures resulting in a reduction in fracture transmissivity and hence reduction in the effective EDZ permeability over time. This sealing of the fractures is a function both of resaturation of the EDZ and recompaction by the Megapacker. Bock et al. (2010) have reviewed self-sealing processes and considered seven mechanisms that might lead to self-sealing and assessed the state of knowledge and potential for sealing of each mechanism summarized in Table 3-3.

It is not possible to determine the interaction between the different sealing mechanisms within the EDZ around the microtunnel and therefore a pragmatic approach is to fit suitable time-dependent permeability or transmissivity functions to the observed behaviour as described in Lanyon et al., 2009 and Lanyon 2012). The choice of permeability reduction function was influenced by results from the EH and EZ-A tests performed at Mont Terri (Blümling et al., 2007).

Table 3.3: Summary of Sealing Mechanisms as Identified by Bock et al. (2010)

	Sealing Mechanism		State of Knowledge	Database	Sealing Potential
M-1	Additional compaction of the rock matrix		Very good		Low
M-2	Increase of the effective normal stress σ_n' across the fracture plane		Good		Moderate to high
M-3	Contraction of fracture when subjected to shear		Good		Moderate to very high
M-4	Creep of fracture wall material		Limited	Limited	High to very high
M-5	Swelling of the fracture wall material		Reasonable	Inadequate	Very high
M-6	Slaking:	Body slaking	Limited	Poor	Limited to moderate
		Surface slaking	Non-existent	Non-existent	Unknown (most likely limited)
M-7	Mineral precipitation onto fracture walls		Reasonable	Reasonable	Limited

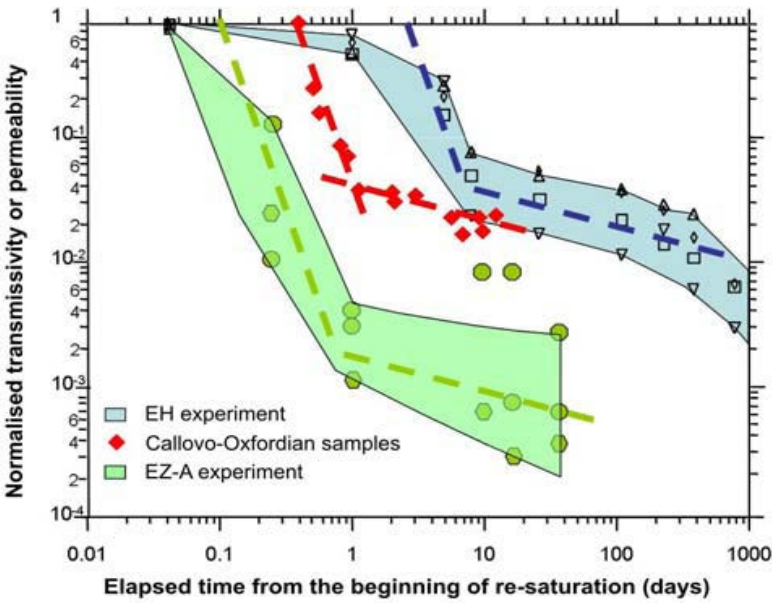

Figure 3.11: Reduction in interval transmissivity with resaturation time from (Blümling et al 2007).

Other coupled hydro-mechanical processes

Strain gauge observations during transients in the multirate tests indicated deformation of the test section due to coupled mechanical effects. These are likely to include both deformation of the pore geometry within the gravel fill and of the tunnel volume itself. These effects are normally treated in hydraulic testing by a wellbore storage term. Lanyon (2008) suggests a test zone storage of 10^{-8} m^3/Pa from analysis of the hydraulic response to testing. Lanyon (2009) uses the same value of compressibility in porous medium simulations of hydraulic testing at

HG-A. This is in reasonable agreement with the estimated pore volume assuming a pore-compressibility of 1.2E-8 1/Pa.

There is likely to be some coupling of the test section volume to the applied Megapacker pressure. This was observed during the multirate test but will be limited during the gas injection phase when a relatively high Megapacker pressure was maintained throughout the testing period.

3.4 INTERPRETATION

Self-sealing

Self-sealing of fractures in claystone rocks has been observed at Mont Terri and other sites (Bock et al., 2010). Lanyon et al. (2009) defined a simple measure of the flow resistance across the seal section as the Sealing Index S (ml/min/kPa) based on the injection rate and test section pressure as:

$$S = \frac{Q}{P_{Test\,section} - 100}$$

where Q is the flow into the test section in ml/min and $P_{TestSection}$ is the absolute test section pressure in kPa. Assuming linear flow and a flow-path length of 3 m (seal section), an EDZ conductance (m^3/s) can be obtained by multiplying the Sealing Index S by a factor 5×10^{-7} (considering only resistance along the seal section). Figure 3.12 shows the calculated Sealing Index after filtering for flow rate changes to minimize storage effects.

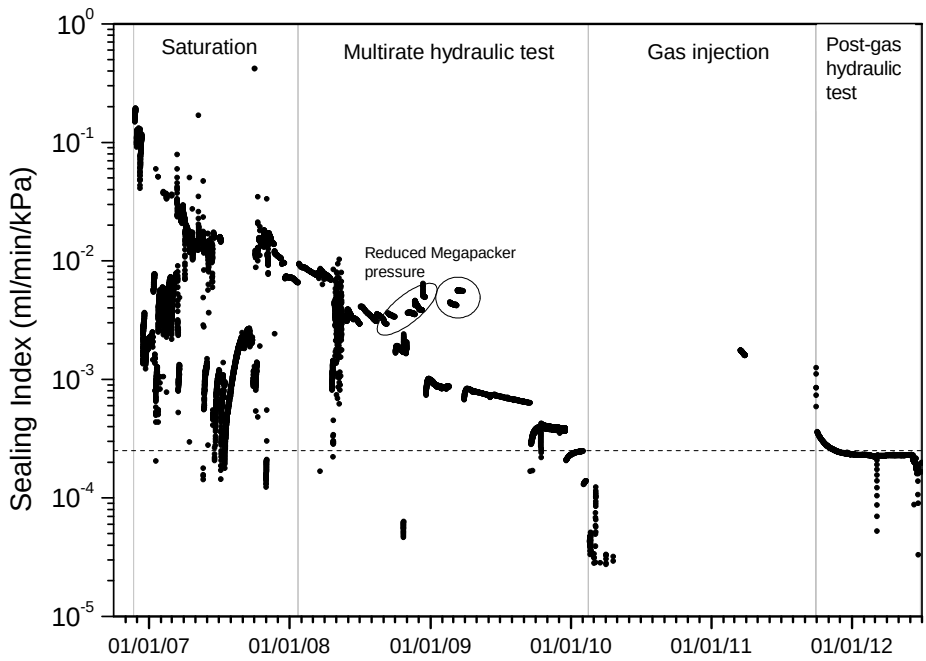

Figure 3.12: Sealing Index during water injection. Periods of reduced Megapacker pressure (low effective stress) are marked.

In the year prior to gas injection the sealing index reduced from 10^{-3} to almost 10^{-4} (ml/min/kPa) equivalent to a hydraulic conductance of 5×10^{-11} m^3/s.

Effective stress dependence

The higher sealing index (seen in Fig. 3-12) and observed test section pressure response during periods when the Mega-packer pressure was reduced so that the measured stress (TP cells) was close to the test section pressure indicate EDZ permeability dependence when effective

stresses are low. This is likely to be due to fracture/feature opening (normal dilation). The response to the subsequent increase in megapacker pressure suggests that the effect is largely reversible and does not significantly hinder ongoing self-sealing.

Figure 3-13 shows the test and seal section pressures during periods of water injection with high and low Megapacker pressure. In the period of high Megapacker pressure injection at 6 ml/min results in an ongoing linear increase in test section pressure. When the Megapacker pressure is reduced the test section pressure levels off close to the measured radial stress (TP cell at 4h, 8.8m). Increasing the injection to 8ml/min then results in only a small increase in test section pressure, which is mirrored by the measured radial stress.

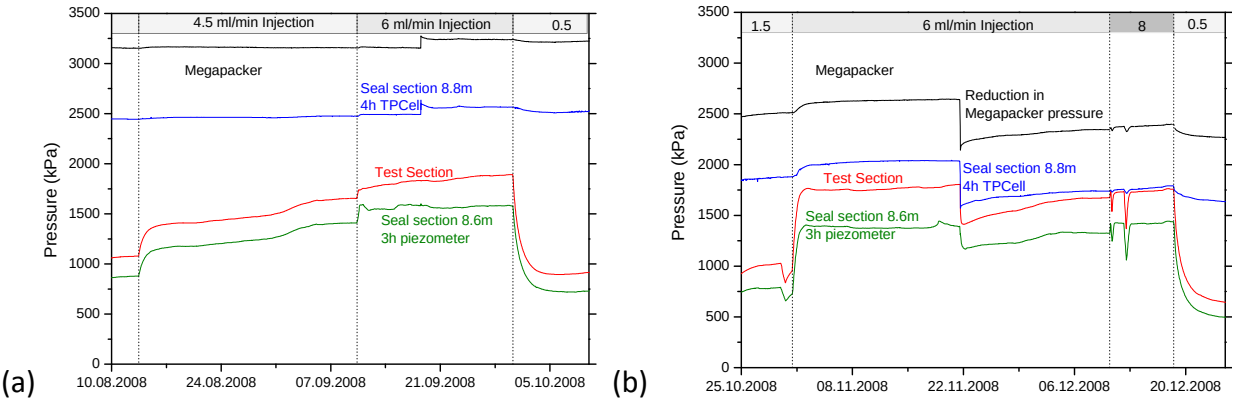

Figure 3-13: Test and seal section pressure and stress during a) high b) low effective stress testing.

Gas transport

The observed response of the test section to gas injection suggests that the dominant pre-breakdown processes are: test section compressibility, gas dissolution in pore water, and water leakage from the test section. This results in a) an initial storage period with linear log-log response, followed by b) a transitional period when leakage along the EDZ becomes important as test section pressure rises and c) a final breakdown when the gas level in the Microtunnel has been driven down to the point where the gas is in contact with a permeable feature and gas over-pressure is sufficient to enter that feature as illustrated in Figure 3.14.

Independent of the gas injection rate, the peak pressures during gas injection are in the order of 1300 – 1400 kPa, suggesting that gas breakthrough is controlled by the percolation process in the sparse channel network along the EDZ. No evidence of gas-"fracturing" has been observed and test section peak pressures (~1350 kPa) and during continued gas injection (~1025 kPa) are well below the measured radial stress along the seal section (minimum of 8 sensors at 1950 kPa).

The pressure data support a model of a heterogeneous EDZ/contact zone along the sealing section with a potential channel associated with the 3 o'clock position (close to one of the notches observed immediately after excavation). However, this channel appears to be poorly connected to any outflow from the system (atmospheric boundary condition). Other sensors at 8.60 m show high pressures after degassing, suggesting that they are not well-connected to the test section. The small oscillations and pressure build-ups also observed suggest either a meta-stable or developing gas flow field rather than steady flow through an established pathway.

The analysis of the pore pressure measurements in response to the gas injections gives clear evidence for localised gas leak-off along the EDZ.

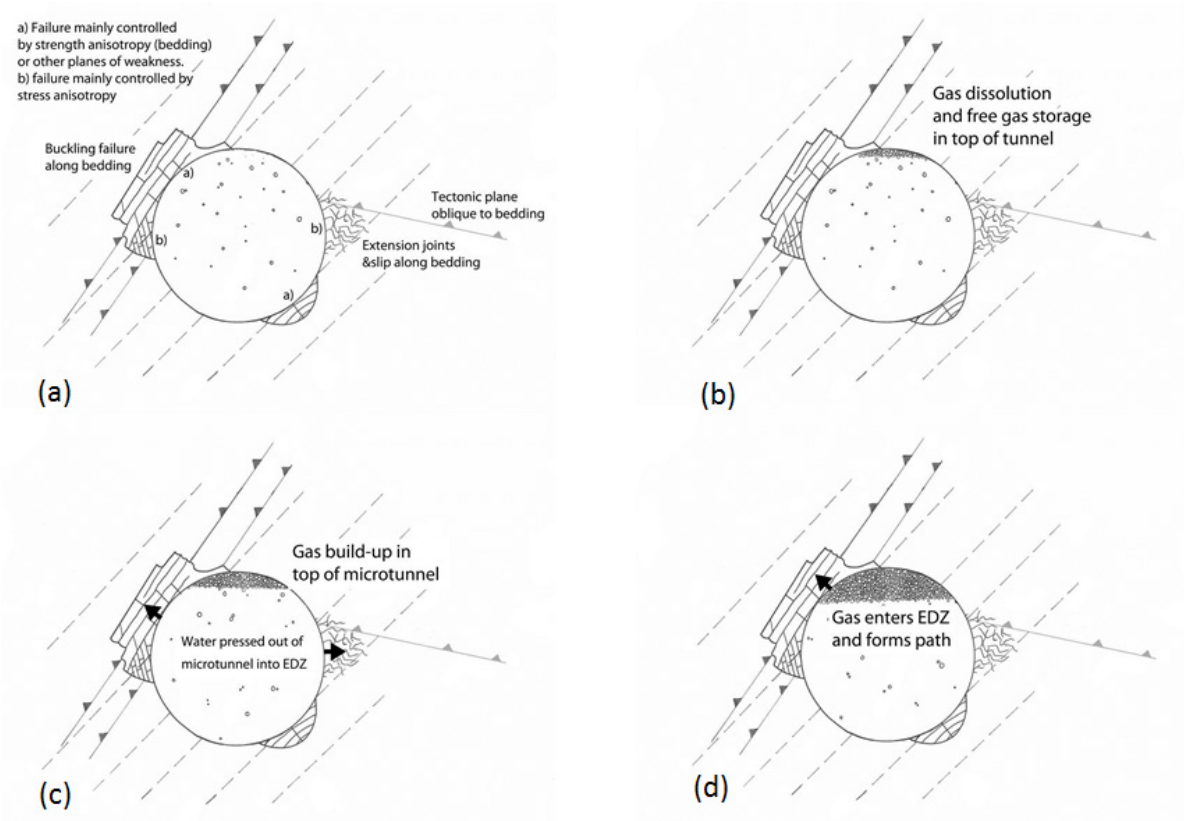

Figure 3.14: EDZ schematic (from Marschall et al. 2008) with stages of gas injection: a) EDZ structure, b) storage & dissolution, c) storage & leakage, d) breakdown and gas flow into the EDZ.

Post-gas hydraulic properties

The water injections following the gas injection sequence confirm a long-term sealing tendency of the EDZ. The effective conductance shows an ongoing reduction during saturation and hydraulic testing. Following gas injection the effective conductance swiftly reduces to values which are even lower compared to that prior to gas injection. The test zone response suggests a rather linear flow behavior (e.g. in a channel or some part of a cylindrical shell with conductance ~ $>5\times10^{-10}$ m^3/s.

3.5 OUTLOOK

The HG-A experiment at the Mont Terri URL is an ongoing long-term experiment, aimed at improving understanding of hydro-mechanical coupled processes in response to gas pressure buildup for the near-field around a sealed tunnel section. Emphasis has been placed not only on the gas transport processes in the EDZ and the host rock during gas injection, but also the resealing process in the subsequent resaturation phase.

The experiment showed clearly that gas tends to move along localised pathways in the EDZ. Repeated gas injection tests demonstrated, that the gas paths appear relatively stable in space; however, the gas transport capacity increases from one gas injection event to the next one. On the other hand, there is clear evidence that the hydraulic conductance of the EDZ decreases with time. After 4 years of testing, the conductance of the EDZ is only 1-2 orders of magnitudes higher than the intact rock.

A series of new gas injection tests have been scheduled at the HG-A site, which will be complemented by 4-D seismic monitoring before, during, and after the gas injection. The purpose of this experiment is the visualisation of the gas paths along the EDZ and the temporal and spatial evolution thereof. It is expected that the detailed monitoring of the propagation of the gas front will give new insight into the coupled gas transport mechanisms and will help to improve the numerical codes for modelling gas transport in deformable media.

4 HG-C/D experimental results and interpretation

4.1 DESCRIPTION OF THE SEQUENCE OF EXPERIMENTS AT SITE

The HG-C / HG-D experiment (previously called GP-A/GS) at Mont Terri URL was set up to investigate coupled hydro-mechanical processes associated with water and gas flow at different gas pressures ranging from below pore water pressure to high pressures leading to dilatancy-controlled gas flow.

The HG-C experiment was performed in four boreholes of the GP-A/GS site at the Mont Terri URL which had been instrumented with piezometers for pore pressure measurements and fixed installed micrometers (FIMs) for measuring axial deformation along the borehole. The boreholes were drilled inclined with respect to the tunnel floor, but perpendicular to bedding planes present in the formation.

Figure 4.1 shows the layout of the tunnel and the four boreholes. Boreholes GS-1 and GS-2 had identical completions and were instrumented with triple packer systems for accurate recording of interval pressures. Boreholes GS-3 and GS-4 also had identical completions and were instrumented with a triple FIM system. The detail in Figure 4-1 shows a schematic of the FIM system, which measures the displacements between fixed anchors in the middle section of the borehole pipe. The spatial resolution of the micrometer systems is in the order of 1 µm at a basal distance of 1 m, resulting in a typical resolution of a microstrain.

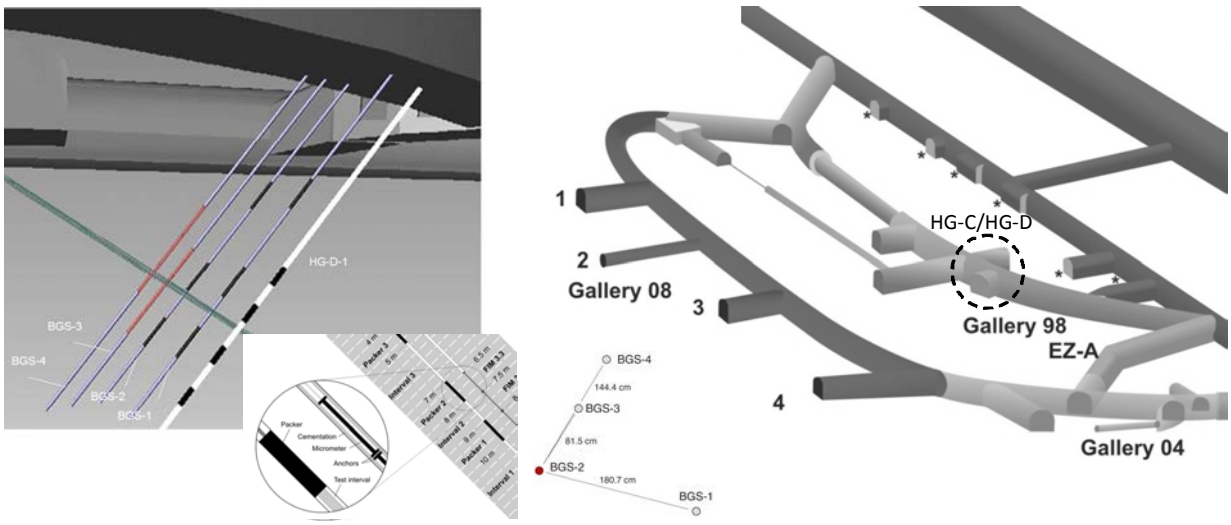

Figure 4.1: Location and layout of HG-C/HG-D site - right: location at the Mont Terri Laboratory; left: Schematic drawing of the borehole configuration and the site instrumentation.

In June 2009, a fifth 10-m long parallel borehole was drilled in the HG-C site as part of the newly launched project HG-D. The new borehole HG-D1 (see chapter 2) was instrumented with a hydraulic triple-packer system, which was designed to resist injection pressures up to 10 MPa. Hydraulic tests were conducted in the central packer interval HG-D1-I2 to determine interval transmissivities and to infer the formation pressure. Pressure transducers were installed for monitoring pore pressure in the three pore pressure monitoring intervals. Long-term monitoring of pore pressures in the piezometers and axial displacements in the micrometer boreholes was managed via the central data acquisition system of the Mont Terri URL.

An overview of the site instrumentation is given in Table 4.1.

Table 4.1: Overview of the HG-C site instrumentation

Borehole-ID	Instrumentation	Remarks
BGS-1	Multi-packer system (3 measurement intervals)	Central test interval: 1 m long
BGS-2	Multi-packer system (3 measurement intervals)	Central test interval: 1 m long; max. injection pressure: 10 MPa
BGS-3	Fixed installed micrometer (3 sections)	3 micrometers (length: 1 m; axial resolution: 1 μm) positioned at mid-distance of the borehole
BGS-4	Fixed installed micrometer (3 sections)	3 micrometers (length: 1 m; axial resolution: 1 μm) positioned at mid-distance of the borehole
HG-D1	Multi-packer system (3 measurement intervals)	Central test interval: 1 m long; max. injection pressure: 10 MPa

During the early stages of the Mont Terri investigation programme (1999- 2004) water and gas injection tests were conducted in zone 2 of borehole GS-2 as part of the GP-A/GS experiment. Full details are presented in Enachescu et al (2000a-e). The detailed objectives of the tests were (Enachescu et al 2002):

- Describe formation parameters under undisturbed conditions by testing the formation with water and gas. Derive transmissivity, static formation pressure, gas threshold pressure, flow geometry.
- Starting from GS-2 Zone 2, create a hydro-frac along a bedding plane that would intersect the middle intervals (Zone 2) in GS1, 3 and eventually 4. Derive frac pressure and reopening pressure.
- Test the formation after the frac with water and gas and compare results with undisturbed formation. Conduct test phases at different pressure levels, to derive transmissivity-pressure dependency.
- Monitor and evaluate interference responses in borehole GS-1.
- Measure rock deformation using FIMs installed in boreholes GS-3 and GS-4, and correlate measurements with pressure observed in GS-2.
- Repeat water and gas tests after a long lasting re-hydration phase to characterize fracture self sealing behaviour in the Opalinus Clay.

In the context of the HG-C/HG-D experiment, complementary water and gas tests were performed in the old GS-boreholes to investigate the self-sealing capacity of the Opalinus Clay and to determine re-frac pressures after long-term pressure recovery. Pressure dependence of water and gas permeability was investigated in turn of repeat tests. After completion of the new borehole HG-D1, a new series of water and gas tests at moderate and elevated injection pressures was conducted in an initially intact borehole section.

The complete experimental sequence included the following 8 phases as listed in Table 4.2.

Table 4.2: Overview of GS/GP-A, HG-C and HG-D experimental phases.

Test Phase			Method	Aim
GS/GP-A Experiment				
Hydro-1	25/11/99	01/02/00	Pulse and constant head rate tests using synthetic porewater	Characterisation of hydraulic behaviour of the undisturbed formation
Gas 1	01/02/00	11/04/00	Stepwise increasing gas pressure test	Calculation of the gas threshold pressure and gas mobility of the undisturbed formation
Frac	12/04/00	13/04/00	Hydrofracture test	Propagate a fracture from GS-2 to intersect Zone 2 of the other three boreholes
Hydro-2	13/04/00	14/04/00	Stepwise increasing pressure pulse test with synthetic porewater	Characterisation of the pressure-transmissivity relationship after the hydro-frac.
Gas-2	14/04/00	19/06/00	Nitrogen gas pulse injection	Characterisation of the ability of the formation to transport gas after the hydro-frac
Gas-3	21/06/00	21/11/00	Constant rate nitrogen gas injection	Confirm the formation behaviour observed during the Gas 2 phase and create a high gas saturation along the fracture plain.
Hydro-3	21/11/00	25/06/01	Resaturation and constant head tests with synthetic porewater	Long-term re-hydration of the fracture plane and the determination of the system transmissivity after fracture self-sealing.
Gas-4	25/06/01	15/04/02	Constant rate nitrogen gas injection	Derive the gas mobility and geometry of gas flow after a long term fracture self-sealing process.
HG-C / HG-D Experiment				
HG-C Phase 12	14/12/06	27/04/07	Multi-step hydraulic test 12-58bar	Hydaulic characterisation of test interval GS2-I2; pressure dependent K
HG-C Phase 13	05/02/08	18/09/08	Gas injection varying back pressure	Gas-related characterisation of test interval GS2-I2; pressure dependent k
HG-D	24/11/2009		Installation of triple packer system	
HG-D Hydrotest	29/04/10	16/08/10	Multi-step constant pressure test 10-20bar	Hydaulic characterisation of test interval HG-D1-I2; pressure dependent K
HG-D Gas test	28/10/10	09/04/11	Gas injection	Gas-related characterisation of test interval HG-D1-I2; pressure dependent k

4.2 EXPERIMENTAL RESULTS AND INTERPRETATION

4.2.1 Water and gas tests as part of the HG-C experiment

Experimental data base / hydrotests

The hydrotest during the HG-C Experimental Phase 1 is described in Trick (2007). The measured pressures in the injection borehole BGS2 and in the observation borehole BGS1 are shown in Figures 4.2a. At total of six injection steps increasing in pressures from 12 MPa to 57 MPa were followed by step decreases. The measured responses in the guard intervals BGS2-3 shows a slight step increases from about 750 to 770 kPa which are probably caused by slight packer movements associated with the injection pressure steps in the injection interval BGS2-2. The pressures in the bottom interval BGS2-1 show no response to the injection test and are at 87 kPa corresponding to atmospheric pressure conditions. The measured responses in the three test intervals in the observation borehole BGS1 indicate relatively low pressures in interval BGS1-1 and BGS1-2 of less than 150 kPa, whereas the pressure in interval BGS1-3 shows a pressure of about 700 kPa, which corresponds to the expected formation pressure.

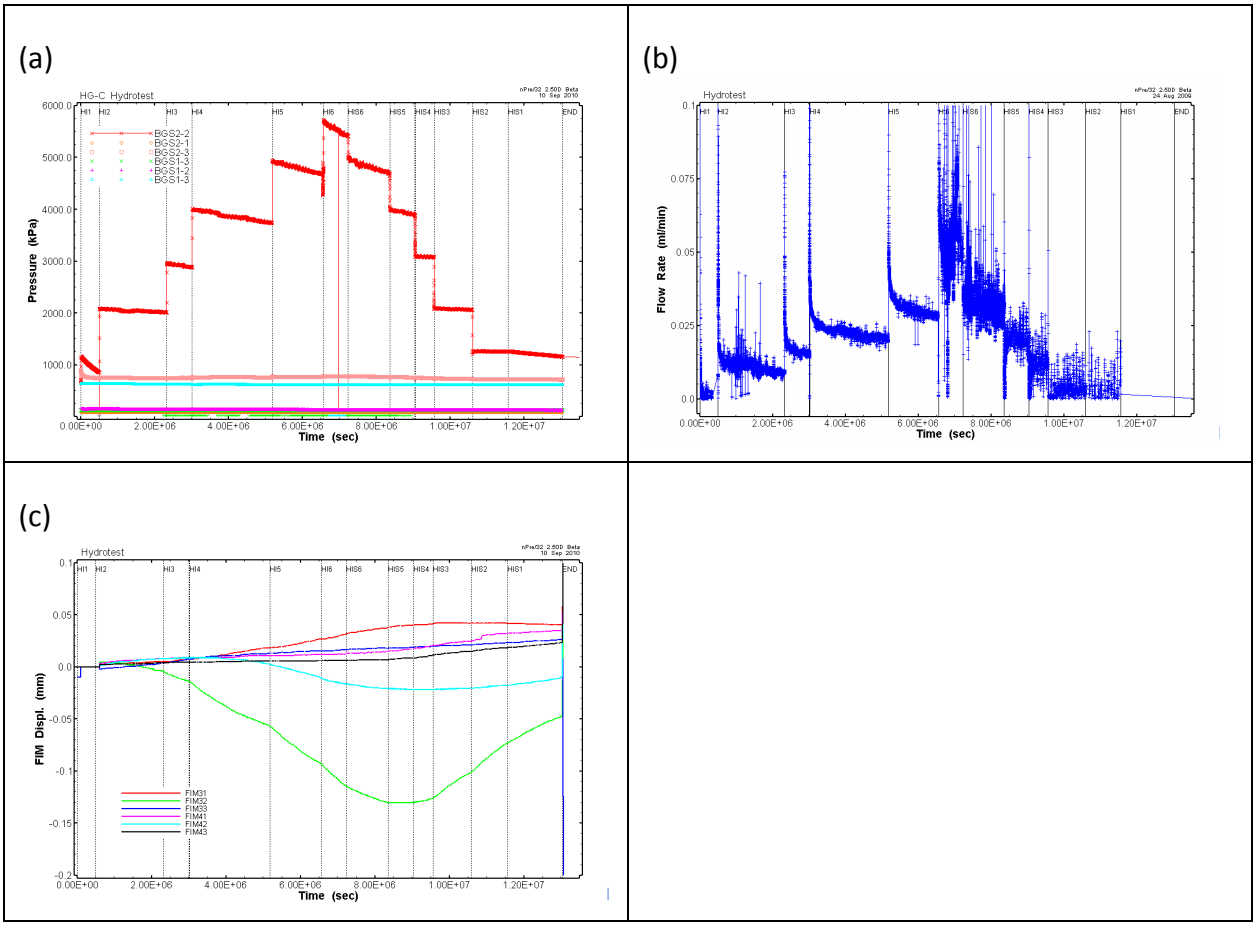

Figure 4.2 Pressure responses in the injection borehole (BGS2-2) and observation borehole (BGS1-1, BGS1-2, BGS1-3) during the HG-C multi-step water injection (a), measured flow rates (b) and axial displacements (c).

The measured flow rates exhibit significant fluctuations, especially during the HIS recovery periods (Figure 4.2b). The reasons for the fluctuations are explained in greater detail in Trick (2007). The flow data required a smoothing and filtering procedure to be suitable for further analysis (Senger 2008). The filtering and smoothing had to be done to such an extent that the variability associated with the injection pressure can still be accounted for in the variation of the flow rate data.

The mechanical observation boreholes BGS3 and BGS4 were instrumented with FIMs to measure axial deformation in the clay rock during the constant-head tests. The two boreholes are at distances of 0.7 m and 1.5 m, respectively, from the injection borehole BGS2 (Fig. 4.1) and contain three FIMs each. The FIM measurements in response to the hydrotest are shown in Figure 4.2c. The FIM responses of the middle sensors indicate dilation in BGS3 and extend to BGS4, with the adjacent sensors indication compaction. The dilation occurs rather gradual indicating only slight increases in slope (Fig. 4.2c), except for FIMGS4-1 which shows an abrupt change during the latter recovery step (HIS2).

Interpretation / hydrotests

The multi-step hydrotest sequence was subjected to detailed diagnostic analyses and numerical simulations with the borehole simulator nSights (Senger 2008). The nSights analysis and optimization was performed for each test sequence to estimate the formation properties in terms of hydraulic conductivity and specific storage of the Opalinus Clay. Figure 4.3 displays the simulation of flow rates of the entire test sequence for the prescribed interval pressures as given in Figure 4.2a. The simulation indicates that the simulated flow rates compare well with those during HI5, but are slightly higher than HI2 – HI4, and lower for HI6.

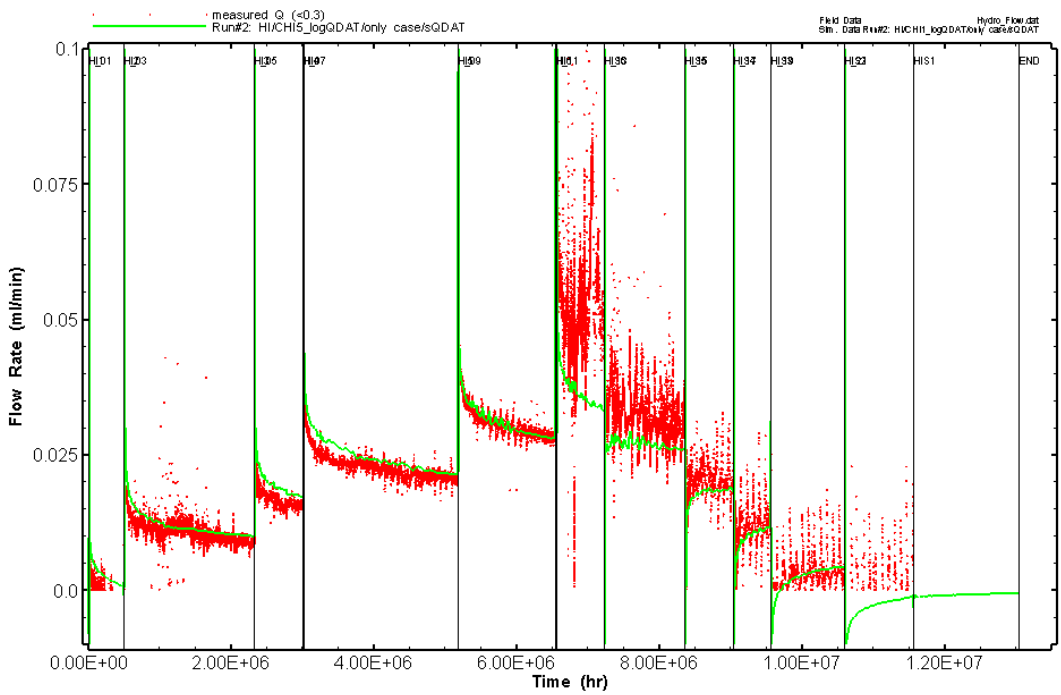

Figure 4.3: Simulated response of the entire test sequence based on the best-fit parameters from the HI5 optimization for injection flow rates.

A summary of the estimated parameters from the different injections steps is given Table 4.3 and in Figure 4.4, showing a cross plot of formation specific storage and formation hydraulic conductivity with the associated 95% confidence regions. The results indicate a distinctly lower

conductivity for HI1, whereas the conductivities for HI2 – HI5 cluster in a narrow range between 5.6E-13 and 7.1E-13 m/s. The conductivity estimate for HI6 is distinctly higher at 1.38E-12 m/s, but the corresponding estimate of specific storage gave a very low value of 3.88E-7 1/m compared to those from HI1 – HI5 which yielded very similar values of between 1.3E-6 to 1.75E-6 1/m.

Table 4.3: Summary of parameter estimates from nSights optimization of HI1 through HI6.

	Best-Fit Parameters		$K = k\rho g/\mu$	$S_s = \rho g\,(C_p/\phi + \phi\beta)$
Seq.	**K [m/sec]**	**Ss [1/m]**	**k(m2)**	**Cp(1/Pa)**
HI1	3.09E-13	1.34E-06	3.15E-20	7.85E-10
HI2	6.19E-13	1.53E-06	6.32E-20	9.62E-10
HI3	5.66E-13	1.73E-06	5.77E-20	1.15E-09
HI4	6.51E-13	1.35E-06	6.64E-20	7.97E-10
HI5	7.06E-13	1.42E-06	7.20E-20	8.58E-10
HI6	1.38E-12	3.88E-07	1.40E-19	-8.47E-11

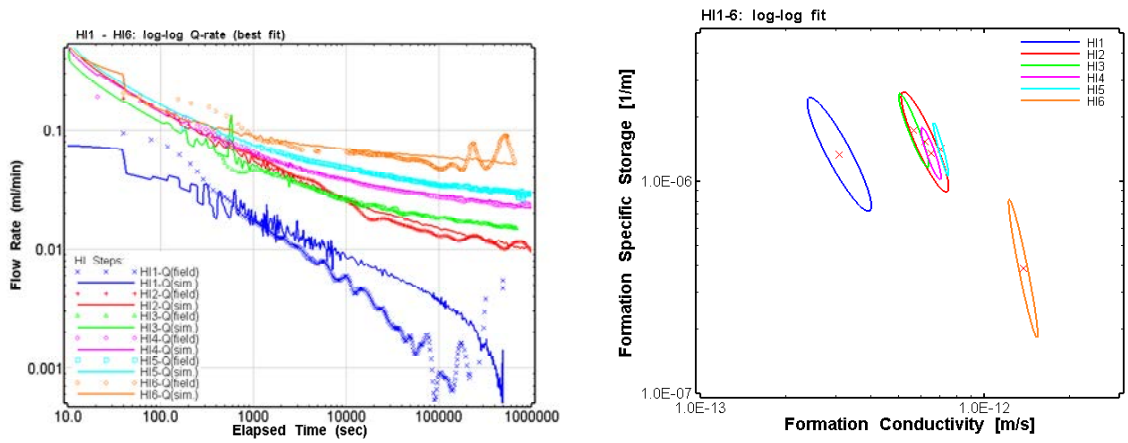

Figure 4.4: Log-log diagnostic plot of the measured and simulated flow rates for the step increases for HI1 through HI6 (left). Computed 95% confidence regions of parameter estimates based on the optimization of the log-log flow rates (right)(.

Experimental data base / gastests

The gas tests during the HG-C Experimental Phase 2 are described in detail in Rösli and Trick (2008) and shown in Figure 4.5. Prior to the constant head gas injection test, the pressures were stable in all three intervals of both boreholes. Because of faulty pressure readings the transducer for BGS1-2 was replaced prior to the test (Rösli and Trick, 2008) and the measured pressure data from the observation borehole were used for the analyses. The gas injection occurred in borehole BGS2 interval 2 (BGS2-2). During the first two steps, the pressures in BGS2-2 remained nearly constant; the third test GHI3 did indicate a slight pressure decline. The gas flow rates were calculated from the pressure changes measured in BGS2-2, indicating a noisy pattern near zero flow during GHI1 through GHI3. During GHI4, the injection pressure showed a distinct decline, and the corresponding gas flow rate showed a slight increase.

The measured pressures in Interval 2 of the observation borehole (BGS1-2) did show an immediate increase with a total pressure increase to 1.23 MPa at the end of GHI4. The last injection step GHI5 to 3.01 MPa resulted in an immediate pressure decline, which leveled off to about 1.5 MPa at the end of GHI5 (Fig. 4.5a). The pressures in BGS1-2 showed a rapid increase

to as high as 1.9 MPa which was followed by the more gradual decline to about 1.2 MPa at the end of the test data. The corresponding gas flow rates similarly showed an initial peak followed by an asymptotic decline to flow rates of about 0.025 ml/min (Fig. 4.5b).

The measured displacements (FIMs) in the observation boreholes BGS3 and BGS4, which are at 0.7 m and 1.4 m distances, respectively, from the injection borehole BGS2 are shown in Figure 4.5c. The data indicate a decreasing trend for FIMGS3-2 starting with the gas injection tests, whereas FIMGS3-1 and FIMGS3-3 indicate an increasing trend. Relatively large responses are associated with GHI4 and GHI5, whereby the latter indicates sudden short decreases of all the FIMs.

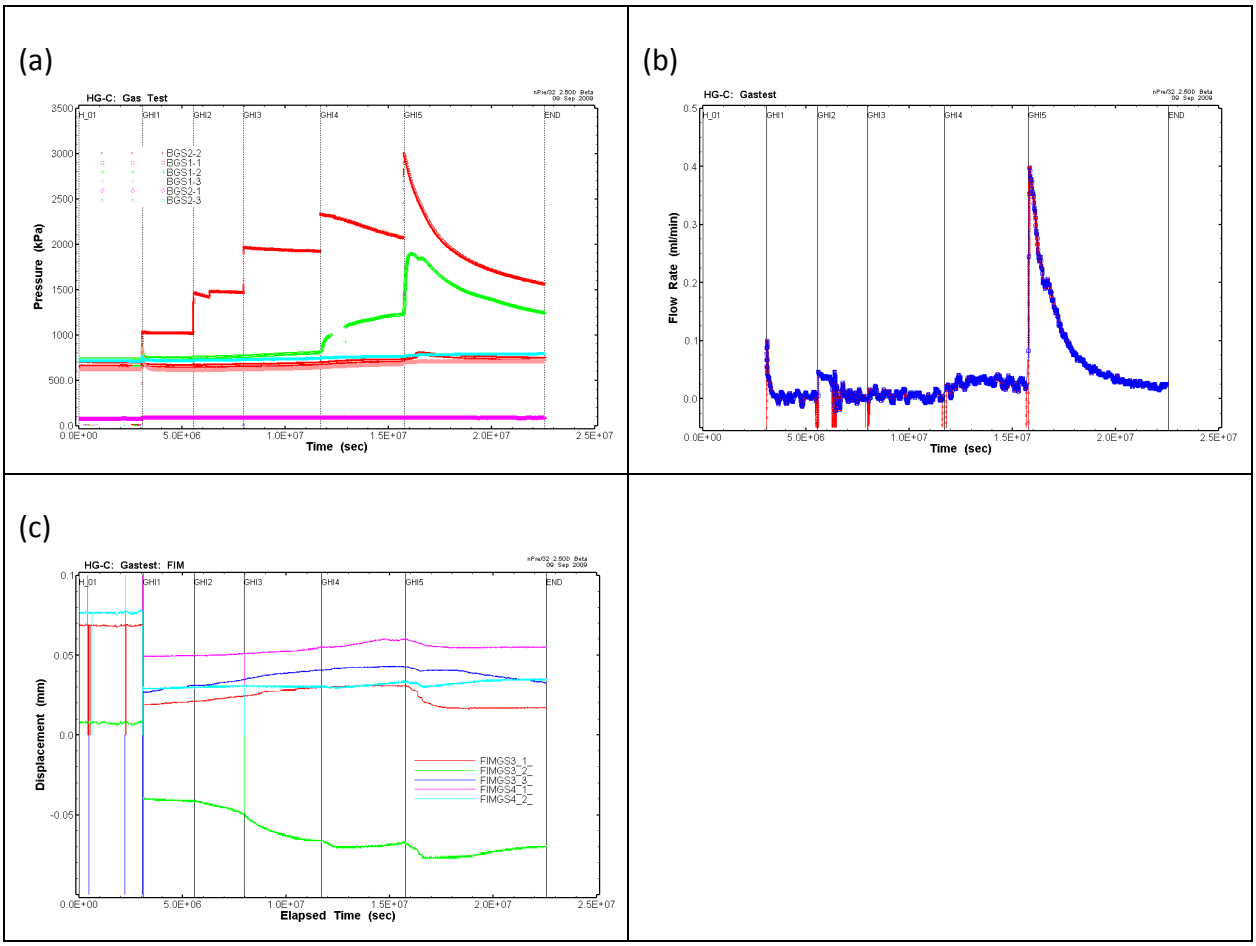

Figure 4.5: Pressure responses in the injection borehole (BGS2-2) and observation borehole (BGS1-1, BGS1-2, BGS1-3) during the HG-C multi-step gas injection (a), measured flow rates (b) and axial displacements (c).

Interpretation / gastests

The gas test was simulated with the two-phase flow code TOUGH2 and the inverse code ITOUGH2 was used for parameter estimation. A detailed description of the corresponding analyses and simulations is given in Senger (2008). For the estimation of formation properties, both the pressure responses in the injection interval (BGS2-2) and in the observation borehole interval (BGS1-2) were used for calibration. That is, the initial gas pressures for each injection step was prescribed based on the increased backpressure in the gas bottle, accounting for the total gas volume of the injection configuration. The subsequent pressure response in the injection interval for each step was then used for calibration, in addition to the monitored pressure in the observation borehole interval BGS1-2. Based on the apparent difference in the

observed responses, three separate optimizations were performed for (a) GHI1-3, (b) GHI4, and (c) GHI5 to estimate hydraulic and two-phase flow properties. The hydraulic properties include:

- permeability,
- pore compressibility,
- porosity

The two-phase flow properties include:

- capillary strength parameter in the van Genuchten constitutive relationship for the capillary pressure – saturation function,
- van-Genuchten 'n' parameter, and residual water saturation (Slr), describing the shape of the capillary pressure and relative permeability curves

Permeability and capillary strength parameter are of particular importance to identify possible pathway dilation at increasing gas pressures. Similar to the hydrotest analyses, described above, the measured data were filtered for each interval and the number of data points for the calibration were specified to get approximately equal weighting for the inverse modeling (i.e., 50 data points for GRI1-3, 20 for GRI4, and 25 for GRI5).

The results of the inverse simulations with ITOUGH2 for the GHI1-3 steps, where the injection pressure steps increase up to 2 MPa and produced only minor pressure responses in both injection and observation intervals (Fig. 4.5), yielded a formation permeability of 5.0E-20 m^2 which compared reasonably well with the estimate 3.9E-20 m^2 from the hydrotest during HI1 (Tab. 4.2). The parameter estimates for the GHI4 indicated a noticeable increase to 1.7E-19 m^2 and reproduced well the injection pressure and observation pressure responses (Fig. 4.6). The final injection step (GHI5) produced about a one order of magnitude increase in permeability to 1.3E-18 m^2. Moreover, the inverse modeling yielded decreasing values in the capillary strength parameter P_0 of the van Genuchten model for the capillary pressure – saturation relationship. This is consistent with the pressure-dependent pathway dilation resulting in a permeability increase and corresponding decrease in capillary pressure. The geomechanical effect of pathway dilation is also indicated by the measured displacements in the boreholes BGS3 and BGS4 (Fig. 4.5c). The estimates for porosity and pore compressibility also decreased whereby the estimate for pore-compressibility reached a lower bound for realistic values, suggesting a localized response within the assumed total width of the test zone (1 m).

The estimated parameters and relevant statistical information from the inverse simulation are summarized in Table 4.4 for the different sequences.

Table 4.4: Summary of parameter estimates from ITOUGH optimization of GHI13-GHI5.

Parameter Estimates:

	GHI13	GHI4	GHI5
K	5.01E-20	1.35E-19	1.45E-18
Por	1.00E-01	3.48E-02	2.50E-02
Cp	3.98E-10	1.00E-10	1.00E-10
vG-n	2.50E+00	2.20E+00	3.70E+00
vG-Po	2.00E+06	7.94E+05	3.80E+05
Slr	*5.00E-01*	4.80E-01	2.30E-01

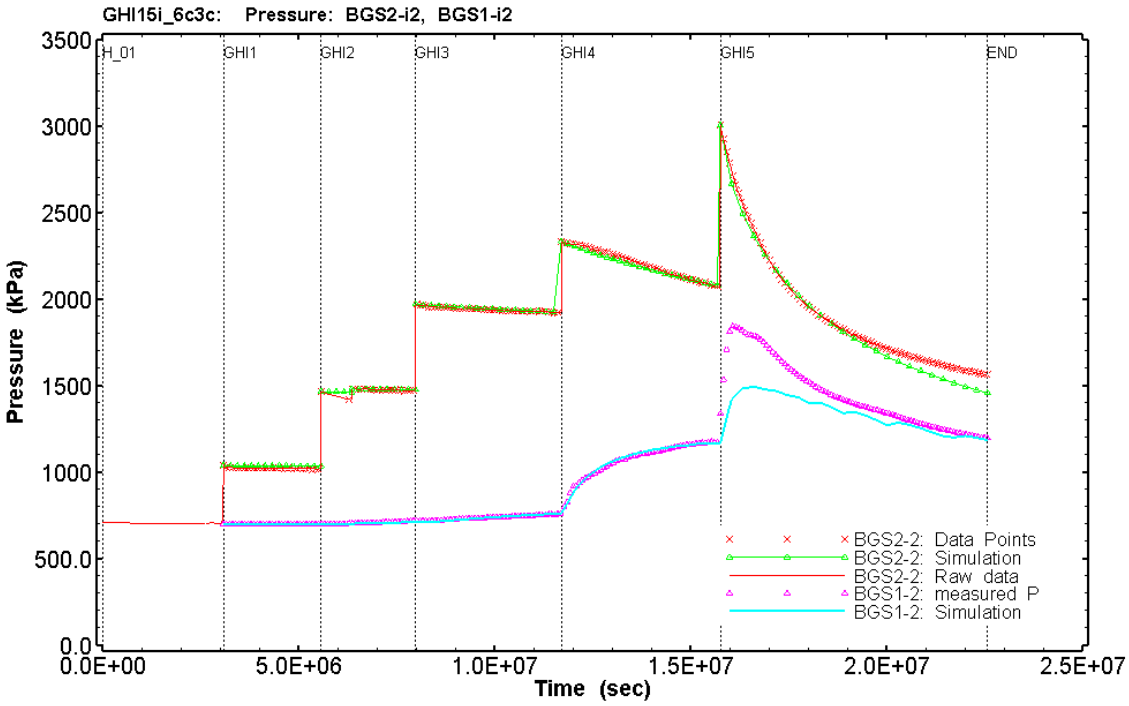

Figure 4.6: Simulated pressure responses in the injection borehole (BGS2-1) and observation borehole (BGS1-2) during the HG-C Experimental Phases 2, based on individual fits of Sequences GHI1–3, GHI4, and GHI5.

Overall, the simulated responses suggest potential pressure-dependency of parameters (i.e. k and vG-P_0) particularly during GHI5 because of the large pressure range. To evaluate the potential impact, a forward simulation was performed of the GHI5 sequence which involved a linear dependency of permeability on pressure. For this a special version of the TOUGH2 code was used incorporating the pressure-dependent permeability and dependency of the capillary-strength parameter P_0 in the van Genuchten model on permeability.

The pressure-dependent permeability is defined as follows:

$$k = k_0 \times (1 + (k_factor - 1) \times \frac{(P - P_1)}{(P_2 - P_1)}$$

Where k_0 is the reference permeability, *k_factor* is a scaling factor, P_1 is the starting pressure of dilation, and P_2 is maximum pressure corresponding to the maximum permeability. The relationship between capillary strength and permeability is typically represented by Leverett's function as:

$$P_0^{'} = P_0 \sqrt{\frac{k_0}{k}}$$

or by a cubic-law function:

$$P_0^{'} = P_0 \sqrt[3]{\frac{k_0}{k}}$$

In the following forward simulation of the GHI5 sequence, the cubic law function was used, and a linear permeability change between a pressure of P1 = 0.75 MPa and P2 = 3 MPa, with a value for k_factor = 15. Initial conditions for the simulation were the simulated conditions at the end of GHI4. The results of the simulation are shown in Figure 4.7. The simulated pressure in the

injection interval shows a much improved pressure response, but are slightly lower at early time than the measured pressures. The simulated pressures in the observation borehole (BGS1-2) shows a very good fit at early time, but tends to be noticeably higher at late time. Overall, the simulations indicate a pressure-dependency, whereby the permeability decrease with decreasing pressure. Most likely, the pressure-dependent properties are non-linear and would require a more complex functional relationship in order to improve the fits, particularly for the BGS1-2. For this, a detailed coupled modeling approach is required to relate the measured deformation in the observation boreholes to the changes in the hydraulic and two-phase flow properties of the formation.

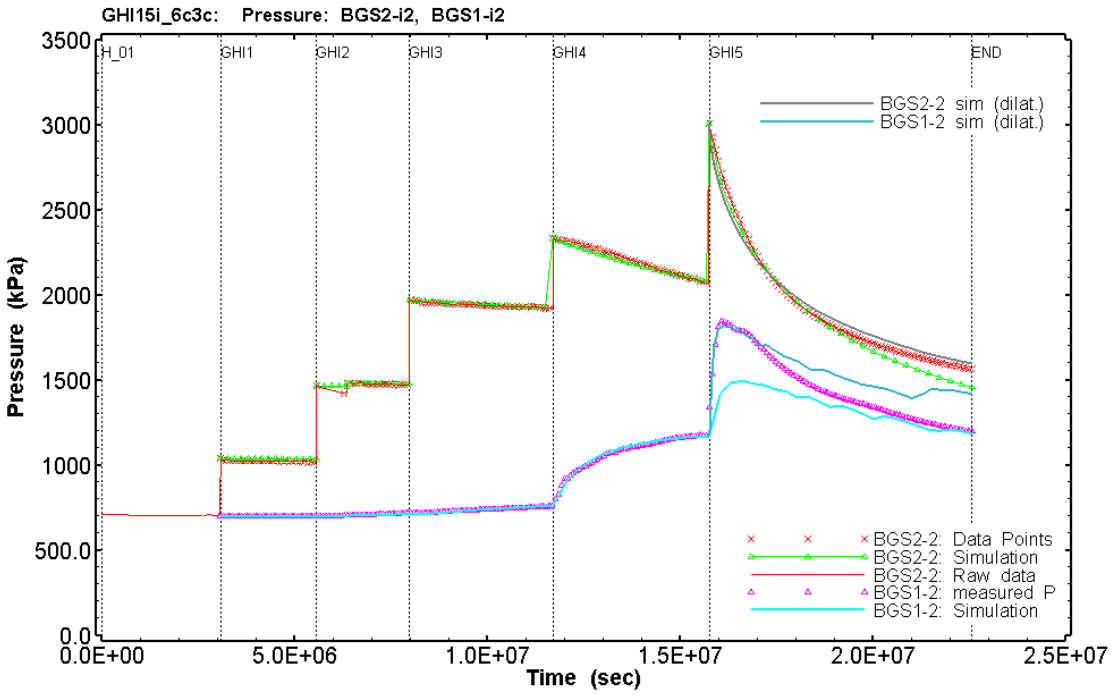

Figure 4.7: Simulated pressure responses in the injection borehole (BGS2-1) and observation borehole (BGS1-2) during the HG-C Experimental Phases 2, based on individual fits of Sequences GHI1–3, GHI4, and GHI5, whereby GHI5 includes the simulated results assuming pressure-dependent permeability.

4.2.2 Water and gas tests as part of the HG-D experiment

The results and the existing interpretations of the HG-C experiments (end of 2006 – 2009) were disseminated to the WP4/WP5 modelling groups for complementary analyses and simulations (section 4.2.1). In addition, data sets of the new water and gas injection tests as part of the HG-D experiment (2011 – 2012) were distributed. The new test data are described in the subsequent paragraphs.

The new test sequence started after drilling and instrumentation of the borehole HG-D1 by the end of 2009. After an extended pressure recovery period, a multistep hydrotest was conducted in the test interval I2 of borehole HG-D1 for hydraulic characterisation of the test interval. The injection pressures were kept below 2 MPa in order to minimise the risk of hydraulic fracturing or pathway dilation. The active test phase was followed by a shut-in period of several months. After full recovery of the pore pressure in HG-D1-I2, a multistep gas injection was started. The test was aimed at determining the gas transport properties of the rock at moderate injection

pressures (two-phase flow regime) and at elevated pressures (pathway dilation regime), respectively.

Figure 4.8a displays an overview of the available long-term monitoring data of the new HG-D experiment, starting early 2009 with an extended long-term monitoring phase and the subsequent packer installation in BHG-D1 by the end of the year. The multistep water injection test starting in June 2010 test is marked in blue in Fig. 4.8a. Crosshole responses on the water injection are observed in intervals I2 of borehole BGS-2 and in BGS-1-I1 and BGS-1-I3.

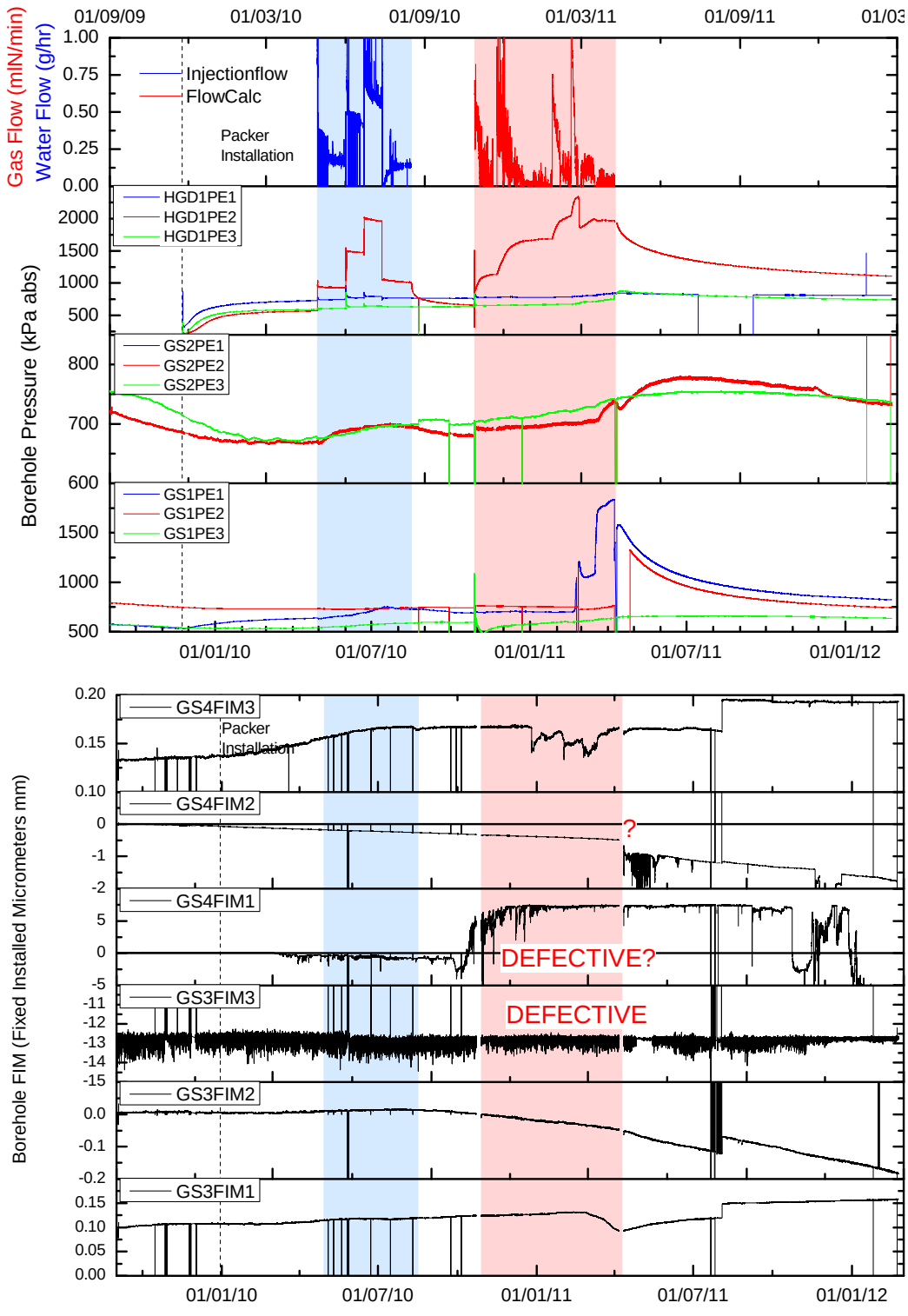

Figure 4.8: HG-D testing: a) flow and pressure response; b) FIM response

The corresponding transients of the FIMs are shown in Figure 4.8b. Unfortunately, the quality of the FIM data is rather poor. In particular BGS-3-FIM3 and BGS-4-FIM4 show strange results indicating, that the sensors might be defective. None of the sensors exhibits a significant mechanical response on the water injection test.

The subsequent gas injection test at the end of 2010 is marked in red in Figure 4.8a. A zoom-in of the pressure and flow transients is given in Figure 4.9. During the first pressure step at 1.2 MPa, the gas flow decreases quickly towards the detection limit of the flowmeter. No significant pressure responses are observed in the observation intervals BGS-1 and BGS-2. Similarly, during the second and the third pressure step (1.7 and 2.0 MPa, respectively) there is no major response observed in the adjacent monitoring boreholes. The behaviour changes when pressure is increased to a value of around 2.3 MPa: a rapid pressure response is observed in GS1-I1 and slow, but significant pressure increases are seen in BGS-2-I1 and –I3. Furthermore GS3-FIM1 displays a marked dilatation.

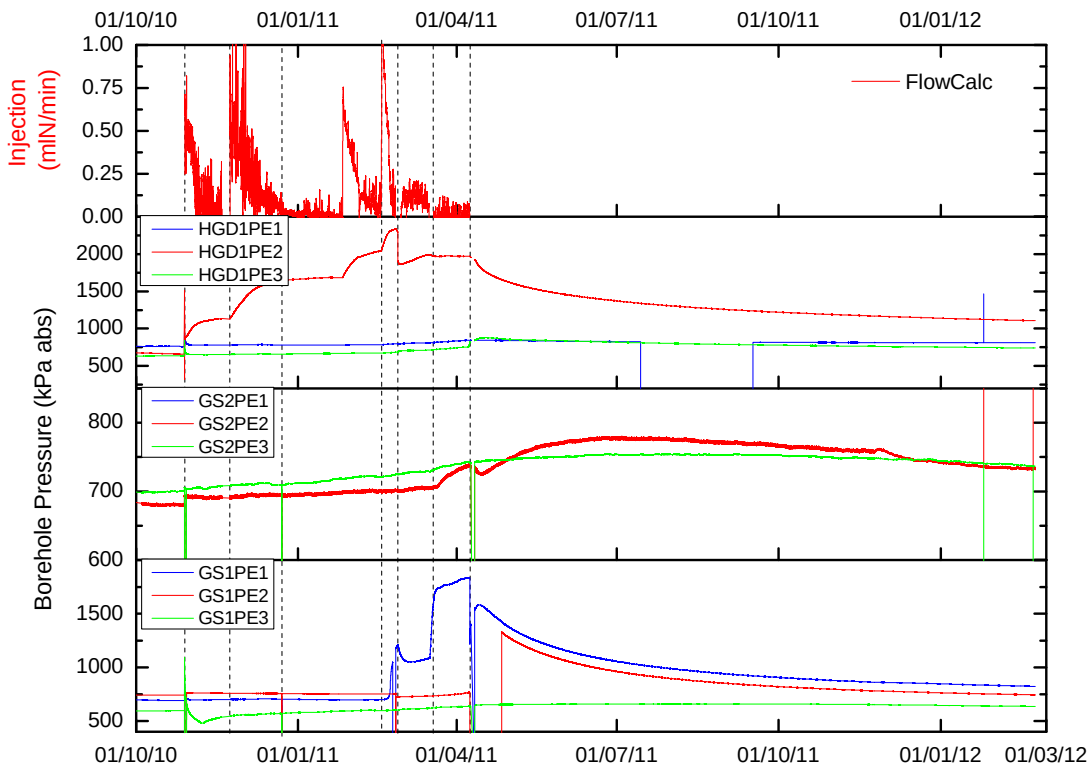

Figure 4.9: HG-D testing gas injection flow and pressure response.

Even though it is evident, that the new HG-D data bases did not exhibit the same quality as the previous HG-C data, some interesting general conclusions can be drawn. Thus, gas invades the rock already at moderate gas pressures (gas threshold pressure of 1.2 MPa, corresponding to an air entry value in the order of 0.7 MPa and a static formation pressure of 0.5 MPa). Furthermore, the opening of the bedding in response to the 4th step of gas injection (at 2.3 MPa) happens at a slightly lower pressure than the previous HG-C gas test (at 2.8 MPa) and significantly lower pressure than the former GS/GP-A tests (at around 4 MPa).

4.3 SUMMARY AND CONCLUSIONS

Due to the limited data quality of the recent HG-D test sequence, the summary and conclusions regarding the HG-C/HG-D experiment are mainly based on achievements from the HG-C test phase.

The aim of the HG-C experiment was to improve the understanding of gas transport processes in the undisturbed Opalinus Clay and to develop coupled THM-models that allow adequate long-term analysis of gas transport in clay-rich formations. The field testing comprised two phases which included (1) long-term step constant head water injection tests conducted between December 2006 and April 2007, followed by (2) long-term constant head gas injection tests conducted between February and September 2008. A detailed interpretation of both water and gas injection test sequences is given in Senger (2010).

During the hydrotest six pressure-controlled injection steps from 1.2 to 5.7MPa were performed while the flow to interval i2 was monitored. Pressure was then decreased in 4 steps. The test data were subjected to diagnostic analyses, followed by optimization (inverse modeling) and calibration with a numerical welltest simulator. The results of the optimization of the individual sequences (HI1 to HI6) indicated a trend of increasing conductivity with increasing injection pressures.

The subsequent gas injection tests used both the pressure responses in the injection interval I2 in borehole BGS2 and interval I2 in the observation borehole BGS1, which have been shown from previous testing campaigns (GS/GP-A) to be hydraulically and geomechanically connected along a bedding plane. For the gas test, the pressures in the observation borehole BGS1-I2 showed a distinct response during the GHI4 and GHI5, corresponding to a decline in the injection pressure (BGS2-I2). For the two-phase flow inverse simulation both the pressure responses in the injection interval (BGS2-2) and in the observation borehole interval (BGS1-2) were used for calibration. Based on the apparent difference in the responses, three separate optimizations were performed for (a) GHI1-3, (b) GHI4, and (c) GHI5 to estimate hydraulic properties as well as two-phase properties. The results of the inverse simulations with ITOUGH2 for the GHI1-3 steps, where the injection pressure steps increase up to 2 MPa and produced only minor pressure responses in both injection and observation intervals, yielded a formation permeability of 5.0E-20 m^2, which compared well with the estimate from the hydrotest during HI2 at a similar injection pressure. The parameter estimates for the GHI4 indicated a noticeable increase to 1.4E-19 m^2 and reproduced well the injection pressure and observation pressure responses. The final injection step (GHI5) produced a more than one order of magnitude increase in permeability of 1.45E-18 m^2. Moreover, the inverse modeling yielded decreasing values in the capillary strength parameter vG-P_0 of the van Genuchten model for the capillary pressure – saturation relationship. This is consistent with the concept of pressure-dependent pathway dilation which results in a permeability increase and corresponding decrease in capillary pressure. The geomechanical effect of pathway dilation is also indicated by the measured displacements in the boreholes BGS3 and BGS4. Further analyses of the hydraulic and two-phase flow responses together with the measured geomechanical responses would be desirable to couple explicitly the two-phase flow behavior of the two mobile phases with the deformation behavior of the solid skeleton with a suitable constitutive HM-model. Thus, further insight could be gained in the self-sealing processes associated with reconsolidation of the rock during the subsequent pressure recovery phase after the shut-in of gas injection. Based on experimental evidence from previous gas injections in the GS-2-2 intervall (e.g. Marschall et al. 2005) it can be expected that the interval transmissivity will approach closely the values which would be expected for intact rock.

5 Summary and conclusions

During the past decade a comprehensive gas-related data base has been elaborated in the context of the Mont Terri project, comprising both laboratory investigations on core samples and in-situ experiments in the Mont Terri URL. Emphasis was on the identification of gas related phenomena and on the development of conceptual models of coupled THM processes associated with gas transport in intact and fractured Opalinus Clay. This report was aimed at compiling relevant data from the Mont Terri URL as input for the benchmark exercises to be tackled by the THM-modelling groups of WP4 (WP 4.3.1: Modelling of gas migration through disturbed argillaceous media) and WP5 (WP 5.3.1 Modelling of gas transport in indurated clay). A survey of laboratory and field experiments is presented in the report, which (i) provides insight in important gas related phenomena, (ii) compiles characteristic two-phase flow parameters of the Opalinus Clay at Mont Terri, and (iii) can be used for the validation of coupled models of multiphase flow in deformable media.

The reported achievements on gas related research in the Mont Terri URL are summarised in the subsequent paragraphs.

Gas related phenomena and HM processes (including self-sealing)

Dedicated laboratory experiments were conducted to pinpoint the high sensitivity of Opalinus Clay on capillary (and osmotic) suction. The experiments included water retention measurements and measurements of the volumetric response on suction changes.

New experimental techniques were tested for measuring the water retention curves at ambient / elevated temperature and at confined / unconfined conditions. Furthermore, water retention behaviour was investigated along wetting / drying paths. The main findings are:

- A marked inverse correlation of the water retention behaviour with temperature was found. The correlation can be explained by the temperature dependence of surface tension of the water/air/solid system. The temperature dependence of the viscosity of water could have an additional (minor) impact.
- The confining pressure (external stress) has a significant impact on the water retention behaviour. The increase in confining pressure tends to shift the pore size distribution towards lower pore modes. This results in steeper capillary pressure curves and higher gas entry pressures.
- A clear hysteretic behaviour of the water retention behaviour along the wetting / drying path has been confirmed. Gas trapping was observed along the drying path which led in some cases to significant values of irreducible gas saturation along the wetting path.

The volumetric response of the rock on changes of liquid and gas pressure was determined in oedometric and triaxial cells. The main findings are:

- Consolidation and swelling were observed as key mechanisms in response to the application of pore pressure. A clear dependency of water permeability on effective stress was confirmed. In this context, the self-sealing capacity of the rock is a direct consequence of its swelling capacity.
- Gas permeability tests in a triaxial cell indicated, that the volumetric strain was mostly recovered after shut-in of the gas injection, suggesting that expansion due to swelling is the main mechanism associated with the gas injection. Recovery of strain followed

largely the slope of the swelling/reconsolidation line with swelling coefficients, which are typical for Opalinus Clay. On the other hand, the occurrence of irreversible volumetric strains (dilatancy) should not be ruled out completely.

- Both laboratory and in-situ experiments suggest that the Opalinus Clay has the capacity to self-seal after being subjected to dilatant deformation processes. The permeability of dilated Opalinus Clay recovers mostly to the intrinsic values of the intact rock, when the effective stress increases to values above the swelling pressure of the rock (typically 0.5 – 1MPa; see chapter 2.2). Another indicator for the self-sealing capacity of the rock are the measured swelling strains of the unloaded rock, ranging typically between 1 and 8%.

Gas related properties of the Opalinus Clay

Laboratory and in-situ experiments were performed to derive basic two-phase flow parameters of Opalinus Clay, including porosity, pore size distribution, intrinsic permeability, capillary pressure and relative permeability relationships. The experiments provided a quite consistent picture of flow and transport parameters in the Opalinus Clay of the Mont Terri URL:

- Porosity exhibits a clear dependence on the stress conditions, as confirmed by experiments in response to changes of total stress, effective stress, capillary suction and osmotic suction. Typical unconfined porosities between 16 and 19% were derived. Pore size distributions were determined with mercury intrusion porosimetry, providing dominant pore modes between 11 and 23 nm.
- Intrinsic permeability of the rock is typically in the range between 5E-20 and 1E-21 m^2 in flow direction normal to bedding and by a factor of 3-5 higher when flow occurs parallel to bedding.
- The capillary pressure curves determined along the wetting and the drying path respectively, exhibit a typical van Genuchten behaviour with a steep increase of capillary pressure in the range of high water saturations. Typical values of capillary strength in the order of 10 – 30 MPa were derived in laboratory experiments along the drying path. In-situ test display lower values, typical in the low MPa-range. This apparent discrepancy can be attributed to a scale effect associated with the pore size distribution of the rock. At the field scale the probability increases to cover a broader pore size distribution, with the largest pores dominating both the capillary strength and the capillary entry pressure. Such macro-pores may either be associated with excavation induced effects or with facial or structural variabilities on the larger scale (sandy intercalacions; tectonic features).
- Gas entry pressures of the intact rock were determined both, from laboratory experiments and in-situ tests. The laboratory experiments suggest threshold pressure values which are often close to the confining stress, whereas the in-situ tests revealed gas entry at significantly lower gas pressures, typically in the range of 1-2 MPa. This apparent discrepancy can be attributed to the scale effect, described in the previous paragraph.

Data for the validation of coupled models of multiphase flow in deformable media

A wealth of data suitable for the validation of coupled models of multiphase flow in deformable media was compiled in this report. The survey includes laboratory data aimed at validating the various aspects of the constitutive hydro-mechanical behaviour of Opalinus Clay, such as water

retention behaviour, volumetric behaviour in response to stress changes and coupled flow&transport behaviour. Furthermore, data from in-situ tests were compiled, emphasising the validation of the evolution of various elements of the repository system, such as the EDZ evolution during construction and operations phases and the behaviour of the backfilled tunnel nearfield in post-operational times. Necessary pre-conditions for the validation of the system evolution is not only a sound understanding of the constitutive behaviour of the different system components (backfill material, EDZ, intact host rock, fracture systems) but also the knowledge of the environmental conditions (stress state, pore pressure distribution, humidity distribution) which are forming the initial and boundary conditions for any prediction-evaluation exercise. In the present report, data bases have been compiled for the following modelling benchmarks:

- Constitutive hydro-mechanical behaviour of fully saturated Opalinus Clay in response to gas overpressures (gas permeability tests by UPC / chapter 2.2.3).
- Constitutive water retention and gas transport behaviour of intact Opalinus Clay in the strictly poro-elastic regime (core desaturation experiment / chapter 2.2.5; gas transfer test by RWTH Aachen / chapter 2.3.4).
- Creation of the EDZ around a circular tunnel and it's evolution during the operational phase (HG-A experiment / chapter 3).
- Evolution of the tunnel nearfield of a backfilled tunnel section after closure (HG-A experiment / chapter 3).
- Initiation and propagation of gas induced fractures around boreholes (HG-C/D experiment / chapter 4).

References

BIRCHALL DJ , HARRINGTON JF, , NOY DJ, CUSS RJ. 2007. LABORATORY STUDY EXAMINING PERMEABILITY EVOLUTION ALONG AN ISOTROPIC UNLOADING STRESS PATH. BGS OPEN REPORT OR/07/016.

BLÜMLING P., F. BERNIER, P. LEBON & C.D. MARTIN. 2007. THE EXCAVATION DAMAGED ZONE IN CLAY FORMATIONS TIME-DEPENDENT BEHAVIOUR AND INFLUENCE ON PERFORMANCE ASSESSMENT. CHEMISTRY OF THE EARTH 32, 588-599.

BOCK. H. 2000. RA EXPERIMENT - ROCK MECHANICS ANALYSES AND SYNTHESIS: DATA REPORT ON ROCK MECHANICS. MONT TERRI TECHNICAL REPORT TR 2000-02.

BOCK, H., DEHANDSCHUTTER, B., MARTIN, C.D., MAZUREK, M., DE HALLER, A., SKOCZYLAS, F. & DAVY, C. (2010): SELF-SEALING OF FRACTURES IN ARGILLACEOUS FORMATIONS IN THE CONTEXT OF GEOLOGICAL DISPOSAL OF RADIOACTIVE WASTE – REVIEW AND SYNTHESIS. OECD/NEA 6184, OECD NUCLEAR ENERGY AGENCY, PARIS, FRANCE, 310 PP.

BOSSART, P., WERMEILLE, S.: THE STRESS FIELD IN THE MONT TERRI REGION - DATA COMPILATION. IN: HEITZMANN, P. & TRIPET, J.-P. (ED.): MONT TERRI PROJECT – GEOLOGY, PAEOHYDROLOGY AND STRESS FIELD OF THE MONT TERRI REGION – REPORTS OF FEDERAL OFFICE FOR WATER AND GEOLOGY (FOWG), GEOLOGY SERIES 4, 65-92.

BROMMUNDT, J., CROISÉ, J. (2010) INTERPRETATION OF GAS TESTS IN OPALINUS CLAY CORE: SPECIMEN: TEST IMPROVEMENTS. MONT TERRI TECHNICAL NOTE TN 2009-52.

CROISÉ, J., MAYER, G.,. MARSCHALL, P., MATRAY, J.M., TANAKA, T. AND P. VOGEL (2006). GAS THRESHOLD PRESSURE TEST PERFORMED AT THE MONT TERRI ROCK LABORATORY (SWITZERLAND): EXPERIMENTAL DATA AND DATA ANALYSIS. OIL & GAS SCIENCE AND TECHNOLOGY - REV. IFP, VOL. 61 (2006), NO. 5, PP. 631-645 DOI: 10.2516/OGST:2006003

CROISÉ, J., MAYER, G. (2006): INTERPRETATION OF HYDRAULIC AND MECHANICAL RESPONSE DURING GP-B LONG-TERM HYDROTEST AND INTERPRETATION OF GAS TESTS IN OPALINUS CLAY CORE SPECIMEN. MONT TERRI TECHNICAL NOTE TN 2006-53.

CORKUM, A.G., MARTIN, C.D. 2007. MODELLING A MINE-BY TEST AT THE MONT TERRI ROCK LABORATORY, SWITZERLAND. INT. J. ROCK MECH. MIN. SCI. 44(6): 846-859.

DAVY, C., SKOCZYLAS, F., BARNICHON, J.-D., LEBON, P. (2007): PERMEABILITY OF MACRO-CRACKED ARGILLITE USING A 3-D ADAPTIVE CONTINUUM/DISCONTINUUM APPROACH. INT. MEETING "NATURAL AND ENGINEERED CLAY-BASED BARRIERS FOR THE CONTAINMENT OF RADIOACTIVE WASTE. TOURS 14-18, MARCH 2005, PP. 681-690.

DAVIES, P.B. 1991: EVALUATION OF THE ROLE OF THRESHOLD PRESSURE IN CONTROLLING FLOW OF WASTE-GENERATED GAS INTO BEDDED SALT AT THE WASTE ISOLATION PILOT PLANT (WIPP). SANDIA REPORT SAND90-3246 UC-721. SANDIA NATIONAL LABORATORIES, ALBUQUERQUE, NEW MEXICO.

ENACHESCU, C., JÄGGI, K., SCHMID, A., WOZNIEWICZ, J. (2000A). MONT TERRI - PHASE V / GP-A PRE-FRAC HYDRAULIC AND GAS LONGTERM TESTS IN BOREHOLE BGS-2: DATA ACQUISITION AND ANALYSIS REPORT. MONT TERRI TECHNICAL NOTE TN 2000-07.

ENACHESCU, C., JÄGGI, K., SCHMID, A. & WOZNIEWICZ, J. (2000B). GP-A EXPERIMENT: PRE-FRAC HYDRAULIC AND GAS LONG-TERM TESTS IN BOREHOLE BGS-2. MONT TERRI TECHNICAL NOTE TN 2000-007.

ENACHESCU, C., JÄGGI, K., SCHMID, A. & STEFFEN, P. (2000C). GP-A AND GS EXPERIMENTS; REPORT ON HYDRAULIC LONG TERM TESTING (WATER AND GAS) IN BOREHOLES BGS-2 (ACTIVE) AND BGS-1 (OBSERVATION) MONT TERRI TECHNICAL NOTE TN 2000-008.

ENACHESCU, C., JÄGGI, K., SCHMID, A. & STEFFEN, P. (2000D). GS – HYDRAULIC AND GAS LONG-TERM TESTS AFTER HYDRAULIC FRACTURING – ANALYSIS REPORT. MONT TERRI TECHNICAL NOTE TN 2000-009.

ENACHESCU, C., JÄGGI, K., PINE, R.J. & SCHMID, A. (2000E). GS - HYDRAULIC FRACTURING IN BOREHOLE BGS2. MONT TERRI TECHNICAL NOTE TN 2000-010.

ENACHESCU, C., BLÜMLING, P., CASTELAO, A., STEFFEN P., (2002). MONT TERRI GP-A AND GS EXPERIMENTS SYNTHESIS REPORT. NAGRA INTERNAL REPORT NIB 02-51.

FERRARI, A., P. WITTEVEEN AND L. LALOUI (2012). MATERIAL PROPERTIES AND GEOMECHANICAL TESTS ON BHG-D1 CORES. MONT TERRI TECHNICAL NOTE TN 2010-52.

FERRARI A. AND LALOUI L. 2012. ADVANCES IN THE TESTING OF THE HYDRO-MECHANICAL BEHAVIOUR OF SHALES. IN L. LALOUI AND A. FERRARI EDITORS. MULTIPHYSICAL TESTING OF SOILS AND SHALES, PAGES 57-68, SPRINGER, 2012.

GIRARDIN, C., T. THEURILLAT, N. BADERTSCHER AND C. NUSSBAUM (2008): DRILLING CAMPAIGN OF PHASE 13: DRILLING DATA, PHOTO DOCUMENTATION AND DRILLCOREDOCUMENTATION. MONT TERRI TECHNICAL NOTE 2008-05

HORSEMAN ST, HARRINGTON JF, BIRCHALL DJ, NOY DJ, CUSS RJ. 2003. HYDROGEOLOGIC ANALYSES AND SYNTHESIS (HA EXPERIMENT): CONSOLIDATION AND REBOUND PROPERTIES OF OPALINUS CLAY: A LONG-TERM, FULLY DRAINED TEST. MONT TERRI PROJECT, TECHNICAL NOTE 2003-03

HORSEMAN, S.T., HARRINGTON, J.F. (2002). LABORATORY EXPERIMENTS ON GAS MIGRATION IN OPALINUS CLAY SAMPLES FROM THE BENKEN BOREHOLE, SWITZERLAND. NAGRA INTERNAL REPORT NIB 02-31

LALOUI L, FERRARI A. 2008. ANALYSIS OF OPALINUS CLAY SELF SEALING: EXPERIMENTAL INVESTIGATION (SWELLING TESTS). HA-PROJECT, TECHNICAL NOTE 2008-45.

LALOUI, L., FERRARI, A. & SALAGER, S. (2012). TESTING THE THERMO-HYDRO-MECHANICAL BEHAVIOUR OF A SHALE. SHALE PHYSICS AND SHALE CHEMISTRY: NEW PLAYS, NEW SCIENCE, NEW POSSIBILITIES, PROC. OF THE 3RD EAGE SHALE WORKSHOP, BARCELONA, SPAIN, 23-25 JANUARY 2012.

JÄGGI, K. & STEFFEN, P. (2000): BOREHOLE INSTRUMENTATION OF BGS1 AND BGS2. MONT TERRI TECHNICAL NOTE TN 2000-006.

KROOSS, B.M., ALLES, S. (2006). INVESTIGATION OF GAS TRANSPORT PROCESSES IN THE OPALINUS CLAY, UNPUBLISHED MONT TERRI REPORT

LANYON, G. W.; MARSCHALL, P; TRICK, T; DE LA VAISSIÈRE, R, SHAO, H & LEUNG, H. (2009). HYDROMECHANICAL EVOLUTION AND SELF-SEALING OF DAMAGE ZONES AROUND A MICROTUNNEL IN A CLAYSTONE FORMATION OF THE SWISS JURA MOUNTAINS. IN 43RD U.S. ROCK MECHANICS SYMPOSIUM & 4TH U.S. - CANADA ROCK MECHANICS SYMPOSIUM, JUNE 28 - JULY 1, 2009 , ASHEVILLE, NORTH CAROLINA.

LANYON, G. W. (2008). DISCRETE FRACTURE NETWORK MODELS OF EXCAVATION DAMAGE ZONE AT THE HG-A SITE. MONT TERRI TECHNICAL NOTE TN 2007-07.

LANYON, G. W. (2009). ANALYSIS AND MODELLING OF HYDRAULIC AND GAS TESTING FOR THE MONT TERRI HG-A EXPERIMENT (PHASE 14). MONT TERRI TECHNICAL NOTE TN 2009-04.

LANYON, G. W. (2012). HG-A (GAS PATH THROUGH HOST ROCK AND ALONG SEALS) EXPERIMENT: PRELIMINARY INTERPRETATION OF GAS INJECTIONS DURING PHASE 15 &16. MONT TERRI TECHNICAL NOTE 2010-40.

LANYON, G. W.; MARSCHALL, P; TRICK, T; DE LA VAISSIÈRE, R, SHAO, H & LEUNG, H. (2012 ; SUBMITTED FOR PUBLICATION). SELF-SEALING EXPERIMENTS AND GAS INJECTION TESTS IN A BACKFILLED MICROTUNNEL OF THE MONT TERRI URL. CLAYS IN NATURAL AND ENGINEERED BARRIERS FOR RADIOACTIVE WASTE CONFINEMENT. GSL SPECIAL PUBLICATIONS.

MARSCHALL, P., CROISÉ, J., SCHLICKENRIEDER, L., BOISSON, J.-Y., VOGEL, P. AND YAMAMOTO, S. 2004. SYNTHESIS OF HYDROGEOLOGICAL INVESTIGATIONS AT THE MONT TERRI SITE (PHASES 1 TO 5). -HEITZMANN, P. ED. 2004: MONT TERRI PROJECT- HYDROGEOLOGICAL SYNTHESIS, OSMOTIC FLOW. REPORTS OF THE FEDERAL OFFICE FOR WATER AND GEOLOGY, FOWG, GEOLOGY SERIES NO. 6.

MARSCHALL, P., HORSEMAN, S., GIMMI,T. (2005). CHARACTERISATION OF GAS TRANSPORT PROPERTIES OF THE OPALINUS CLAY, A POTENTIAL HOST ROCK FORMATION FOR RADIOACTIVE WASTE DISPOSAL. OIL AND GAS TECHNOLOGY REVUE DE L'INSTITUT FRANÇAIS DU PÉTROLE, 60, NO. 1&2.

MARSCHALL, P., M. DISTINGUIN, H. SHAO, P. BOSSART, C. ENACHESCU & T. TRICK. 2006. CREATION AND EVOLUTION OF DAMAGE ZONES AROUND A MICROTUNNEL IN A CLAYSTONE FORMATION OF THE SWISS JURA MOUNTAINS. SPE PAPER 98537.

MARSCHALL, P., T. TRICK, G.W. LANYON, J. DELAY AND H. SHAO. 2008. HYDRO-MECHANICAL EVOLUTION OF DAMAGED ZONES AROUND A MICROTUNNEL IN A CLAYSTONE FORMATION OF THE SWISS JURA MOUNTAINS. ARMA 2008, SAN FRANCISCO.

MARTIN, C.D., G.W. LANYON, P. BLÜMLING, & J.-C. MAYOR. 2002. THE EXCAVATION DISTURBED ZONE AROUND A TEST TUNNEL IN THE OPALINUS CLAY. *PROC. 5TH NORTH AMERICAN ROCK MECHANICS SYMPOSIUM AND 17TH TUNNELLING ASSOCIATION OF CANADA CONFERENCE: NARMS/TAC 2002*, UNIVERSITY OF TORONTO PRESS, VOL. 2, P1581-1588.

MARTIN, C.D. & LANYON, G.W. 2003. EDZ IN CLAY SHALE: MONT TERRI, MONT TERRI TECHNICAL REPORT. 2001-01

MEIER, O., O. MASSET, N. BADERTSCHER, G. JOLLIAT & CH. NUSSBAUM. 2006. GAS PATH TROUGH HOST ROCKS AND ALONG SEALS (HG-A EXPERIMENT) DRILLING OF A RESIN IMPREGNATED SAMPLING BOREHOLE BHG-A28 FOR LABORATORY TESTS. MONT TERRI TECHNICAL NOTE TN 2006-67.

MUÑOZ, J.J. (2007). THERMO-HYDRO-MECHANICAL ANALYSIS OF SOFT ROCKAPPLICATION TO A LARGE SCALE HEATING TEST AND LARGE SCALE VENTILATION TEST. PHD DISSERTATION, UNIVERSITAT POLITÈCNICA DE CATALUNYA, SPAIN

NAGRA. 2002. PROJEKT OPALINUSTON – SYNTHESE DER GEO-WISSENSCHAFTLICHEN UNTERSUCHUNGSERGEBNISSE. ENTSOR-GUNGSNACHWEIS FÜR ABGEBRANNTE BRENNELEMENTE, VERGLASTE HOCHAKTIVE SOWIE LANGLEBIGE MITTELAKTIVE ABFÄLLE. NAGRA TECHNICAL REPORT NTB 02-03. NAGRA, WETTINGEN, SWITZERLAND

NAGRA (2008). EFFECTS OF POST-DISPOSAL GAS GENERATION IN A REPOSITORY FOR LOW- AND INTERMEDIATE-LEVEL WASTE SITED IN THE OPALINUS CLAY OF NORTHERN SWITZERLAND. NAGRA TECHNICAL REPORT NTB 08-07.

NUSSBAUM, CH. AND BOSSART P.: "TECTONICS OF THE MONT TERRI AREA BASED ON SMALL-SCALE TUNNEL MAPPING IN THE OPALINUS CLAY AND CORRELATION WITH THE SURROUNDING MAP SCALE STRUCTURES". *ECLOGAE GEOL. HELVETICAE*, SWITZERLAND (2006).

PERON, H., SALAGER, S., EICHENBERGER, J, RIZZI, M., LALOUI, L. 2008. HG-A EXPERIMENT: EXPERIMENTAL AND NUMERICAL ANALYSES OF EXCCAVTION DISTURBED ZONE (EDZ) ALONG TUNNELS. MONT TERRI TECHNICAL NOTE TN 2008-54

ROESLI, U., TRICK, T. (2008): TERRI HG-C EXPERIMENT PHASE 2: HYDRAULIC AND GAS TEST SERIES IN BGS2 BOREHOLE AND DEFORMATION MEASUREMENTS IN BOREHOLE BGS-3 AND BGS-4 BOREHOLES. MONT TERRI TECHNICAL NOTE TN 2008-30.

ROMERO, E., SENGER, R. & MARSCHALL, P. (2012). AIR INJECTION LABORATORY EXPERIMENTS ON OPALINUS CLAY. EXPERIMENTAL TECHNIQUES, RESULTS AND ANALYSES. 3RD EAGE SHALE WORKSHOP, BARCELONA, JANUARY 23-25, 2012.

ROMERO, E., SENGER, R., MARSCHALL, P., GÓMEZ, R. 2012. GAS TESTS ON LOW-PERMEABILITY ARGILLACEOUS ROCKS. EXPERIMENTAL RESULTS AND SIMULATIONS. IN L. LALOUI AND A. FERRARI EDITORS. MULTIPHYSICAL TESTING OF SOILS AND SHALES. SPRINGER, 2012.

SENGER, R.K. (2010): ANALYSIS OF THE HG-C EXPERIMENTAL PHASE 1 FOR THE DEVELOPMENT OF THM MODELS FOR THE LONG-TERM ANALYSIS OF GAS TRANSPORT IN CLAY-RICH FORMATIONS. . MONT TERRI TECHNICAL NOTE TN 2008-56.

STEIGER, H., P. BOSSART. 2003. HYDROGEOLOGIC ANALYSES AND SYNTHESIS (HA EXPERIMENT) BOREHOLE BHA-1: DOCUMENTATION OF DRILLING AND SAMPLE CONDITIONING. MONT TERRI TECHNICAL NOTE TN 2003-32.

TRICK, T. (2007): MT TERRI HG-C EXPERIMENT PHASE 1: FIRST HYDRAULIC TESTS AND DEFORMATION MEASUREMENTS IN BOREHOLE BGS-2. MONT TERRI TECHNICAL NOTE TN 2007-13.

VILLAR, M.V.AND ROMERO, F.J. 2012.WATER RETENTION CURVES OF OPALINUS CLAY. INFORMES TÉCNICOS CIEMAT 1262. OCTUBRE 2012. CIEMAT, MADRID, 33 PP.

VILLAR, M.V., A.M., FERNANDEZ AND MELON, A.M., 2009. MONT TERRI VENTILATION TEST PHASE II. WATER RETENTION CURVES DETERMINED ON ARGILLITE SAMPLES TAKEN BEFORE AND AFTER AN IN SITU VENTILATION PHASE. INFORMES TÉCNICOS CIEMAT 1170, MADRID.

Appendix – Data Packages 1 - 11

In the course of the FORGE project a total number of 11 data deliveries were initiated, concerning relevant laboratory and field data from Mont Terri. The data packages were distributed to the modelling teams of Work Package 4 and 5. The entire data base is available on request in electronic form. The enclosed table gives a survey of the data packages and the contents thereof.

FORGE DATA Deliveries

1	Data Package 1	First HG-A dataset & supporting reports Also includes sensor locations etc.
2	Data Package 2	Selected reports on laboratory testing of Opalinus Clay
3	Data Package 3 Stress	Information on expected stress field at Mont Terri URL
4	Data Package 4 HG-C	Dataset for HG-C to 30/06/09
5	Data Package 5 GS GPA	Dataset for GS/GPA experiments (HG-C related)
6	DataPackage 6 HGA Hydro	HG-A dataset to 13/02/12
7	DataPackage 7 HG-D	Dataset for HG-D to 28/10/09 (continuation of HG-C) omits observation zone responses
8	Data Package 8 HG-D 20110503	Dataset for HG-D to 03/05/11
9	DataPackage 9 HGA 300611	Complete HG-A dataset to 30/06/11
10	DataPackage 10 HGA 130212	Complete HG-A dataset to 13/02/12
11	DataPackage11 HG-D 230312	Dataset for HG-D to 23/02/12
	LBL HG-A	Data for LBNL (Jens Birkholzer)